1981

Atmospheric pressure active nitrogen (APAN) - a new source for analytical emission spectroscopy

Gary Wayne Rice
Iowa State University

Rice, Gary Wayne

ATMOSPHERIC PRESSURE ACTIVE NITROGEN (APAN) - A NEW SOURCE FOR ANALYTICAL EMISSION SPECTROSCOPY

Iowa State University PH.D. 1981

Atmospheric pressure active nitrogen (APAN) - A new source for analytical emission spectroscopy

by

Gary Wayne Rice

A Dissertation Submitted to the
Graduate Faculty in Partial Fulfillment of the
Requirements for the Degree of
DOCTOR OF PHILOSOPHY

Department: Chemistry
Major: Analytical Chemistry

Approved:

Signature was redacted for privacy.

In Charge of Major Work

Signature was redacted for privacy.

For the Major Department

Signature was redacted for privacy.

For the Graduate College

Iowa State University
Ames, Iowa

1981

TABLE OF CONTENTS

CHAPTER I. INTRODUCTION

The Disco Lights of Time Immemorial

Current trends in modern rock and roll music have led to a style in dancing known to the younger generations as disco. Upon entering an establishment that is popular for this type of entertainment, one is immediately overwhelmed by the rapid pace and consistent rhythm of the music. But the truly dominating observation that would be made is the multitude of flashing lights, containing every color in the visible spectrum, which continually attempt to impress upon the mind the diversity that can be achieved from controlled manipulation of light patterns.

As with all trends, disco will undoubtedly become only a passing memory to those who have experienced it. The pulsating colored lights which became a trademark for disco will, however, always remain for future generations. Nature has provided mankind with its own form of disco lights, a phenomenon known as auroras. These vivid and breath-taking displays of light, which are visually observed in the upper atmosphere of the polar regions, could truly be referred to by our passing generation as the disco lights of time immemorial.

Nature of Auroral Phenomenon

Auroras, which are also called "northern lights" or "aurora borealis" in the northern hemisphere, and as "southern lights" or "aurora australis" in the southern hemisphere, occur in a variety of forms, including homogeneous and pulsating arcs or bands, rays, and coronas. Colored

lights are observed in only the most intense auroras, and are usually observed to be yellowish-green in color, or occasionally red or violet.

The colors observed are now known to be caused primarily by emissions from nitrogen and oxygen in the upper atmosphere. The common yellowish-green auroras are the result of emission from atomic oxygen at 557.7 nm. The red auroral emissions are also the result of emission from oxygen at 630.0 nm. Rather intense emission from molecular nitrogen at 391.4 nm and 427.8 nm results in the violet colors observed in some auroras.

The theories which describe the formation of auroras are numerous and in most cases conflicting. The fact that both auroral displays and geomagnetic disturbances are concentrated in the polar regions has led to the general belief that both are excited by high-velocity charged particles, such as protons or electrons, which originate from the sun. The impact of these charged particles upon the earth's atmosphere gives rise to auroral emissions from interactions with oxygen and nitrogen. There still remains many questions, however, about the mechanisms through which these charged particles interact with the atmospheric nitrogen and oxygen to create auroras.

Active Nitrogen - A Man-made Aurora

The difficulties manifested in obtaining detailed analysis of naturally occurring auroral phenomenon led to numerous investigations using man-made auroras. The man-made nitrogen aurora, in particular, has been the subject of more investigations than any other element. Metastable and emissive excited states from nitrogen can readily be

produced by a variety of excitation sources, which has allowed for extensive analysis of atomic and molecular transations, as well as mechanisms for excitation.

The first known report on the luminescent afterglow of nitrogen occurred in 1865 by Morren, who demonstrated that a persistent luminescence, or afterglow, could be produced from nitrogen at low pressures following an electrical discharge through the gas (1). The first extensive study on the nature of nitrogen afterglows was made in 1900 by E. P. Lewis, who identified the band spectra from the afterglow as originating from molecular nitrogen (2-4). A series of papers by R. J. Strutt (Lord Rayleigh) beginning in 1911 demonstrated that the afterglows obtained from nitrogen at low pressures (1-10 torr) were highly reactive with other molecules or atoms introduced into the afterglow (5-8). The high degree of activity observed by Strutt led to the commonly used term "active nitrogen." Well over 2,000 publications on "active nitrogen" have appeared in the literature since the early investigations of Strutt. The entire field of active nitrogen research through 1968 has been extensively reviewed, with over 1,500 references, in a manuscript by Wright and Winkler (9).

Active nitrogen has, in the past, been produced primarily by electrical discharges through the nitrogen maintained at low pressures (2,5,10). High-frequency electrodeless discharges have also been used for generating active nitrogen (11-12), the primary advantage being that the gas is contained within a glass envelope and not contaminated by

metal electrodes during spectroscopic measurements. Other methods of generating active nitrogen have included electron bombardment (13), microwave resonant cavity techniques (14-15), and arc discharges (16-17).

During 1954-1955, Kentz observed that metastable species observed in active nitrogen sources could also be excited in electrical discharges of argon containing traces of nitrogen at pressures of $\sim$ 300 torr (18-19). Later investigations determined that the metastable nitrogen species were produced by energy transfer from argon metastable atoms to ground state nitrogen molecules (20-21). Nitrogen metastables have since then been also excited in helium (22) and krypton (23).

While the vast majority of investigations involving active nitrogen afterglows have been conducted in the 1 to 10 torr pressure range, observations on afterglows produced at atmospheric pressure have been sparse. A few investigators have used electric arc discharges between tungsten or copper electrodes in flowing nitrogen gas to generate afterglows (17,24). Only two investigators have made spectroscopic observations from electrodeless, low-frequency "ozonizer" discharges (25,26) and one investigator utilized excitation by 50 keV electrons (27).

The interaction of active nitrogen afterglows with other elements or molecules has been extensively studied. In the early work of Lewis and Strutt, it was qualitatively demonstrated that characteristic atomic or molecular emission could be observed when vapors of metals or compounds were introduced into a low pressure, active-nitrogen afterglow. It was recognized even then that active nitrogen provided an excellent source for the low-temperature excitation of line and band spectra of many

atoms and molecules. The investigations by Kenty demonstrated that reactions with metallic elements could also be duplicated in the argon induced, active-nitrogen afterglow. Renewed and stimulating interest in the interactions of active nitrogen with various species has been most recently investigated by Winkler et al. (28-31), Duthler (32), and Phillips (10,33). A considerable effort was undertaken in these investigations to determine the nitrogen species and mechanisms responsible for the formation of characteristic emission from species introduced into the afterglow. In contrast to the extensive investigations mentioned above, in which the active nitrogen afterglow was maintained at low pressures, there is no evidence that reactions of elements or molecules introduced into active nitrogen afterglows produced at atmospheric pressure have been reported.

Analytical Applications Utilizing Active Nitrogen

Although active-nitrogen afterglows have been recognized since the turn of the century for exciting emission from a large number of elements and molecules, their development as a source for analytical emission spectroscopy has been over-shadowed by the popularity and commercial availability of flame and plasma excitation sources. Unfortunately, the continual assault of man upon his environment has created an urgent need for developing new methodology to detect trace levels of potentially dangerous substances which threaten the delicate balance of our natural environment.

Recent investigations by Sutton et al. have successfully demonstrated that a low pressure active nitrogen afterglow could be utilized as an

excitation source for analytical spectroscopy (34-38). Detection of gas phase Bi and GeH_4 down to 10^4 atoms/cm^3 and 10^7 molecules/cm^3, respectively, was demonstrated (34-36). The proposed mechanism of excitation involved energy transfer from metastable, active-nitrogen species generated in a microwave cavity. More recently, the same system has been evaluated as a selective detector for gas chromatography (37,38). Selective detection of hydrocarbons, alcohols, and alkylated metals was demonstrated. A limit of detection of 4 ng was obtained for methane by monitoring CN emission at 388.3 nm.

For quantitative analytical purposes, the use of low pressure, active-nitrogen afterglows may present problems in sample introduction and pressure regulation. In contrast, active-nitrogen afterglows produced at atmospheric pressure would be experimentally much easier to manipulate and hence, more attractive to analytical chemists. However, no systematic studies on the behavior of atoms and molecules when they are introduced into an atmospheric pressure, active-nitrogen afterglow have been reported. These considerations led into the investigations reported in this thesis. An atmospheric pressure, active nitrogen (APAN) afterglow system was developed for the purpose of evaluating its potential utilization as an excitation source for analytical spectroscopy. The next chapter discusses the experimental foundations and results obtained in the development of this technique.

CHAPTER II. EXPERIMENTAL EVALUATION OF AN ATMOSPHERIC PRESSURE ACTIVE NITROGEN AFTERGLOW AS A SOURCE FOR ANALYTICAL SPECTROSCOPY

Detection of Trace Levels of Hg and the Hydrides of As, Bi, Ge, Pb, Sb, Se, Sn, and Te

Introduction

The determination of nanogram levels of As, Bi, Ge, Pb, Sb, Se, Sn, and Te via the hydride generation technique, and Hg by reduction to the volatile elemental form, followed by atomic absorption, fluorescence, or emission spectrometry has been extensively documented (39). Physical properties of the hydrides in Groups IV-VI of the periodic table are given in Table 1. The application of hydride generation is analytically appealing for several reasons. The extremely low boiling points readily allow for the separation of the hydrides from a sample matrix which could give rise to spectral interferences. Atomization of the hydrides proceeds rapidly in conventional flame or plasma excitation sources because of the low decomposition temperatures encountered. The low energy requirements for dissociation of the hydrides are desirable in the low temperature active nitrogen afterglows since the dissociation process has been attributed to energy transfer and not thermal processes (37). Finally, aqueous vapors, which are known to quench the active nitrogen afterglow, can be eliminated.

To initially demonstrate the analytical potential of an APAN afterglow, a study on the detection of trace levels of As, Bi, Ge, Hg, Pb, Sb, Se, Sn, and Te was performed, as well as the quantitative determination of As in environmental samples.

Table 1. Physical properties of the hydrides in Groups IV-VI of the periodic table

Group	Element	Hydride	M.P.[a]	B.P.[a]	Decomposition Temp.[a]	Bond Energy (eV)[b]
IV	Germanium	GeH_4	-165°C	- 89°C	350°C	2.96
IV	Tin	SnH_4	-150°C	- 52°C	150°C	2.61
IV	Lead	PbH_4	-c	-c	-c	-c
V	Arsenic	AsH_3	-116°C	- 55°C	300°C	3.08
V	Antimony	SbH_3	- 89°C	- 17°C	200°C	2.65
V	Bismuth	BiH_3	-c	22°C	150°C	-c
VI	Selenium	H_2Se	- 64°C	- 42°C	160°C	3.17
VI	Tellurium	H_2Te	- 51°C	- 4°C	0°C	-c

[a]Reference 40.

[b]Reference 41.

[c]Not found at time of writing.

The experimental approach utilized in the present study was to form either the free atoms (Hg) or the gaseous hydrides of the other elements listed above. These species were then injected into the afterglow region of an electrodeless ozonizer-type discharge in pure N_2.

Apparatus and procedures

A schematic diagram of the APAN afterglow torch is shown in Figure 1. The actual discharge occurs in pure N_2 that flows through the annular space formed by two concentric fused silica tubes approximately 40 cm in length. The copper foil electrodes were positioned in the inside of the inner tube and the outside of the outer tube. The source of N_2 was provided by the boiloff from a pressurized tank of liquid N_2. Our measurements have indicated that the O_2 content of the N_2 boiloff was less than 10 ppm. The N_2 gas initially flowed through the inner tube to facilitate cooling of the inner electrode and then into the annular discharge cavity. The top of the discharge tube was truncated and ended in an 8 cm long, 8 mm I.D. afterglow tube. The exit end of the sample inlet port was positioned approximately 5 mm from the rounded tip of the inner tube and centrally with respect to the afterglow tube.

A schematic diagram of the analytical facilities employed in this investigation is shown in Figure 2. The N_2 gas from the liquid N_2 tank [1] was partitioned into two streams. The main stream, which sustained the discharge [4], flowed through the rotameter [2] and the purification trap [3] at a rate of 30 liters/minute. The purification trap consisted of a glass condenser coil immersed in liquid N_2 and was designed to

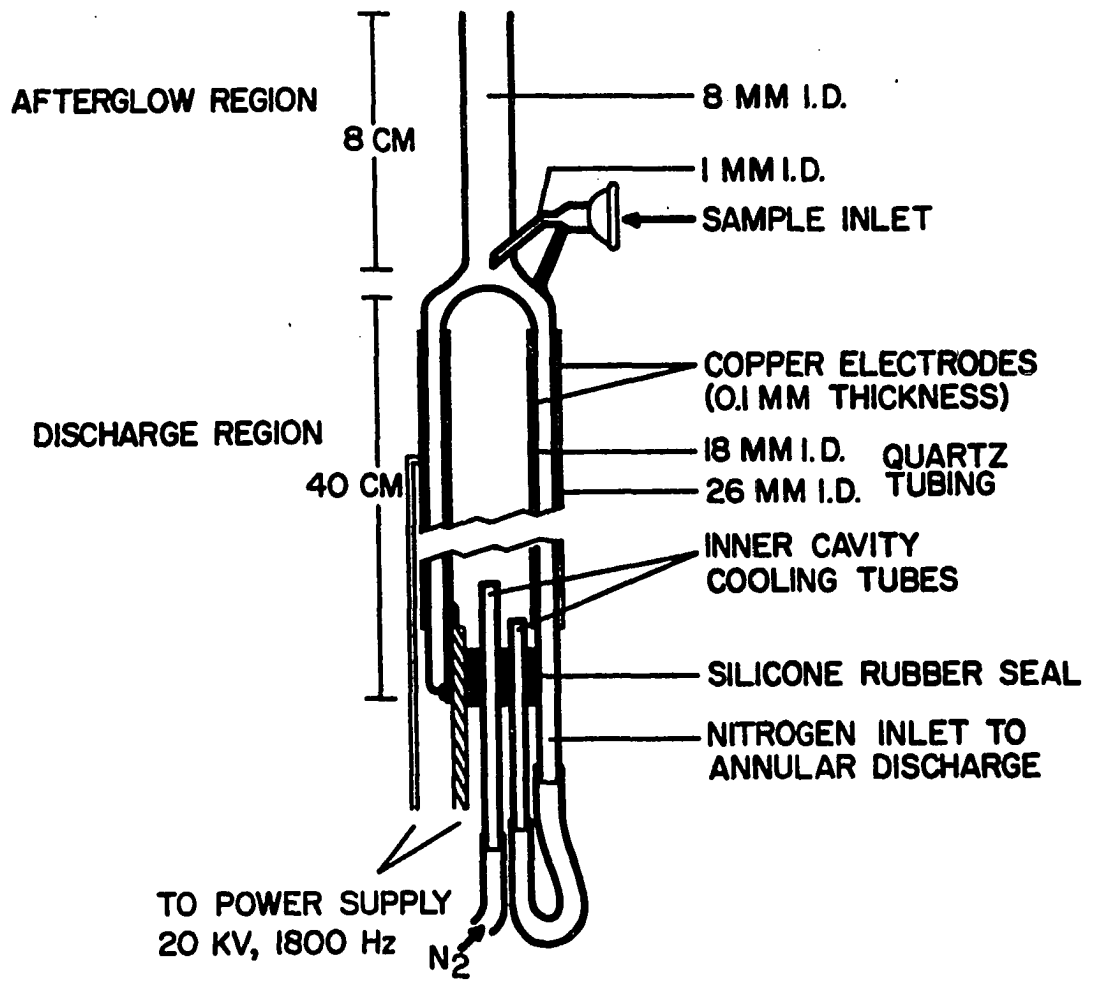

Figure 1. Schematic diagram of the APAN discharge tube

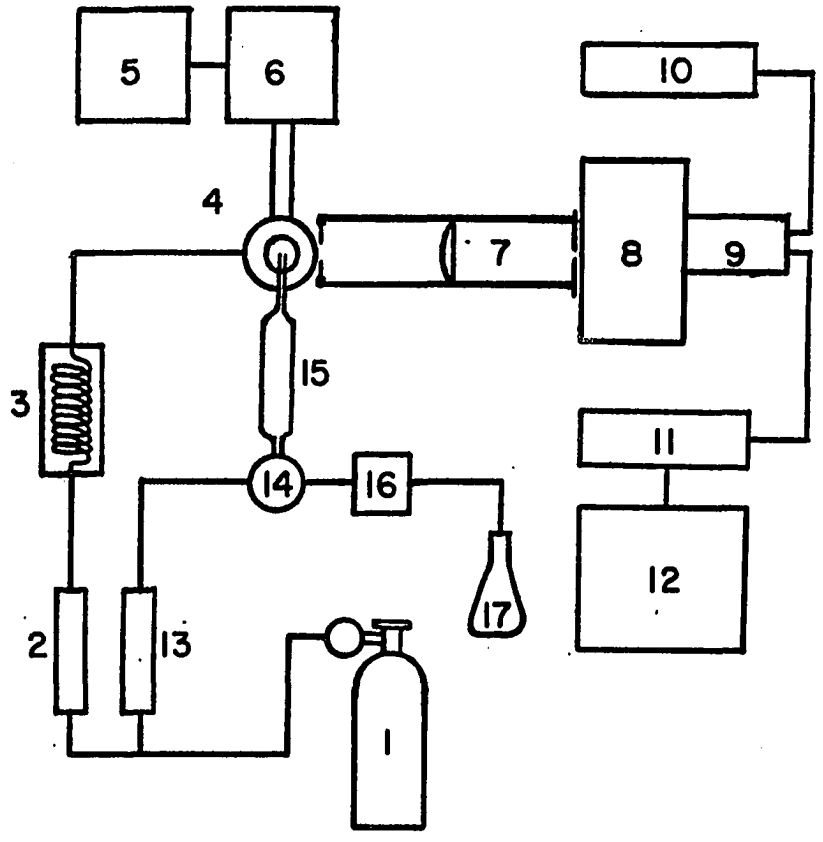

Figure 2. Schematic diagram of instrumentation for APAN system (numbered components are referred to in the text)

condense impurities that may be volatilized during the N_2 boiloff. The inclusion of the trap was found necessary to improve the characteristic emissions of the APAN afterglow.

The power supply assembly that maintained the discharge consisted of a 500 VA, Invertron AC power source [5] (Aiken Industries, 5150 Convoy Street, San Diego, California 92111). The power source contained a built-in oscillator that provided a variable frequency output in the 300 Hz to 2 kHz range. The output from this source provided the input to a 20 kV transformer [6] (Model EGV 20-6, Del. Electronics, Inc., Mount Vernon, New York 10550). The best analytical performance with the present torch design was obtained when the discharge was operated at 1800 Hz.

The central 3 cm of the afterglow tube was imaged by a fused silica plano-convex lens [7] onto the slit of the 0.3 meter scanning monochromator [8] (McPherson Model 218, GCA Corporation, Acton, Massachusetts 01720). For studies in the ultraviolet region, the monochromator was fitted with a 1200 lines/mm grating blazed at 200 nm. A CsTe solar blind photomultiplier tube [9] (EMI, G-26H 315) was used as the detector. An extended S-20 response photomultiplier (Centronic #Q4283S-25, Bailey Instruments Company, Saddle Brook, New Jersey 07662) was used for studies in the 400-900 nm region. For observations in this wavelength region, a 1200 lines/mm grating blazed at 500 nm was used. A spectral slit width of 500 μ (FWHM = 1.4 nm) was normally used for the analytical studies. The photomultipliers were powered by a HV power supply [10]

(Model N-4035, Hamner Electronics Company, Inc., Princeton, New Jersey 08540). The photocurrents produced were amplified by an electrometer amplifier [1] (Model 417, Keithley Instruments, Inc., Cleveland, Ohio 44139) and the spectral information recorded on a strip chart recorder [12] (Model FWD, Texas Instruments, Inc., Houston, Texas 77008).

The N_2 stream that was directed through the second rotameter [13] flowed at a rate of 2 liters/minute into the hydride generating cell [14]. The generated hydrides were transferred through a $CaCl_2$ drying tube [15] into the APAN afterglow tube. A peristaltic pump [16] was used to introduce an aqueous $NaBH_4$ solution [17] into the hydride generator at a rate of 12 mL/minute for five seconds.

The hydride generator is shown schematically in Figure 3. Sample aliquots were pipetted into the sample chamber [5] through the 12/5 socket joint [1] on the top of the generator cell. The ball joint seal [2] contained a rubber septum fitted with #20 gauge Teflon tubing that extended into the sample solution for introducing the $NaBH_4$ solution. The N_2 carrier stream [3] passed through a stopcock [4] into the sample chamber [5], whose internal volume was approximately 15 mL. A gas dispersion tube [6] assured rapid reagent mixing and removal of the gaseous hydrides. The hydrides were swept through a second stopcock [7] into the APAN afterglow [8]. A third stopcock [9], located at the bottom of the cell, was used to drain reacted solutions from the sample chamber.

In the present study, the hydrides of the elements were generated by the introduction of $NaBH_4$ solution (1-5% w/v) into acidified analyte

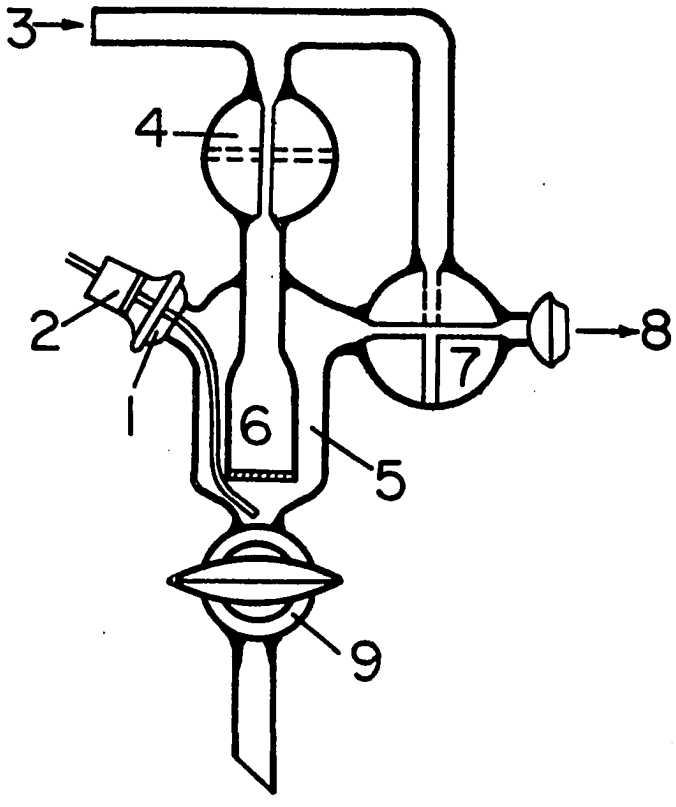

Figure 3. Schematic diagram of the hydride generator (numbered components are referred to in the text)

solutions (1-5 M HCl). For Pb, the analyte solutions were prepared in 1% $HClO_4$ (v/v) to which 1 ml of 12% H_2O_2 (v/v) was added prior to addition of $NaBH_4$ (42). For Sn, the analyte solutions were prepared in 1% HCl (v/v) (43). Mercury (II) solutions were reduced directly to elemental Hg by addition of 2% $SnCl_2$ in 1 M HCl. The results reported here were obtained on 1 mL sample volumes. The hydrides or elemental Hg were detected in the APAN afterglow tube by the characteristic atomic emission spectra of the respective elements. With this system, the hydrides of several elements at ng/mL levels, in sample solutions ranging from 0.1 to 5 mL, could be generated at the rate of 30 to 40 samples per hour.

Results and discussion

On electrical initiation of the discharge, the N_2 gas in the discharge tube attained a violet blue color, but no color was observed in the afterglow tube. Over a period of approximately five minutes a green glow appeared in the discharge tube and slowly migrated into the afterglow tube. The optimum analytical performance of the APAN system was observed when the green 557.7 nm emission from metastable atomic oxygen in the afterglow reached a maximum and constant value.

The spectral background from 180 nm to 700 nm obtained from the afterglow region of the discharge tube is shown in Figure 4. As can be seen from Figure 4, the ultraviolet region is dominated by emissions from NO. Emission in the visible region of the spectrum was limited to atomic oxygen at 557.3 nm. Detailed discussions pertaining to the origin of these species in the afterglow will be given in the following chapter.

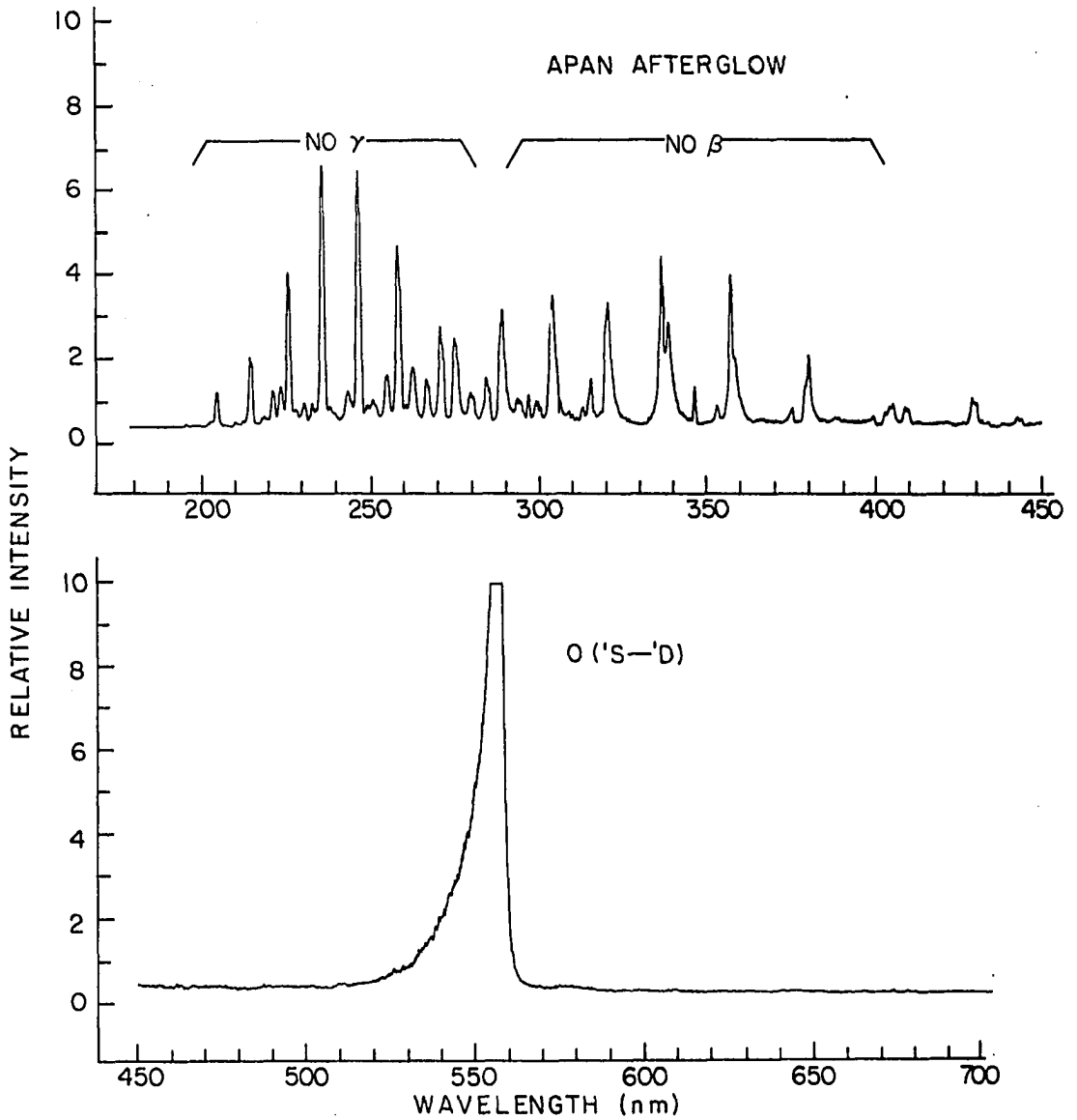

Figure 4. Spectral background observed from the APAN afterglow. Bandpass = 0.3 nm (FWHm)

An initial study was performed to determine the various energy transitions that could be obtained from each hydride forming element in the afterglow region. This study was deemed necessary in order to obtain the most sensitive atomic lines of each element, their accessibility above the afterglow background, and possible spectral interferences that may occur between the elements of interest. A compilation of atomic emission lines for 1 μg/mL samples of As, Sb, Bi, Ge, Pb, Se, and Sn is shown in Table 2.

Resonance as well as nonresonance emissions were obtained for each element. The ability to populate excited states above 6.1 eV (i.e., As at 199.0 nm (7.54 eV), Ge at 211.9 nm (6.52 eV)) suggests that energetic species in the APAN afterglow other than metastable $N_2(A^3\Sigma^+)$ molecules at 6.17 eV are necessary to account for these atomic transitions. Possible species and mechanisms leading to these higher energy transitions will be discussed in the next chapter.

The analytical potential of the APAN technique can be gauged with reference to the data presented in Figure 5 and Table 3. The analytical calibration curves observed for Sb (206.8 nm), Se (196.0 nm), Pb (283.3 nm), and Hg (253.7 nm) showed a linear response through a concentration range of 10^3, similar to that shown for As (193.7 nm). The analytical calibration curves for Bi (306.8 nm), Sn (326.2 nm), Te (214.3 nm), and Ge (265.1 nm) had a linear response of only 10^2. A pronounced curvature was observed in the analytical calibration curve for Bi at concentrations greater than 10 ng. Similar response ranges ($\sim 10^{2.5}$)

Table 2. Atomic emissions detected for As, Sb, Bi, Ge, Pb, Se and Sn using the APAN system

Wavelength (Å)	Energy Transition (eV)	Photocurrent (Amps)	Relative Intensity
	Arsenic (1 μg/mL)		
1937	6.40 - 0	9.2×10^{-8}	92
1972	6.28 - 0	6.5×10^{-8}	65
1990	7.54 - 1.31	7.5×10^{-9}	8
2003	7.54 - 1.35	1.0×10^{-8}	10
2288	6.77 - 1.35	1.1×10^{-7}	110
2350	6.59 - 1.31	9.9×10^{-8}	99
2493	6.28 - 1.31	1.9×10^{-9}	2
2781	6.77 - 2.31	2.9×10^{-8}	29
2860	6.59 - 2.25	3.4×10^{-8}	34
	Antimony (1 μg/mL)		
2068	5.99 - 0	7.5×10^{-8}	75
2176	5.70 - 0	8.0×10^{-8}	80
2311	5.36 - 0	3.7×10^{-8}	37
2529	6.12 - 1.22	4.5×10^{-9}	5
2598	5.83 - 1.06	2.4×10^{-8}	24
	Bismuth (1 μg/mL)		
2062	6.13 - 0	8×10^{-8}	80
2231	5.56 - 0	2.2×10^{-7}	220
2277	5.44 - 0	3.3×10^{-9}	3
2628	6.13 - 1.42	4.5×10^{-9}	5
2697	6.01 - 1.42	2.4×10^{-9}	2
2898	5.69 - 1.42	2.4×10^{-7}	240
2938	6.13 - 1.91	8.0×10^{-8}	80
2989	5.56 - 1.42	1.3×10^{-7}	130
3025	6.13 - 1.91	1.9×10^{-7}	190

Table 2. Continued

Wavelength (Å)	Energy Transition (eV)	Photocurrent (Amps)	Relative Intensity
3068	4.04 - 0	1.9×10^{-5}	19000
3596	6.13 - 2.69	4.2×10^{-8}	42
	Germanium (1 µg/mL)		
2065	6.07 - 0.07	1.6×10^{-8}	16
2199	6.52 - 0.88	3.8×10^{-9}	4
2652	4.67 - 0	2.5×10^{-8}	25
2691	4.67 - 0.07	1.6×10^{-9}	2
2709	4.64 - 0.07	5.4×10^{-9}	5
3040	4.96 - 0.88	8.1×10^{-8}	81
3270	4.67 - 0.88	3.6×10^{-9}	4
4227	4.96 - 2.03	5.1×10^{-8}	51
	Lead (1 µg/mL)		
2170	5.71 - 0	8.1×10^{-9}	8
2394	6.50 - 1.32	1.6×10^{-9}	2
2614	5.71 - 0.97	5.9×10^{-9}	6
2663	5.97 - 1.32	6.9×10^{-9}	7
2802	5.74 - 1.32	1.2×10^{-8}	12
2823	5.71 - 1.32	7.7×10^{-8}	77
2833	4.37 - 0	3.0×10^{-8}	30
2873	5.63 - 1.32	2.4×10^{-9}	2
3640	4.37 - 0.97	5.5×10^{-8}	55
3684	4.33 - 0.97	2.3×10^{-7}	270
4058	4.37 - 1.32	1.7×10^{-7}	170

Table 2. Continued

Wavelength (Å)	Energy Transition (eV)	Photocurrent (Amps)	Relative Intensity
	Selenium (1 μg/mL)		
1960	6.32 - 0	2.7×10^{-8}	27
2040	6.32 - 0.25	2.1×10^{-8}	21
2063	6.32 - 0.31	1.4×10^{-8}	14
2075	5.97 - 0	1.4×10^{-7}	140
	Tin (10 μg/mL)		
2073	5.98 - 0	3.6×10^{-9}	0.4
2210	6.03 - 0.42	9.0×10^{-9}	0.9
2246	5.52 - 0	5.4×10^{-9}	0.5
2317	6.42 - 1.07	2.3×10^{-9}	0.2
2335	5.52 - 0.21	2.6×10^{-9}	0.3
2422	6.19 - 1.07	1.0×10^{-8}	1.0
2429	5.53 - 0.42	1.1×10^{-8}	1.1
2496	6.03 - 1.07	1.9×10^{-9}	0.2
2547	4.87 - 0	1.0×10^{-8}	1.0
2661	4.87 - 0.21	5.1×10^{-9}	0.5
2707	4.79 - 0.21	2.5×10^{-8}	3.0
2840	4.79 - 0.42	1.6×10^{-7}	16
2863	4.33 - 0	6.0×10^{-8}	6.6
3009	4.33 - 0.21	4.6×10^{-8}	5.0
3034	4.29 - 0.21	$5.8 - 10^{-8}$	6
3175	4.33 - 0.42	1.5×10^{-7}	15
3262	4.87 - 1.07	3.7×10^{-7}	37

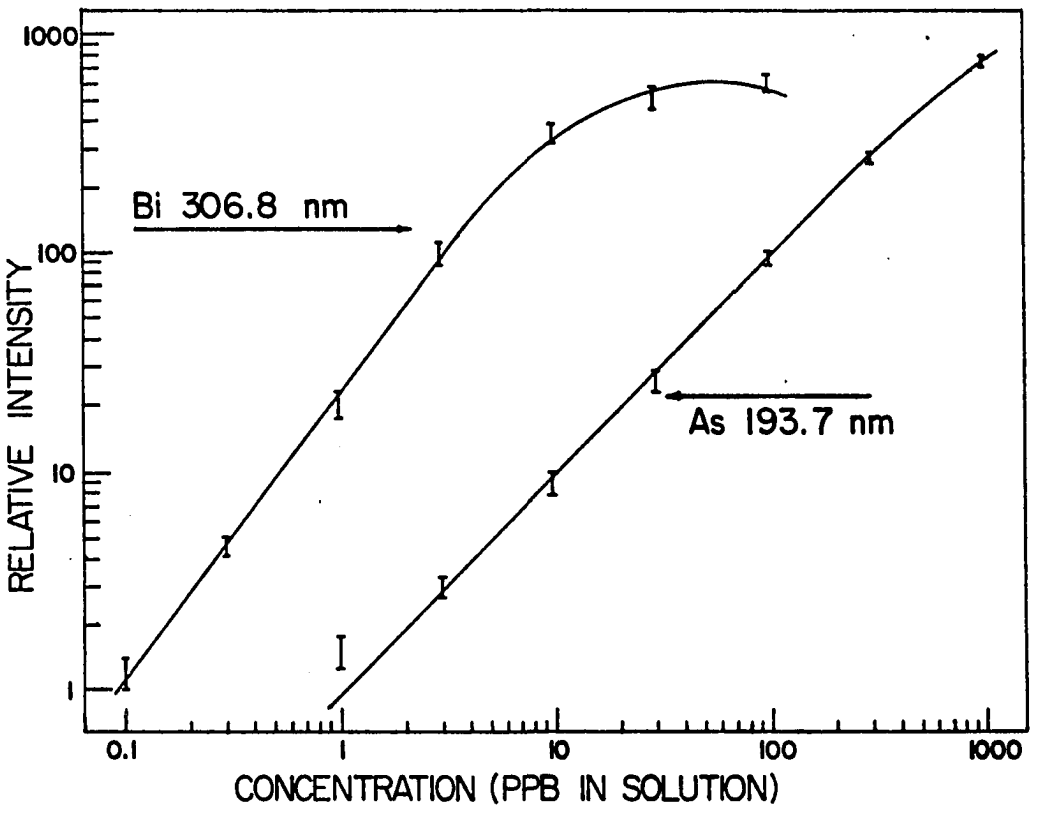

Figure 5. Analytical calibration curves for As and Bi

Table 3. Comparison of detection limits (ng)[a] for spectrometric techniques utilizing hydride generation

Element	ICP-AES[b]	AAS[c]	AFS[d]	MP[e]	DCD[f]	APAN
As	2.5	0.8	0.1	7	1	0.2
Bi	2.5	0.2	-	-	-	< 0.1[g]
Ge	-	50	-	3	9[h]	20
Hg[i]	-	0.3	2[k]	0.01[ℓ]	0.4[m]	< 0.02[g]
Pb	-	100	-	-	-	5
Sb	3	0.5	0.1	10	0.5	1
Se	2.5	1.8	0.06	25	-	5
Sn	-	0.5	-	40	-	20
Te	3	1.5	0.08	-	-	50

[a]Calculated on the basis of a 1-mL sample volume.

[b]Inductively coupled plasma-atomic emission spectroscopy, Ref. 44.

[c]Atomic absorption spectroscopy, Refs. 45 and 46.

[d]Atomic fluorescence spectroscopy, Ref. 47.

[e]Microwave plasma, Ref. 48.

[f]dc discharge, Ref. 49.

[g]Limited by reagent blank.

[h]Ref. 50.

[i]Reduced to the free metal.

[j]Ref. 51.

[k]Ref. 52.

[ℓ]Ref. 53.

[m]Ref. 54.

have been observed in the determination of Be at 306.8 nm and Te at 238.6 nm by ICP-AES via the hydride generation technique (44).

Table 3 shows a comparison of limits of detection (in nanograms) reported for several atomic absorption, emission, and fluorescence techniques that have used the hydride generation technique. All the data in this table are calculated on the basis of a 1 mL sample volume. As seen from Table 3, the APAN technique provides limits of detection similar to values measured by other conventional atomic spectroscopic techniques based on hydride generation.

The reproducibility obtained from 10 successive 1.0 mL aliquots containing 10 ng As/mL is illustrated in Figure 6. A relative standard deviation from the mean of 4.9% was calculated from measured peak heights. The reproducibility of other elements at various concentration levels was observed to be less than 10% in relative deviation. Signal fluctuations are thought to be the result of several factors. These include, in order of decreasing significance, errors in measuring and introducing the 1.0 mL aliquot, variations in the rate of hydride formation, and fluctuations in the active nitrogen population.

The ability to measure the relative intensities of the atomic emissions as peak heights is accounted for by the rapid evolution of the hydrides. Figure 7 illustrated the evolution patterns observed for Se, Te, Sb, Bi, As, and Ge.

To enhance detection sensitivity, several investigators in the past have used collection (i.e., balloon) or condensation systems to trap the

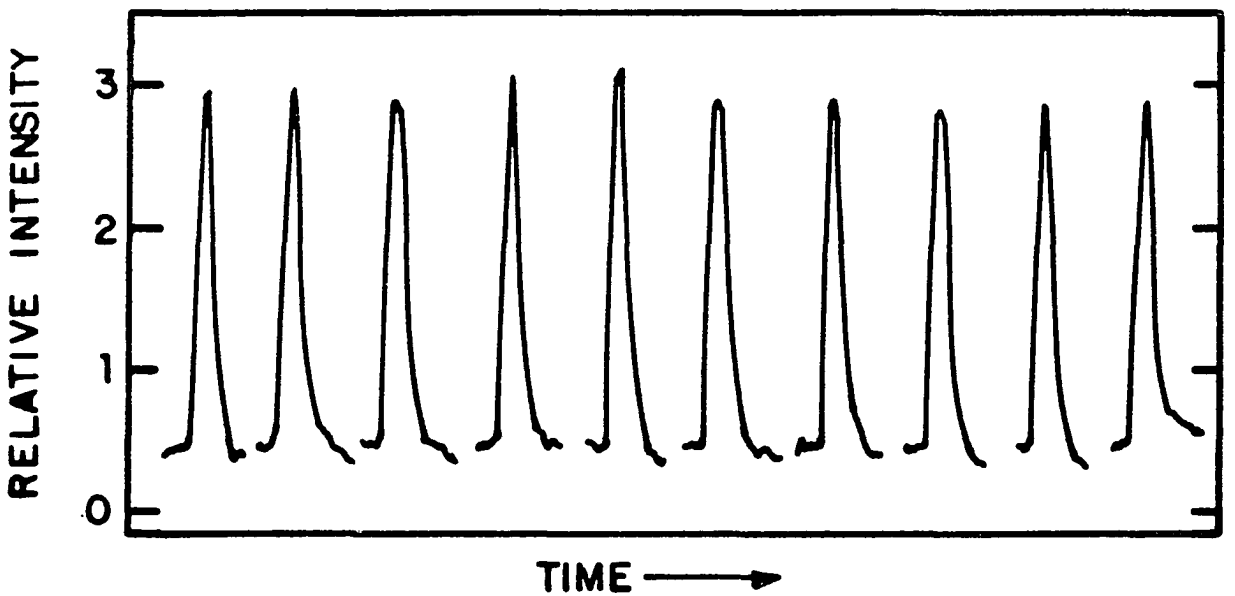

Figure 6. Reproducibility obtained from ten successive hydride generations of 10 ng/mL As reference solutions

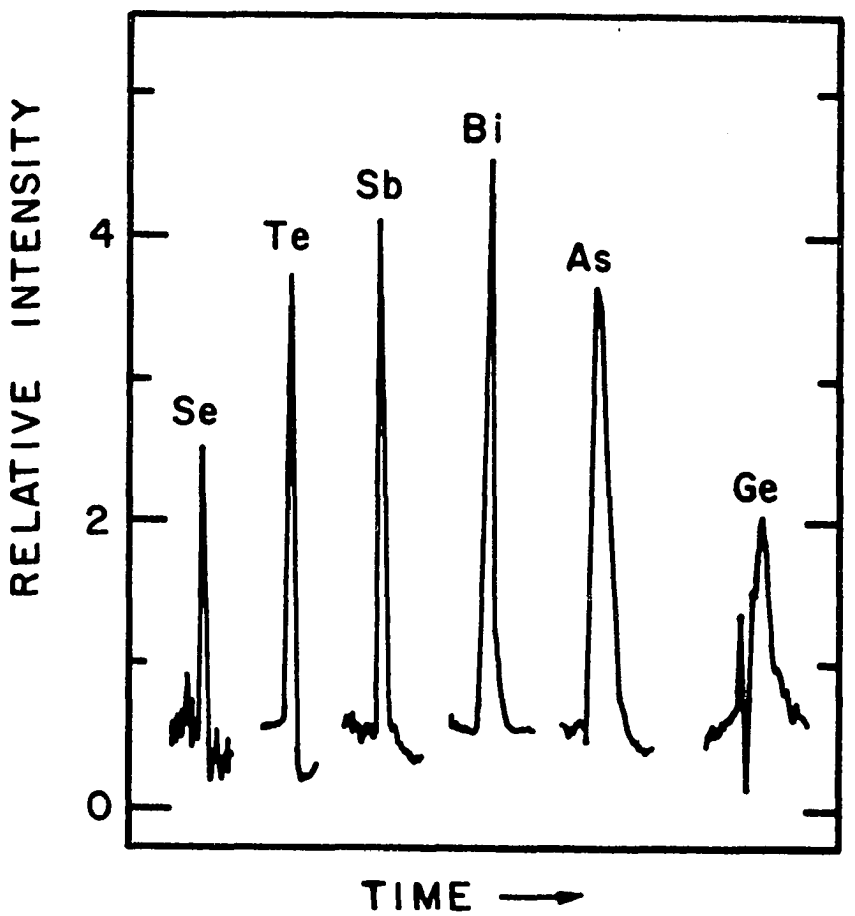

Figure 7. Comparison of peak shapes from hydride generation of Se, Te, Sb, Bi, As, and Ge

liberated hydrides prior to their introduction into the analytical system. These approaches were not used in this investigation. In contrast, the evolved hydrides, or Hg, and molecular hydrogen generated in the reaction were introduced directly into the APAN afterglow without any prior separation or condensation. The quenching effects of the hydrogen often observed when the mixtures are introduced into other plasmas were not evident in the afterglow. Although the green emission from atomic oxygen was quenched immediately above the sample inlet upon passage of the sample carrier gas, the atomic emissions appeared to be unaffected when the hydrides or Hg were directly introduced into the afterglow region. The atomic emissions from analyte species were quenched if the O_2 concentration increased in the liquid N_2 boiloff that maintained the discharge. As noted earlier, the O_2 content of the N_2 boiloff was less than 10 ppm, and no attempt was made to reduce the level further.

The determination of hydride-forming elements in a number of complex samples; i.e., steel, food, biological matrices, has been performed using hydride generation technique combined with atomic absorption or atomic fluorescence detection (50,55,56). A preliminary evaluation of the analytical potential of the APAN system was performed by determining As in several NBS standard reference materials of interest in environmental studies.

Samples were prepared by the sodium fusion technique, the resulting melt being dissolved and diluted to 100 mL with 40 mL of concentrated HCl and the remainder with deionized water. Initially, the arsenic

concentration was determined by forming the hydride from a 1.0 mL sample aliquot and comparing the resulting peak height to an analytical calibration curve produced by standards prepared from the sodium fusion blanks. Results indicated the recovered As, as compared to the NBS values, was significantly lower and varied on all three samples.

The addition to the sample, prior to generation of the hydride, of 0.3 M EDTA (pH ≈ 9) as a masking agent (57) or 10% KI as a reductant for As (V) to As (III) (56) had insignificant affects on the As recoveries. It should be noted, however, that investigators who have used EDTA or KI effectively have incorporated semi-automated mixing techniques for hydride generation. This technique involves the use of multistage pumping of the reagents and sample into glass mixing coils. The reacted solution and gaseous hydrides formed are then separated in a gas-liquid separator and the hydrides swept into the analytical system for measurement. The utilization of such a system has been found to be virtually free of all interferences in the reacting solutions and gives excellent detection limits for a number of hydride forming species.

Although direct determination of arsenic as previously discussed was not successful, close agreement to the NBS values was obtained by using the methods of additions. A comparison of the data obtained on duplicate samples with those certified by NBS is shown in Table 4.

Although the APAN afterglow has proven to be a useful excitation source for detecting trace levels of a number of environmentally important elements, there are several disadvantages which should be disclosed.

Table 4. Determination of As (μg/g) in NBS reference materials

Sample	APAN	NBS
Coal No. 1632	5.4 ± 0.3	5.9 ± 0.6[a]
Fly ash No. 1633	63 ± 4.0	61 ± 6.0[a]
River sediment No. 1645	65 ± 1.0	66[b]

[a]Certified value.

[b]Information value.

The wide spectral bandpass ($\sim$ 1.4 nm) used for the analytical results obtained may prove to be a disadvantage when attempting to determine several hydride forming elements present in a complex matrix. Compromises between sensitivity and spectral resolution may be necessary to guarantee freedom from spectral interferences. The background from afterglow emissions also limits the sensitivity of the APAN system for several of the elements. The background encountered at optimum emission wavelengths in the region above 200 nm is ten to one hundred-fold higher than the background below 200 nm. Sensitivity is thus severely limited by the amplifier gain necessary to observe changes from emission signals produced. The analytical wavelengths used in this investigation were, however, well resolved from the NOγ and NOβ background in the afterglow, as illustrated in Figure 8. Finally, the afterglow is limited to the introduction of dry vaporized samples. The presence of water vapors extinguishes the afterglow. Expansion of the technique to a number of other elements is thus limited to thermal atomization of aqueous samples to remove water from the system (i.e., graphite furnace).

Spectral Observations and Analytical Evaluation of B, P, S, Cl, Br, and I in the APAN Afterglow

Introduction

The determination of trace levels of many of the nonmetallic elements is becoming increasingly important in industrial, agricultural, and environmental analysis.

Low pressure (< 10 torr), active-nitrogen afterglows have been extensively utilized in the past for qualitative studies of the reactions of

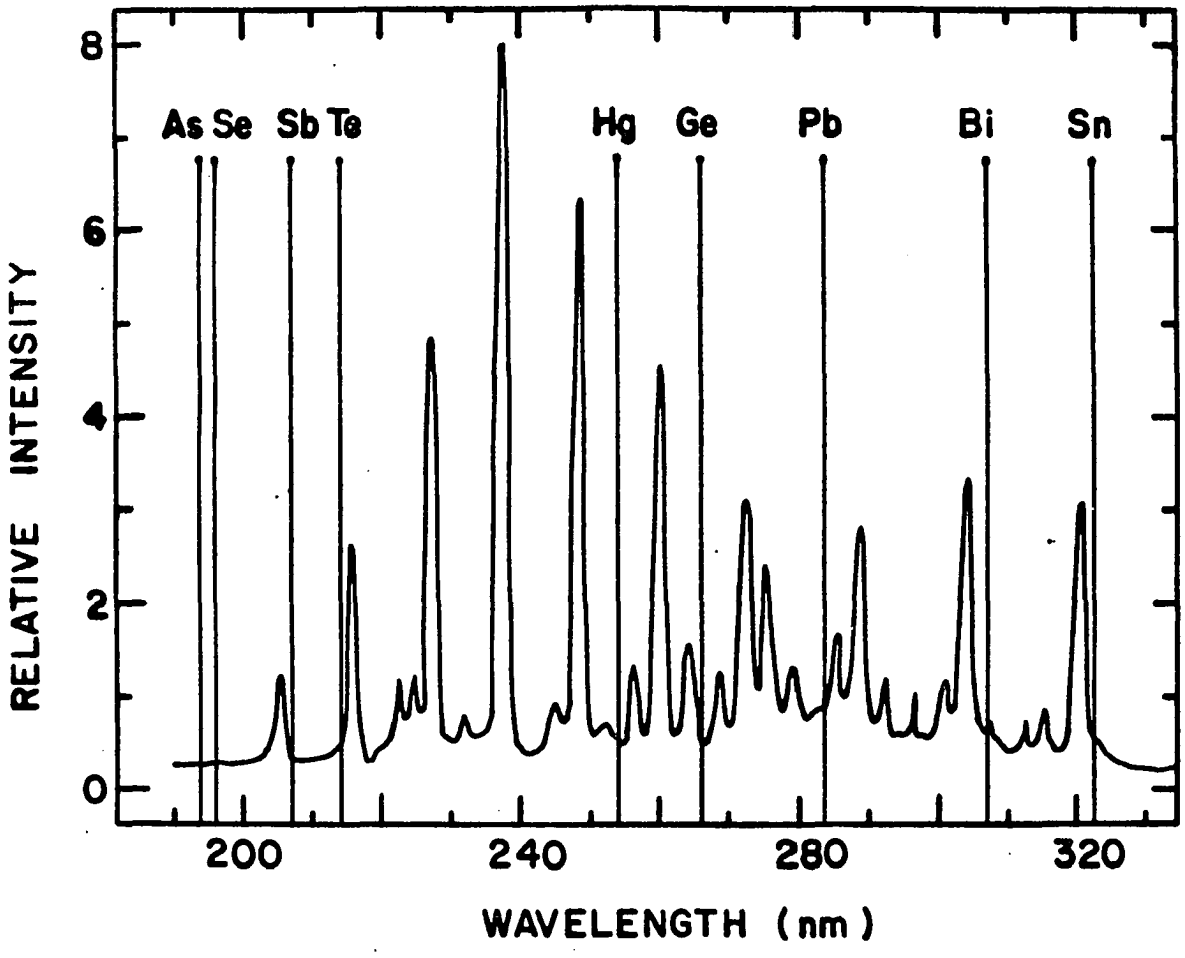

Figure 8. Position of analytical wavelengths used for the detection of hydride forming elements and Hg in relation to the NO background observed in the afterglow

metastable nitrogen atoms and molecules with B, S, P, Cl, Br, and I (9). The results to be given reveal for the first time that these elements also give characteristic atomic and/or molecular emission in an APAN afterglow.

Apparatus and procedures

The APAN discharge tube, instrumentation, and operating conditions were described in the previous section of this chapter.

For spectral observations in the 180 nm to 500 nm wavelength region, a 1/3-meter McPherson monochromator was fitted with a 1200 lines/mm grating blazed at 300 nm. An EMI 6256 photomultiplier tube was used as the detector. The monochromator and optical region of the detection system was flushed with argon for obtaining spectra down to 180 nm. For observations in the 500 nm to 900 nm region, a 1200 lines/mm grating blazed at 700 nm was used in conjunction with an extended S-20 response PMT.

For Br and I, A.C.S. grade Br_2 and I_2 were used without further purification. For B, a lecture gas bottle containing BCl_3 (99.9% min. purity) was used. For S, P, and Cl, certified gas standards were obtained containing 100 ppm H_2S, COS, and SO_2, 50 and 1000 ppm PH_3, and 0.092% Cl_2, respectively (Matheson, Lyndhurst, N.J. 07071). All gas mixtures were prepared in a balance of nitrogen.

All gases were introduced through the sample inlet located in the afterglow region of the discharge tube. Bromine and iodine were introduced into the afterglow as vapors in a nitrogen carrier gas produced from the sealed hydride generator cell previously described. Boron

trichloride was fed directly into the discharge tube from the gas cylinder at a rate of < 1 cm^3/min. All gas mixtures were regulated through a flow meter prior to introduction into the APAN afterglow. Spectral observations from each element were recorded from 180-900 nm.

For analytical studies, the gas mixtures were diluted with N_2 through a mixing tee. Both gas flow rates were monitored through separate flow meters so that the amount of analyte per second introduced into the afterglow could be calculated. The combined gas flows into the afterglow were maintained at 10 cm^3/s. All analyte wavelengths were selected from spectral data obtained for each compound in the APAN afterglow.

The feasibility of determining halogen concentrations in aqueous solutions was also evaluated by generating Cl_2, Br_2, and I_2 from acidified, standard solutions of Cl^-, Br^-, and I^- by addition of 30% H_2O_2.

Results and discussion

The introduction of BCl_3 transformed the afterglow from its characteristic green to a brilliant blue color from the molecular electronic transitions of $BO[A^2\pi \rightarrow X^2\Sigma^+]$, whose spectrum is shown in Figure 9. No atomic B emission or molecular emission from BN were observed, although these transitions may be concealed by the afterglow background and intense BO emissions. The formation of BO is undoubtedly due to the O_2 impurity present in the N_2 discharge gas flow, although why BO is formed in preference to BN is not known at this time.

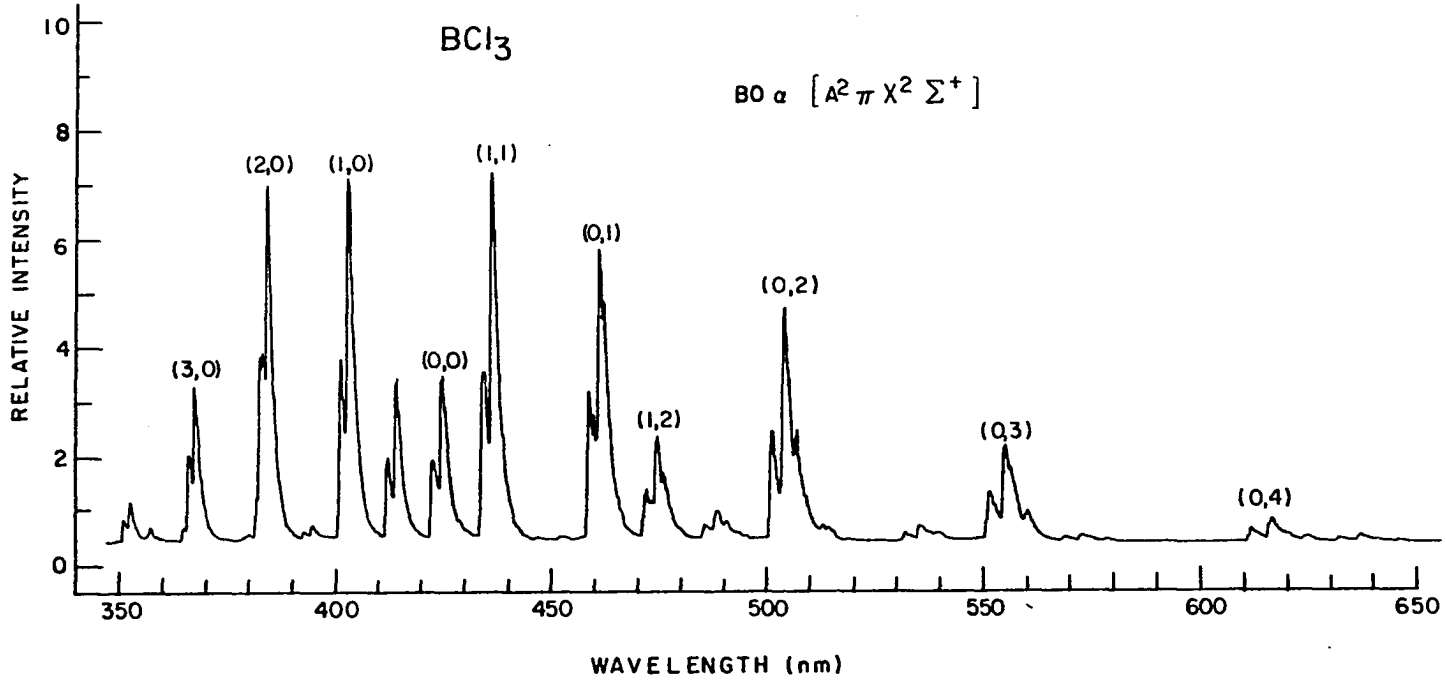

Figure 9. Spectrum of BO [$A^2\pi \rightarrow X^2\Sigma^+$] obtained from BCl_3 when introduced into the afterglow. Bandpass = 0.3 nm

The introduction of 100 ppm H_2S, COS, or SO_2 into the afterglow caused a transformation from green to a deep blue due to the formation of S_2 [$B^3\Sigma_\mu^- \rightarrow X^3\Sigma_g^-$], whose spectrum is shown in Figure 10. The blue afterglow created by S_2 emissions was observed to extend throughout the length of the afterglow tube and was still readily produced 0.5 m above the point of introduction. No atomic sulfur emissions as well as molecular emissions from the formation of NS were observed, although, once again, emission from NS may have been concealed by the NO background and S_2 emissions.

The passage of either 50 ppm or 1000 ppm PH_3 into the afterglow resulted in only weak emissions from the formation of PN [$A^1\pi \rightarrow X^1\Sigma^+$] as shown in Figure 11. No atomic emission or formation of emitting PO species were observed.

Introduction of Cl_2 into the afterglow produced a faint red emission resulting from the formation of NCl [$b^1\Sigma^+ \rightarrow X^3\Sigma^-$]. The spectrum of NCl is shown in Figure 12. No Cl_2 emissions were observed.

Introduction of Br_2 into the afterglow produced brilliant orange-red emissions. These emissions resulted from the production of NBr [$b^1\Sigma^+ \rightarrow X^3\Sigma^-$] and Br_2 [$^3\pi_{1u} \rightarrow X^1\Sigma_g^+$], the spectrum of which is shown in Figure 13. The most intense emission was found to result from Br_2 at 674.2 nm.

Both molecular and atomic emission were observed when I_2 was introduced into the afterglow as shown in Figure 14. The molecular emission was the result of the I_2 [$D\text{-}B^3\pi_{o+u}$] transition. No emission was observed which would indicate the formation of NI.

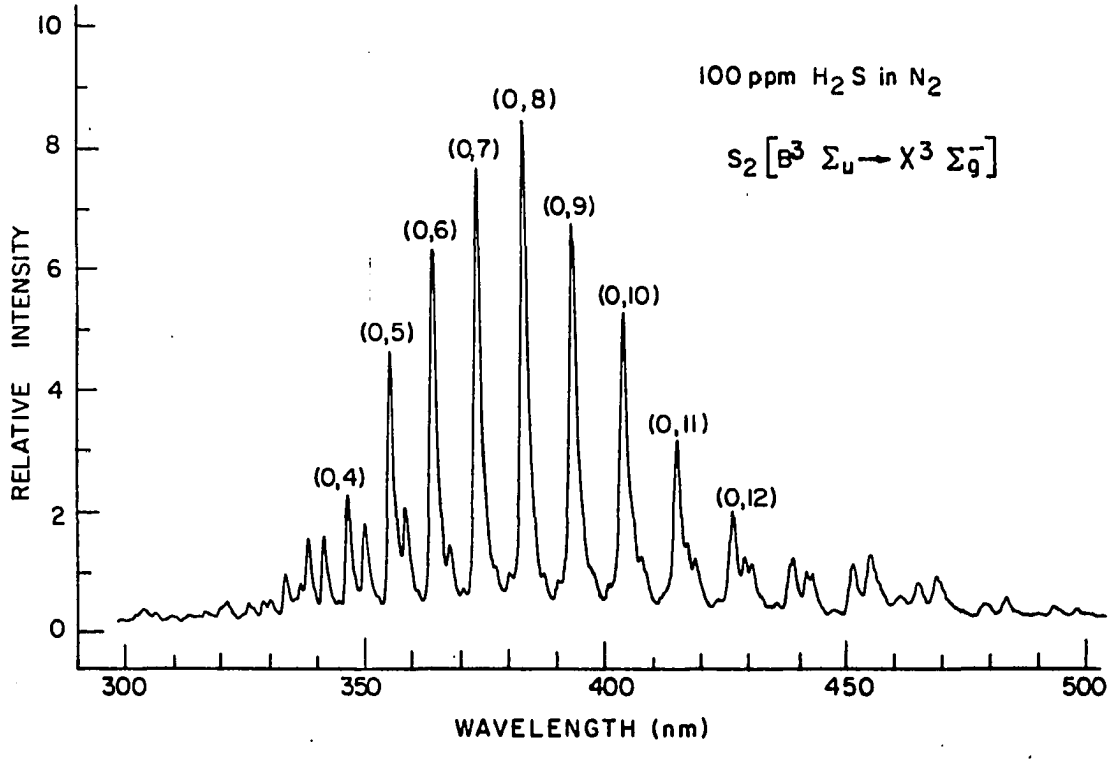

Figure 10. Spectrum of S_2 $[B^3\Sigma_u^- \rightarrow X^3\Sigma_g^-]$ obtained from 100 ppm H_2S when introduced into the afterglow. Bandpass = 0.3 nm

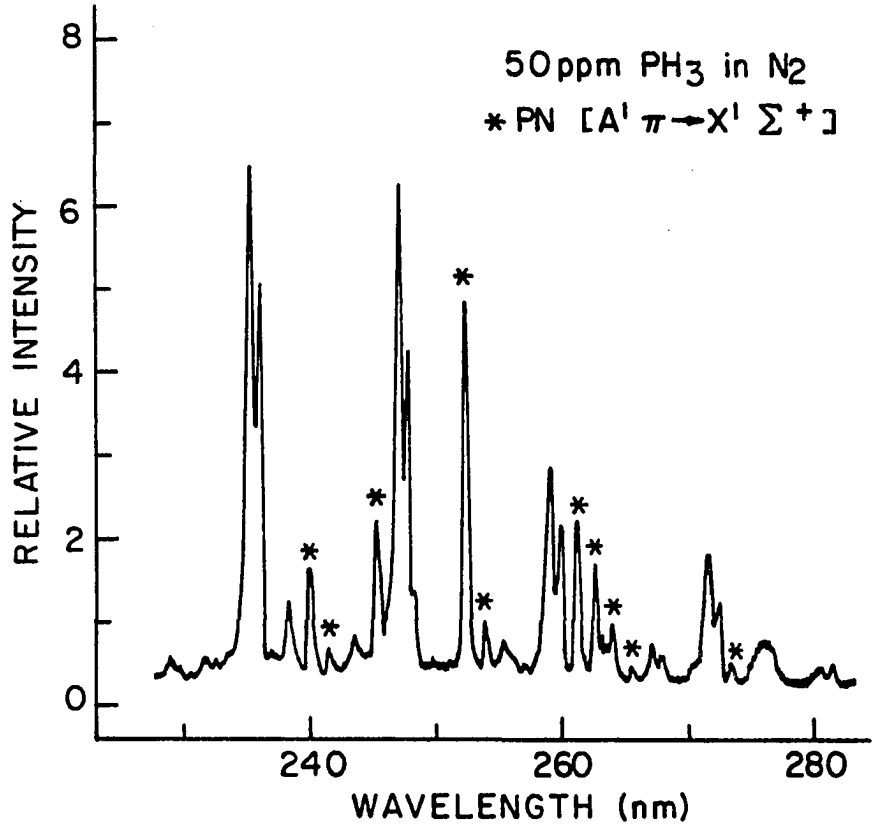

Figure 11. Spectrum of PN [$A^1\pi \rightarrow X^1\Sigma^+$] obtained from 50 ppm PH_3 when introduced into the afterglow. Bandpass = 0.3 nm

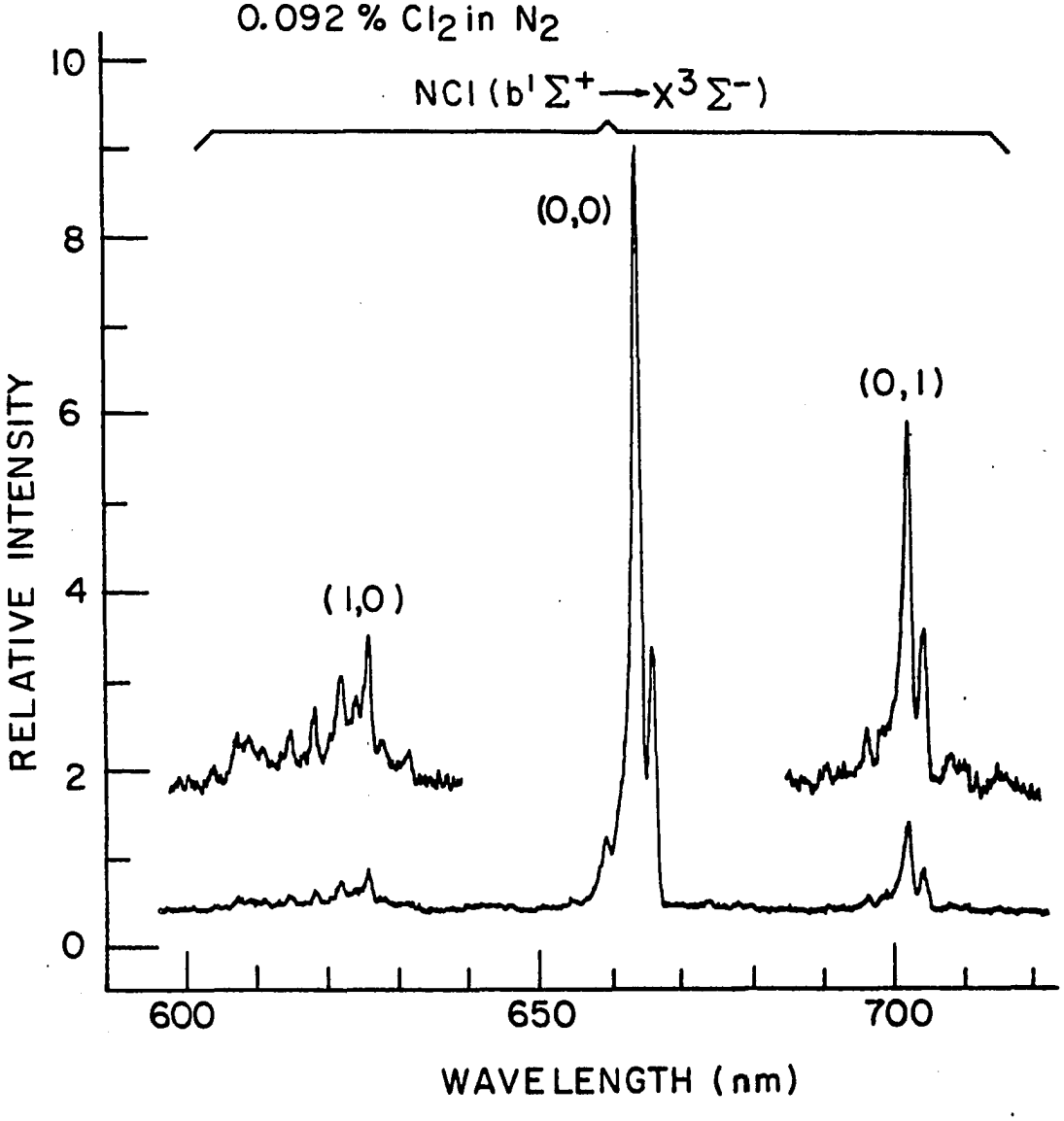

Figure 12. Spectrum of NCl [$b^1\Sigma^+ \rightarrow X^3\Sigma^-$] obtained from 0.092% Cl_2 when introduced into the afterglow. Bandpass = 0.7 nm

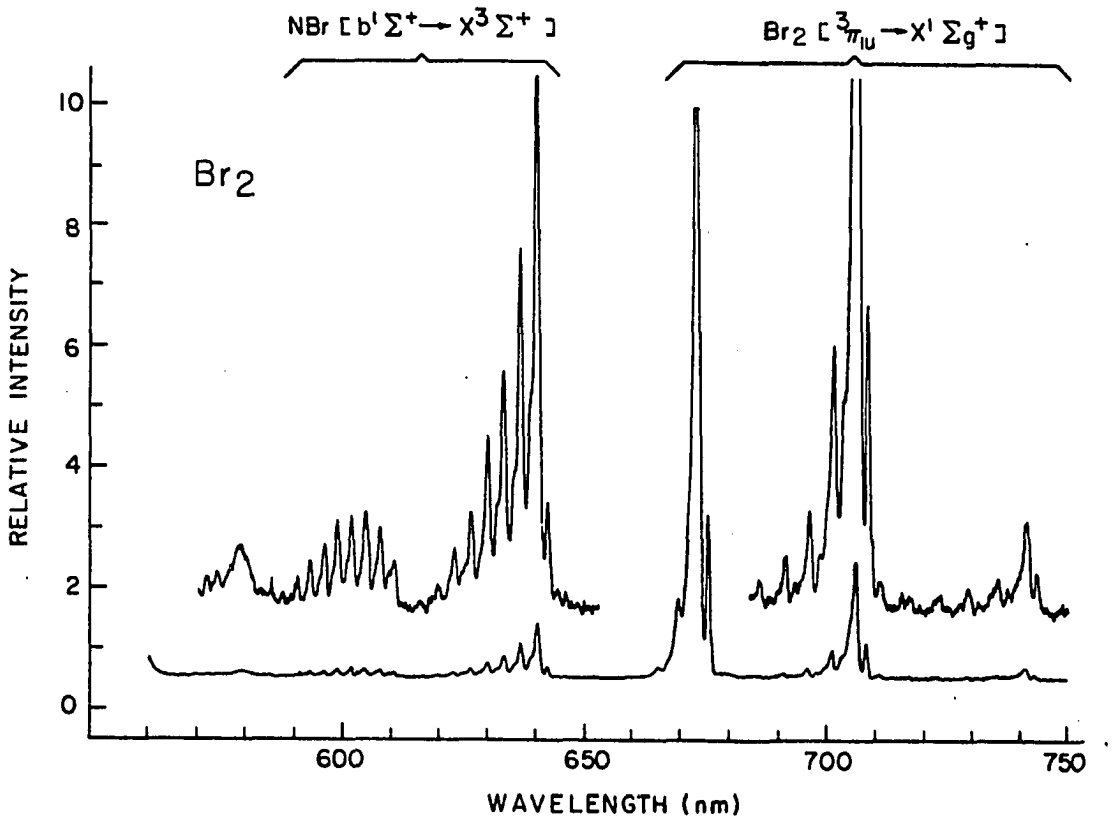

Figure 13. Spectrum of NBr [$b^1\Sigma^+ \rightarrow X^3\Sigma^-$] and Br_2 [$^3\pi_{1u} \rightarrow X^1\Sigma_g^+$] obtained from Br_2 when introduced into the afterglow. Bandpass = 0.7 nm

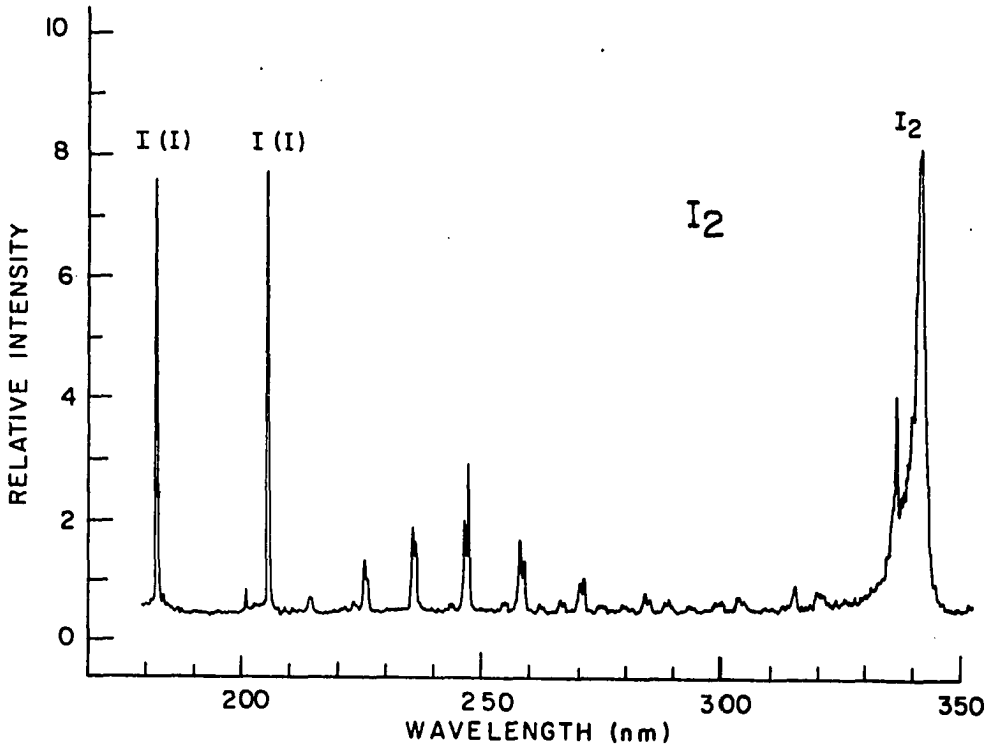

Figure 14. Spectrum obtained from I_2 when introduced into the afterglow. Bandpass = 0.3 nm

A summary of the spectral transitions observed for each element is given in Table 5. The possible mechanisms through which the formation of these species may occur will be discussed in the following chapter.

The analytical potential of detecting Cl^-, Br^-, and I^- in solution by evolution of Cl_2, Br_2, and I_2 was first evaluated. Emissions were monitored at 664.8 nm for the 0-0 NCl transition, 674.2 nm for the 2-0 Br_2 transition, and 183.0 nm for the atomic I line.

The solubility of Cl_2 (14.6 g/l) and Br_2 (41.7 g/l) in water thwarted efforts in obtaining analytical data from these species. The aeration time necessary for removing Cl_2 and Br_2 from solutions was found to be on the order of 20 minutes or more. No solution to this problem has been found thus far.

The time necessary to completely evolve I_2 from the reaction cell was less than one minute, giving the peaks shown in Figure 15 at 100 ppb, 1 ppm, and 10 ppm I^- concentrations. The concentration to peak height ratio was found to be constant up to 100 ppm. A smaller dead volume and more efficient aeration system may improve detection limits. The primary drawback is that the halogen species present must first be reduced to the -1 oxidation state, from which the diatomic molecules can be formed by appropriate oxidation reactions.

An analytical calibration curve was obtained from the introduction of the Cl_2 gas mixture into the afterglow, as shown in Figure 16. A linear response over a concentration range of approximately 1.5 orders of magnitude was obtained, with a detection limit of 50 ng/s.

Table 5. Summary of observed transitions in the APAN afterglow from Cl, Br, I, S, P, and B

Element	Compound Studied	Emissive Species Observed	Transition	Wavelength Region (nm)
Cl	Cl_2	NCl	$b^1\Sigma^+ \rightarrow X^3\Sigma^-$	600 - 710
Br	Br_2	NBr	$b^1\Sigma^+ \rightarrow X^3\Sigma^-$	590 - 645
		Br_2	$^3\pi_{iu} \rightarrow X^1\Sigma_g^+$	660 - 750
I	I_2	I(I)	---	183.0, 206.2
		I_2	$D \rightarrow B^3\pi_{o+u}$	330 - 345
S	H_2S, COS, SO_2	S_2	$B^3\Sigma_u^- \rightarrow X^3\Sigma_g$	330 - 550
P	PH_3	PN	$A^1\pi \rightarrow X^1\Sigma^+$	240 - 275
B	BCl_3	BO	$A^2\pi \rightarrow X^2\Sigma^+$	350 - 650

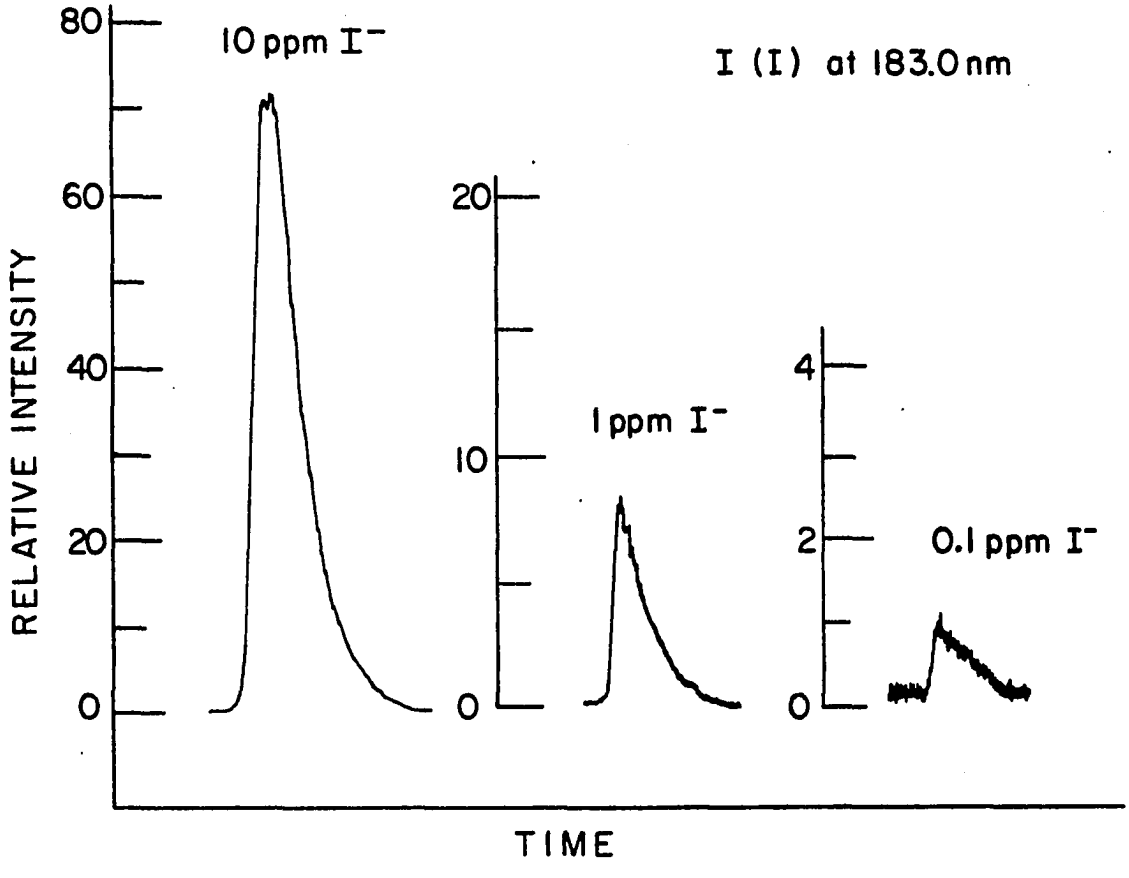

Figure 15. Concentration dependence on I(I) emission at 183.0 nm from evolution of I_2 by oxidation of I^- reference solutions

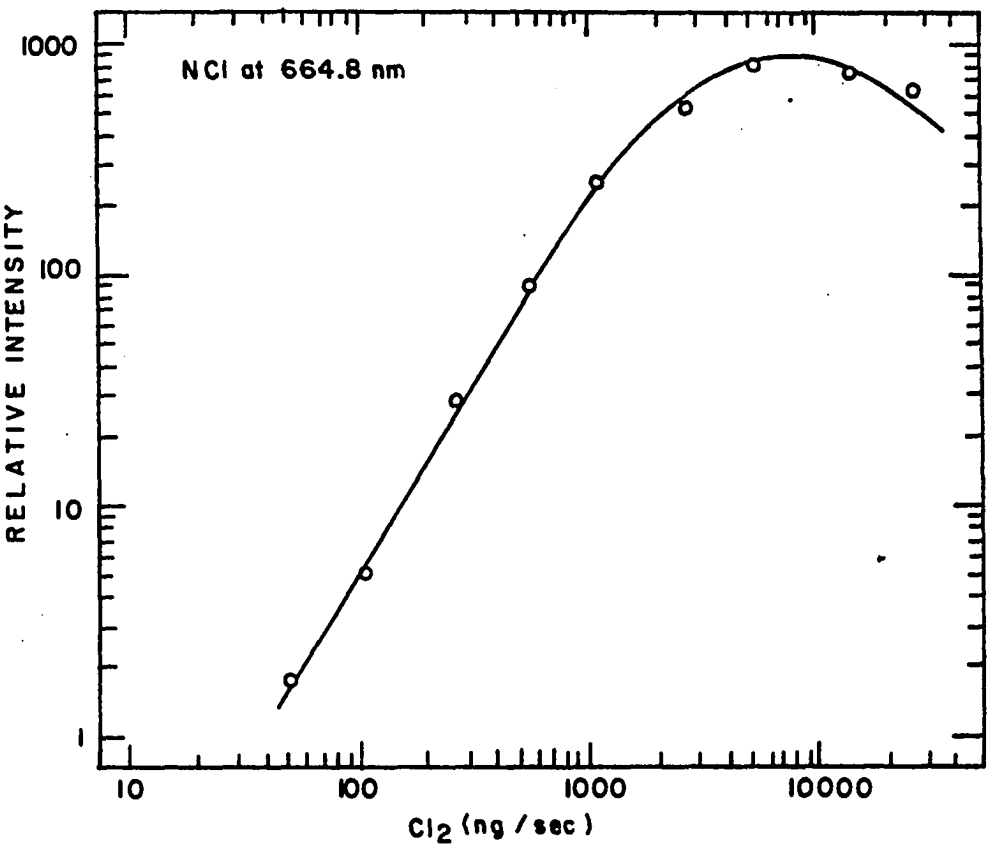

Figure 16. Analytical calibration curve obtained from Cl_2 by detection of NCl emission at 664.8 nm

A secondary method for evaluating the sensitivity for Br was performed by injecting standards of $CHBr_3$ onto the column of a gas chromatograph in order to vaporize the samples prior to introduction into the APAN afterglow. A detection limit of 5 ng Br/sec was obtained by monitoring Br_2 emission at 764.2 nm.

The introduction of either 50 ppm or 1000 ppm PH_3 in a nitrogen gas mixture into the afterglow exhibited no concentration dependence on the intensity of the PN emissions observed. Both concentrations gave PN emissions with no significant difference in intensity. The reasons for this observation are unknown at this time; however, it is reasonable to conclude that the utilization of PN emissions for selective detection of phosphorous compounds appears very remote at this time.

Analytical calibration curves obtained from H_2S, COS, and SO_2 are shown in Figure 17. The amount of each compound was plotted in terms of the sulfur content. Changes in emission intensity were monitored as a function of the amount of compound entering the afterglow per second as detected from the S_2 (0-8) emission band at 374.0 nm. All three compounds exhibited linear response to concentration changes of two to three orders in magnitude. Detection limits of 5 ng/sec were obtained from H_2S.

The slope of approximately 1.8 obtained from the analytical calibration curves for H_2S and COS appears to be similar to results obtained using flame photometric detectors (FPD) for gas chromatography. The response of the FPD to S_2 intensity is related to the S concentration by the

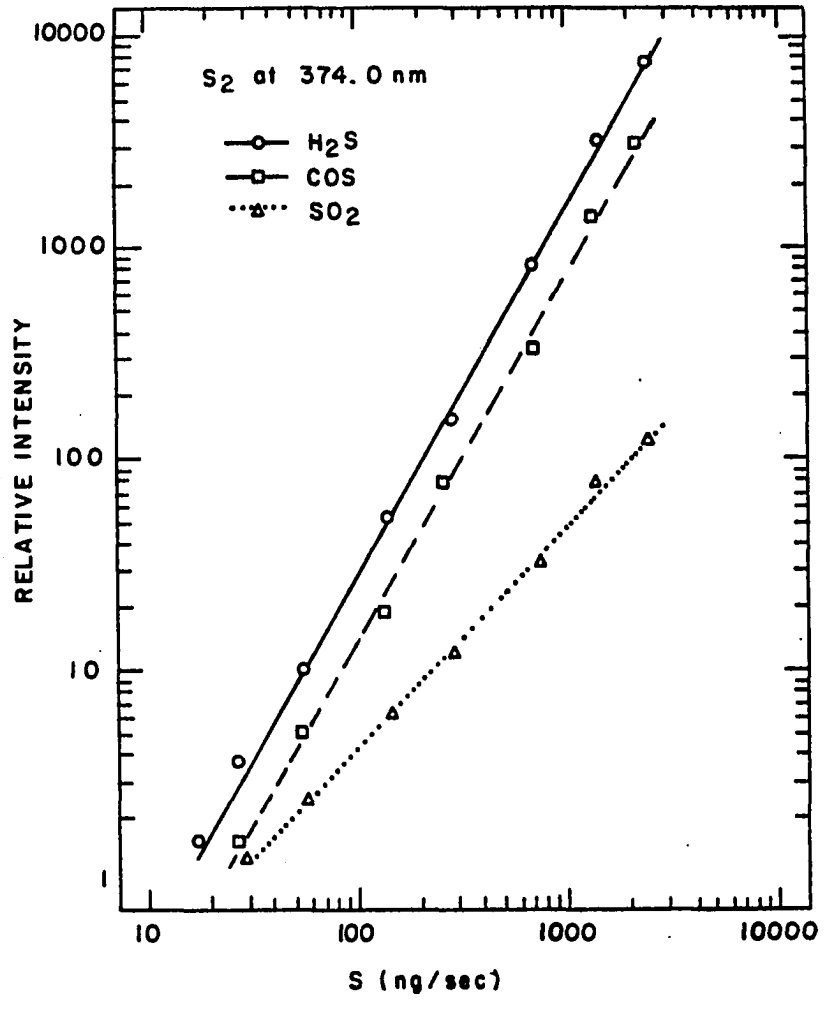

Figure 17. Analytical calibration curves obtained from H_2S, COS, and SO_2 from S_2 emissions at 374.0 nm

relation,

$$I_{S_2} = C[S]^n$$

where I is the intensity of the S_2 emission, and C and n are constants dependent on the experimental conditions used (58). Theoretically, n = 2, however, the slope has been found to range from one to two, a factor dependent on the experimental conditions; i.e., observation height, flame temperature and composition, and the types of sulfur compounds used. Little S_2 emission has been observed from compounds containing C = S and S = O bonds, a factor believed to be due to inefficient decomposition in the low flame temperatures used. The same reasoning may possibly be applied to the decreased slope and sensitivity observed for SO_2 in the APAN afterglow, in which there may be insufficient energy available for complete dissociation of the SO_2 molecule. The nonideal slopes observed may also be due to other interactions in the afterglow, including radiationless deactivation on the wall surfaces of the discharge tube or further reaction of the S_2 with active species in the afterglow.

A summary of the analytical data obtained thusfar for Cl, Br, I, and S using the APAN excitation source is given in Table 6. These data indicate that the APAN afterglow could be a useful detector for trace levels of Cl, Br, I, and S species from detection of molecular or atomic species generated in the afterglow. Improvements in the detection limits may be possible by using narrow bandpass filters to isolate the analyte wavelength. The intense BO emission observed from BCl_3 also

Table 6. Analytical data obtained from Cl, Br, I, and S

Element	Compound	Emissive Species Observed	Analytical Wavelength (nm)	Detection Limits (ng/s)	Linear Range
Cl	Cl_2	NCl	664.6	50	$10^{2.5}$
Br	$CHBr_3$	Br_2	674.2	5[a]	-[b]
I	I_2	I(I)	183.0	10[c]	10^3
S	H_2S	S_2	374.0	5	10^3

[a]Determined by gas chromatographic vaporization of sample into the APAN afterglow.

[b]Not evaluated.

[c]Determined by evolution of I_2 from acidified I^- solutions.

indicates that the APAN afterglow may be an excellent detector for trace levels of boron.

Utilization of the APAN Afterglow as a Detector for Gas Chromatography

Introduction

Although the determination of the concentration of a given element in complex samples has become a routine procedure in analytical laboratories today, the identification of the particular chemical forms which occur still remains a challenge to the analytical chemist. More emphasis is especially being placed on determining organometallic species present in environmental samples, a factor magnified by the discovery of a number of organometallic species being biosynthesized in the environment (59) as well as man-made organometallic pollutants (60). Thus, the development of sensitive analytical systems for the determination of various organometallic species present in a sample is warranted in order to understand how these species are produced and to what extent they may exist in our environment.

The ability to separate organic and organometallic compounds by gas chromatography (GC) is an established technique for which no discussion is necessary at this time. However, the detectors used for organometallic applications and their merits or drawbacks do deserve recognition. Normally the flame ionization detector (FID) is used for the detection of organometallic species unless the compound of interest contains electron absorbing species (i.e., halides) for which an electron capture detector (ECD) is commonly used.

The FID offers the greatest linear range (10^6-10^7) of any GC detector. The primary limitations of the FID can be summarized as follows: 1) limited sensitivity (usually 0.1-10 ng, dependent on the compound of interest); 2) poor selectivity (practically all compounds eluted from the GC will be detected if at sufficient levels); and 3) the solvent must be selected so that compounds do not elute in the solvent front.

Although the ECD has proven to give superior detection limits (0.1-10 pg) in many GC applications, its disadvantages are still numerous: 1) only compounds of highly polar or electron absorbing character will be detected, thus selectivity may be a disadvantage in organometallic studies (i.e., although the ECD is capable of detecting CH_3HgCl at pg levels, sensitivity to diorganomercury compounds is poor (> ng); 2) solvent selection is critical (highly polar solvents as well as halogen containing solvents; i.e., methylene chloride must be avoided); and 3) the detectors have been found to be readily fouled by contaminants and organometallic species, thus frequent detector cleaning is usually a necessity.

Gas chromatography, coupled with element selective detectors, is widely utilized in speciation studies of environmental pollutants, a subject of substantial current interest. In such studies an extended list of detection systems have been investigated to enhance the limits of detection.

A class of such detectors is the microwave induced plasma (MIP) operated at low or atmospheric pressure with He or Ar as the plasma gas

(61-64). Of the MIP detectors, the atmospheric pressure MIP in He, operated in a Beenakker type TM_{010} cylindrical resonant cavity is potentially the most versatile element selective detector (65). Unfortunately, the MIP detectors described to date have several operational limitations. The injection of relatively small amounts (μL) of species into the plasma gas, such as a solvent plug from a GC or excessive hydrogen from dissociated hydrocarbons, can decouple the resonant cavity, resulting in total quenching of the discharge. Such a limitation has been circumvented by adopting one or more experimental manipulations. They are: 1) initiation of the discharge after the solvent peak elutes out of the resonant cavity, 2) selection of a solvent that elutes at the tail of the sample elution sequence, or 3) utilization of elaborate gas switching instrumentation and routines to control the flow of GC columns for reduced sample volumes. A limitation of MIP sources operated at reduced pressure is the buildup of carbonaceous deposits on the walls of the discharge with effluents containing carbon. Such deposits have to be periodically burnt off <u>in situ</u>, by operating the discharge in a mixture of He with O_2 or N_2 (3). To minimize the above limitations, alternate element specific detectors, such as the direct current atmospheric pressure argon plasma (66,67), and inductively coupled plasma (68,69) have also been evaluated.

A chemiluminescence detector, based on the reaction of organic compounds with active nitrogen (AN) sustained at low pressure (20-30 torr) to form excited CN ($B^2\Sigma^+$) molecules, has been recently reported (37,38).

The low pressure AN source, however, is susceptible to a build up of polymeric deposits containing CN and thus requires periodic cleaning similar in nature to the MIP. The addition of HCl gas is also required to enhance the sensitivity for simple saturated hydrocarbon compounds. Finally, the fact that the "chemiluminescent" detector operates at low pressure whereas the GC operates at atmospheric pressure may also introduce some inconvenience in sample introduction.

Thus, the merits of using the APAN afterglow as a GC detector were evaluated with the purpose of eliminating some of the problems previously discussed for other emission selective detectors.

Apparatus and procedures

A conventional GC (Hewlett-Packard, Model 5700A) was modified by cutting a 3 cm diameter hole through the side of the oven wall to accommodate the transfer line from the GC column to the APAN discharge tube. The interface constructed for the transfer line is shown in Figure 18. The glass capillary transfer line minimized peak broadening from dead volume between the GC column and the discharge tube. Copper tubing wrapped with nichrome wire was used to produce uniform heating around the transfer line. A variable temperature control (Omega Engineering, Inc., Stamford, Connecticut) was used to maintain the desired interface temperature.

Details of the operational characteristics of the APAN discharge, spectrometric system used, analytical wavelengths observed,and GC parameters and columns chosen for the investigations are summarized in Table 7.

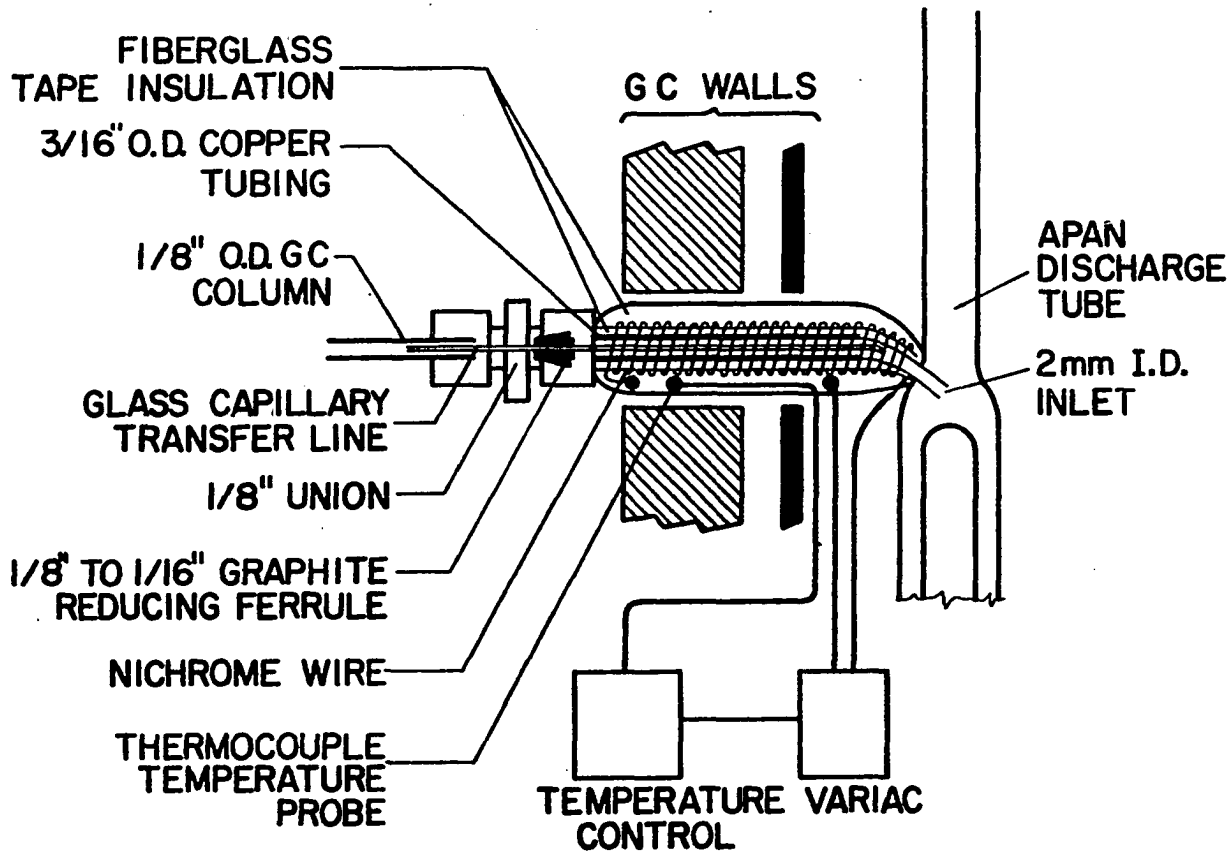

Figure 18. Schematic diagram of the interface between the GC and the APAN afterglow tube

Table 7. Operating conditions of the GC-APAN system

(A)	APAN Discharge	
	N_2 flow rate:	30 L/min (obtained from boil off of 200 L liquid N_2 tank)
	Voltage:	20 KV (Model EGV 20-6 transformer, Del Electronics, Inc., Mount Vernon, NY)
	Frequency:	1800 Hz (Invertron 500 VA ac power supply, Aiken Industries, San Diego, CA)
	Input Power to Discharge:	~400 W
(B)	Spectrometric System	
	Monochromator:	H20 UV/VIS (Instruments SA, Inc., Metuchen, NJ)
	Bandpass (FWHM):	2 nm
	Photomultiplier:	Type R955 (Hamamatsu Corporation, Middlesex, NJ)
	PMT Voltage:	800 V
	Amplifier:	Model 110 (Pacific Precision Instruments, Concord, CA)
	Recorder:	Superscribe Series 4910 (Houston Instruments, Austin, TX)
(C)	Analytical Wavelengths	
	Organolead Compounds:	368.3 nm (Pb I)
	Organotin Compounds:	326.2 nm (Sn I)
	Organomercury Compounds:	253.7 nm (Hg I)
	Organic Compounds:	388.3 nm (CN; $B^2\Sigma^+ \rightarrow X^2\Sigma^+$)
(D)	GC System	
	GC:	Model 5700 A (Hewlett-Packard, Avondale, PA)
	Carrier gas/Flow rate:	N_2 at 80 mL/min
	Interface Temperature:	230°C
	Sample Volumes:	2.0 µL

Table 7. Continued

(E)	GC Columns	
	Organometallic Compounds:	4% SE-30/6% SP2401 on 100/120 Supelcoport (Supelco, Inc., Bellefonte, PA). Packed in 4 ft. x 1/8 in. O.D. glass column.
	Organic Compounds:	5% SE-30 and 3% OV-17 on 100/120 Supelcoport (Supelco, Inc.) for hydrocarbon and aromatic compounds respectively. Packed in 6 ft. x 1/8 in. O.D. stainless steel columns.

Stock solutions of organometallic reference samples were prepared in anhydrous diethylether for the organic Hg, Pb, and Sn compounds (Alfa Products, Danvers, Massachusetts) at a concentration of 1.0 mg/mL. Serial dilutions were also prepared containing from 100 µg/mL to 0.01 µg/mL. Hydrocarbon and aromatic mixtures were prepared in pentane by the same manner from selected GC reference compounds (Chem Service, Inc., West Chester, Pennsylvania).

Results and discussion

The specificity of the GC-APAN system for the detection of organometallic compounds is best exemplified by the chromatogram shown in Figure 19 obtained from a neat 2 µL injection of leaded gasoline.

The Pb specific chromatogram was obtained by monitoring the Pb I emission at 368.3 nm. The species detected were attributed to a mixture of methyl and ethyl lead alkyl compounds normally present in leaded gasoline. No interferences from co-eluting hydrocarbon compounds in the gasoline were observed. The relative sensitivity for organolead compounds can be approximated by the signal that was obtained from a reference sample containing 20 ng of tetrabutyllead, which is also shown in Figure 19.

A chromatogram of several tetraalkyltin compounds, obtained by monitoring Sn I emission at 326.2 nm, is shown in Figure 20. The signal from the diethylether solvent was due to stray light from CN emission. The signal from the solvent, considering that a 2 µL injection would contain 1.4 mg of diethylether, is negligible when compared to the

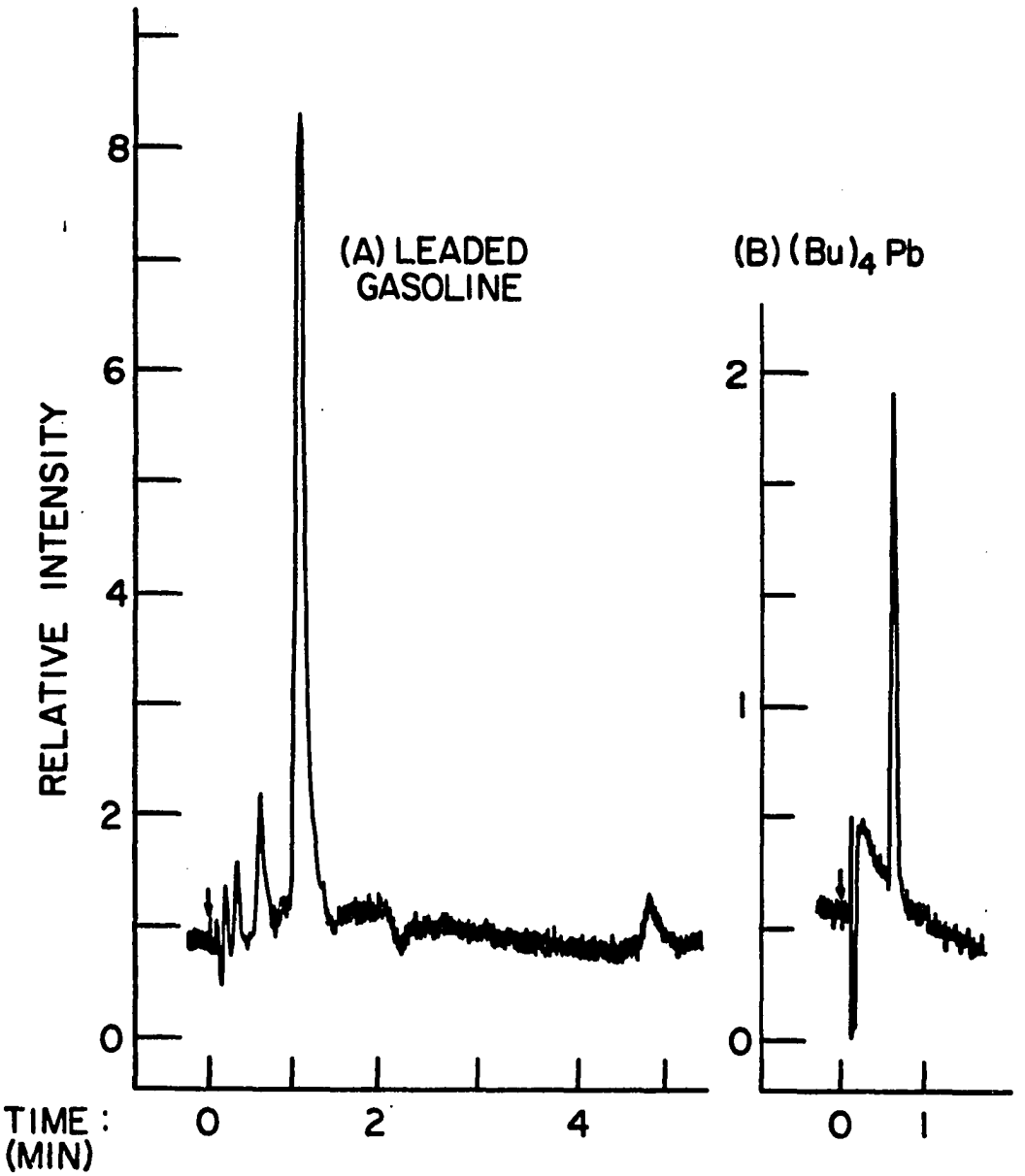

Figure 19. Chromatograms obtained from (A) leaded gasoline (temperature program; initial: 40°C, rate: 8°C/min; final: 80°C with 2 min hold) and (B) 20 ng of tetrabutyllead (isothermal at 175°C)

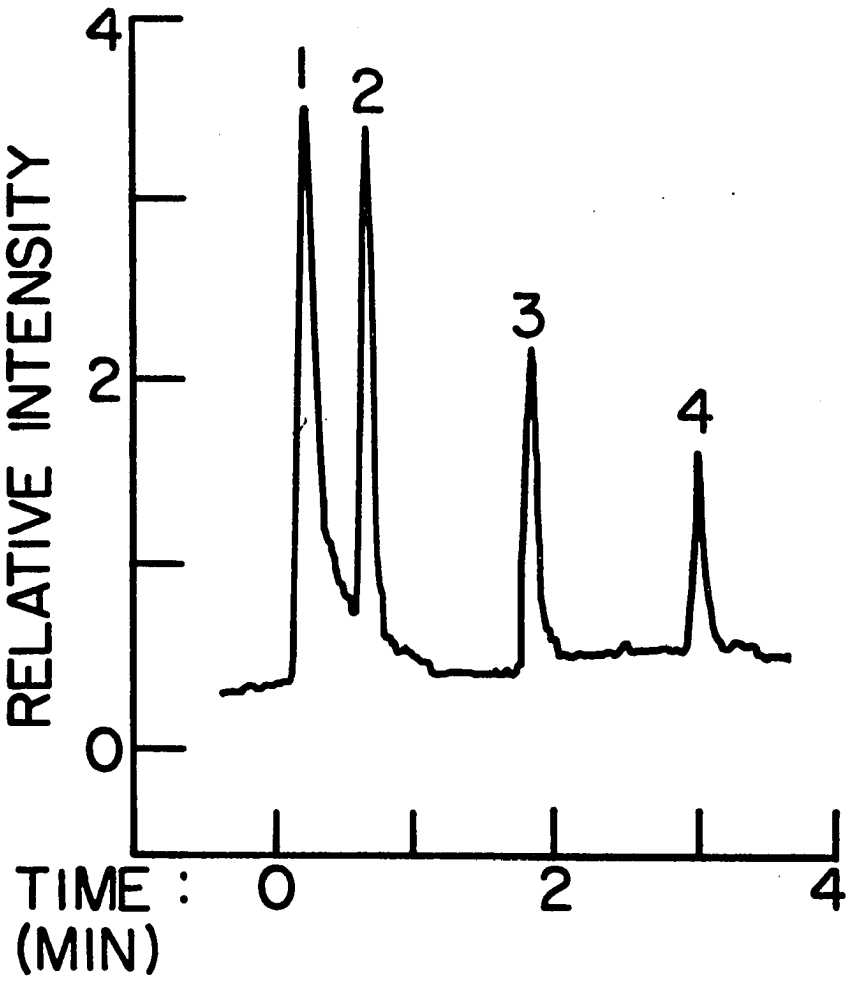

Figure 20. Chromatogram obtained from tetraalkyltin compounds: (1) solvent, (2) $(C_2H_5)_4Sn$, (3) $(C_3H_7)_4Sn$, and (4) $(C_4H_9)_4Sn$ (temperature program; initial: 70°C, rate: 32°C/min; final: 170°C). Each tin compound was present at a 10 ng level

signals obtained from the organotin compounds which were present at a 10 ng level.

A chromatogram for several diorganomercury compounds, obtained by monitoring Hg I emission at 253.7 nm, is shown in Figure 21. Each compound was present at a 2-5 ng level. The excellent resolution obtained with the GC-APAN system for the mercury compounds is exemplified by the near total separation of the di-n-propyl and diisopropyl mercury isomers.

The potentialities of the APAN afterglow as a nonspecific detector for organic compounds were literally stumbled upon when it was observed that organic solvents eluted from the GC column during the organometallic studies transformed the usual green emission of the afterglow into a long-lived blue glow from excited CN molecules. The production and excitation of the characteristic chemiluminescence emission of CN ($B^2\Sigma^+ \rightarrow X^2\Sigma^+$) when hydrocarbon compounds are introduced into low pressure active nitrogen sources is well documented (9). To the best of our knowledge, the observation of CN emission in an APAN afterglow has not been reported in prior investigations on active nitrogen.

The chromatograms obtained from a selected mixture of saturated hydrocarbon compounds and of aromatic compounds using the APAN detector are shown in Figure 22. Emission was monitored from the CN ($B^2\Sigma^+ \rightarrow X^2\Sigma^+$) $0 \rightarrow 0$ transition at 388.3 nm. Each compound was present at a 10 ng level. Irregularities in the baseline were found to be the result of solvent impurities or column bleed at high GC oven temperatures.

It should be noted that the intensity of CN emission was highly dependent on the discharge tube geometry. The discharge tube used in

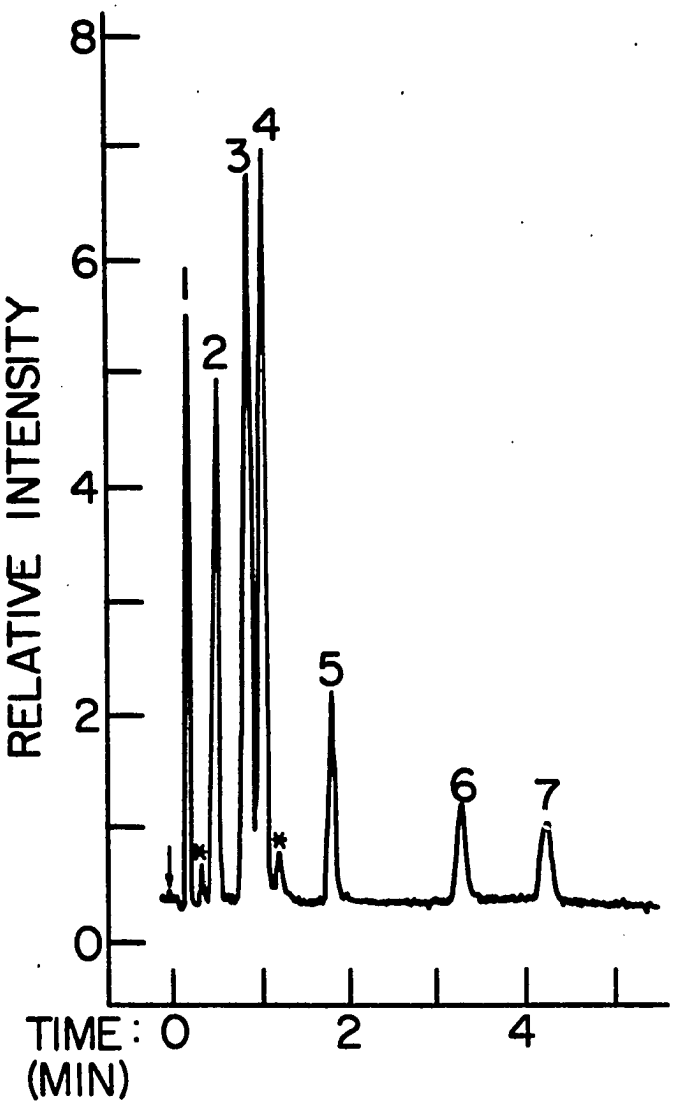

Figure 21. Chromatograms obtained from dioganomercury compounds: (1) $(CH_3)_2Hg$, (2) $(C_2H_5)_2Hg$, (3) $(i\text{-}C_3H_7)_2Hg$, (4) $(C_3H_7)_2Hg$, (5) $(C_4H_9)_2Hg$, (6) $(C_6H_{13})_2Hg$, (7) $(C_6H_5)_2Hg$, and (*) impurities (temperature program; initial: 50°C, rate: 32°C/min; final: 200°C). Each mercury compound was present at a 2-5 ng level

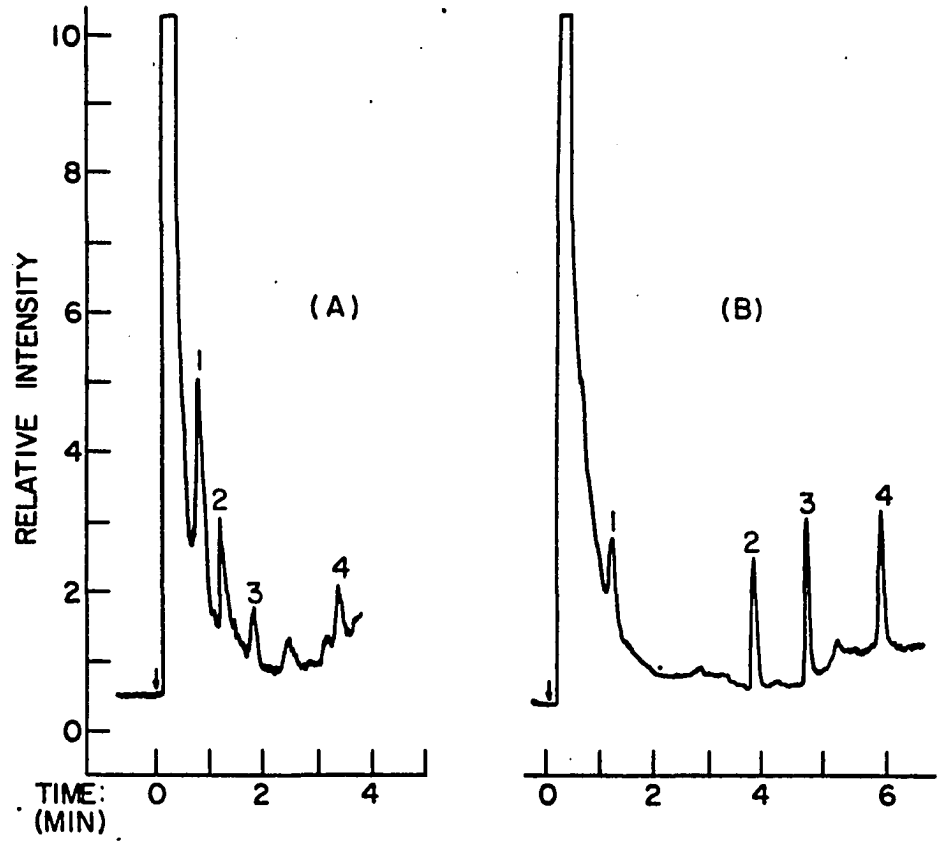

Figure 22. Chromatograms obtained from (A) hydrocarbon mixture in pentane containing (1) octane, (2) decane, (3) dodecane, and (4) hexadecane (temperature program; initial: 50°C, rate: 32°C/min; final: 200°C with 2 min hold) and (B) aromatic mixture in pentane containing (1) toluene, (2) napthalene, (3) biphenyl, and (4) t-stilbene (temperature program; initial: 80°C with 2 min hold, rate: 32°C/min; final: 190°C with 2 min hold). Each compound present at a 10 ng level

earlier work was found to form significantly less excited CN species as compared to the narrower discharge tubes used in this work. The best speculation one can make at this time is that the greater curvature of the glass in the larger tubes, from the discharge region to the afterglow, must reduce the population of active species responsible for the formation of CN species.

Changes in the GC carrier gas were also observed to effect the formation of CN species. Nitrogen gave the best response when used as a carrier gas, hydrogen reduced the signal response by a factor of two, and helium was found to reduce the signal response by a factor of ten or more.

The current limits of detection, linear response ranges, and selectivity ratios for the various organometallic and organic compounds observed in the GC-APAN system are given in Table 8. The limits of detection were obtained from peak heights that gave a signal to background scatter of three. The representative compound on which the limits of detection are based is also given. These limits will vary by factors dependent on the chromatographic conditions used and the mole fraction of the metal present in the organometallic compounds.

It is not surprising that the limits of detection for aromatic compounds are, in general, significantly better than those obtained for the saturated hydrocarbons. Kinetic studies have revealed that unsaturated organic molecules (i.e., alkenes, aromatics) tend to form CN molecules in an active nitrogen environment at a much faster rate than

Table 8. Limits of detection, linear dynamic ranges, and selectivities obtained for various organometallic and organic compounds by GC-APAN

Species	Compound	Analytical Wavelength (nm)	Limit of Detection (ng)	Dynamic Linear Range	Selectivity
Pb	Tetrabutyllead	368.3	3	1×10^3	100
Sn	Tetraethyltin	326.2	2	1×10^3	1,000
Hg	Dimethylmercury	253.7	0.002	5×10^4	10,000
Hydrocarbons	Hexadecane	388.3	0.8	1×10^2	---
Aromatics	Napthalene	388.3	0.2	5×10^2	---

saturated hydrocarbon compounds (70). Thus, a more rapid reaction will undoubtedly be observed more readily for the short reaction time available in the APAN afterglow region due to the high flow rates utilized.

Typical analytical calibration curves obtained for organometallic and organic compounds are shown in Figure 23. The analytical calibration curves for the organometallic compounds, when monitored at an emission wavelength specific for the metal, are generally linear over three to four orders of magnitude in concentration, as shown for diethylmercury. Calibration curves for organic compounds were observed to be linear over two orders of magnitude in absolute amounts up to a maximum of approximately 100 ng, after which a pronounced departure from linearity occurred. This observation may be due to depletion of the active species in the afterglow responsible for the formation of CN molecules.

Selectivity ratios were based on the ratio of the limits of detection for napthalene to the limits of detection for each representative organometallic compound at the analytical wavelengths used for each organometallic compound. Excellent selectivity was observed for the organomercury and organotin compounds, but the selectivity for organolead compounds was observed to be significantly lower. This decrease in selectivity resulted from spectral overlap of the CN ($B^2\Sigma^+ \rightarrow X^2\Sigma^+$) emission, which occurs in the 310-460 nm region, with the Pb 368.3 analytical wavelength. Selectivity can be improved by observing emission from other emission lines not within the CN emission region (i.e., Pb I at 283.3 nm), however, a decrease in sensitivity is observed. Thus, a

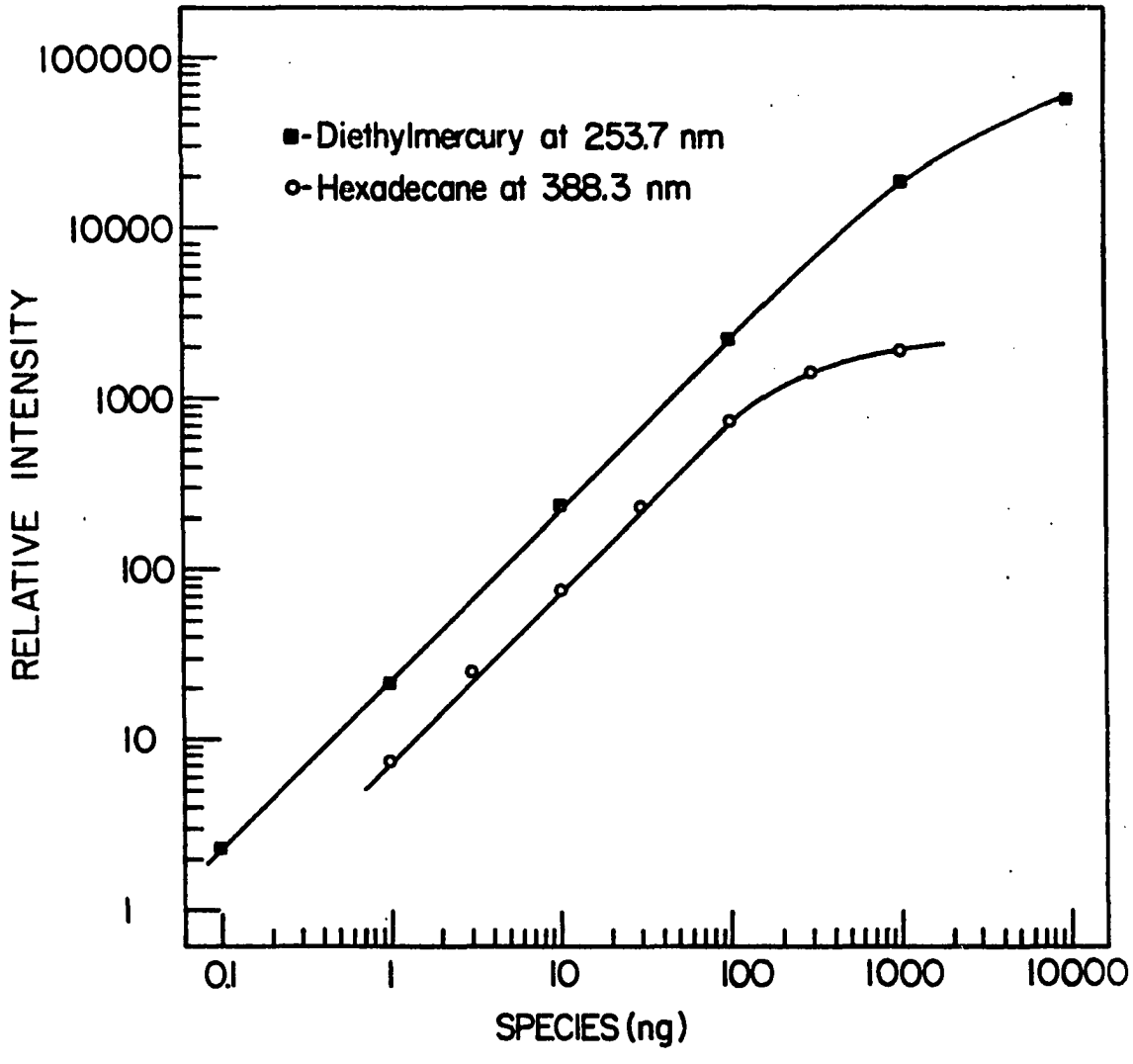

Figure 23. Analytical calibration curves obtained from diethylmercury and hexadecane

compromise must be made in choosing the optimum analytical wavelength as opposed to desired selectivity.

Comparison to other GC emission detectors

The versatility of the GC-APAN system is highlighted by its capabilities as an element specific detector for organometallic compounds, as well as a nonspecific detector for organic compounds.

There are several advantages in utilizing APAN as a detector for organic compounds as opposed to the recent use of low pressure, active-nitrogen detectors. The formation of the excited CN molecules in low pressure afterglows is significantly hampered by the formation of polymeric materials containing CN (37). A constant flow of dilute HCl gas into the afterglow is also required to catalyze a significant enhancement in the emissions from saturated hydrocarbon compounds. The use of HCl has not been effective when used in the APAN afterglow. The formation of the excited CN ($B^2\Sigma^+$) state, being a collision dependent phenomenon, is more favorably produced in the APAN afterglow. Deposits on the windows of the low pressure cells from polymeric materials also give rise to increasing background signals from CN emissions, thus, periodic cleaning of the cell is required. No such deposits have been observed on the APAN afterglow tube.

Finally, the interfacing of the GC column, maintained at atmospheric pressure, to low pressure afterglows is much more difficult to manipulate and maintain than the simple interface design used with APAN. The chromatography developed with the APAN detector has thus far been

characterized by well defined, gaussian shaped peaks. The interface to the APAN detector appears to have negligible effects on the chromatographic capabilities of the GC when compared to chromatograms obtained from the standard flame ionization detector on the GC unit used.

In contrast to the observations with MIP detectors, the APAN afterglow is not extinguished by the introduction of relatively large amounts of organic species. Thus, instrumental modifications and manipulations to vent the solvent effluent prior to the detection of the trace organic constituents are not necessary. The afterglow, being continually generated from the main discharge region of the ozonizer-type tube, is at most, only temporarily quenched by the introduction of excessive amounts of organic effluents. As can be seen in Figure 19, the spectral background from the afterglow is temporarily quenched by the passage of the solvent peak, resulting in the negative deflection in the chromatograms. The characteristic green afterglow is immediately regenerated after the solvent effluent has been swept through the afterglow tube, with no apparent detrimental effects on the performance of the afterglow. Carbonaceous deposits, which can severely effect the performance of MIP sources maintained at reduced pressures, are not formed in the APAN afterglow tube, a factor which is probably the result of the high flow rates and pressure used.

The limits of detection, using GC-MIP systems for the species evaluated in this communication, appear to be better than for those obtained using GC-APAN. The one exception is for organomercury compounds,

in which either detector appears about equivalent (71). Unfortunately, a vast majority of publications to date on the use of MIP detectors show limits of detection based on integrated peak area measurements, typically in terms of ng/sec detected. Thus, a true comparison of the limits of detection for the MIP and APAN detectors was not possible since the limits of detection for the GC-APAN system were based on peak heights.

Application of GC-APAN to the Determination of Organomercury Compounds in Environmental Samples

Introduction

Organomercury compounds are known to have considerably higher toxicity and longer biological half-lifes in organisms than the inorganic forms of the elements (72). Methylmercury and dimethylmercury are now known to be readily formed by bacterial biomethylation of inorganic mercury (73). Of these two compounds, methylmercury has been the predominant species found in biological systems, although the possible presence of dimethylmercury as well as other diorganomercury compounds and organomercury salts does exist (74). The wide spread industrial usage and natural distribution of mercury in the environment has made it imperative to develop analytical methodology for the specific determination of organomercury compounds which may originate from these sources.

In the past 25 years, numerous incidences of methylmercury poisoning from contaminated foods, particularly from fish, have resulted in a number of methods for the specific determination of methylmercury in fish and

other environmental samples. Early work by Westöö (75,76) consisted of liberating the protein bound methylmercury as methylmercury chloride by the addition of HCl. The CH_3HgCl was extracted into benzene and then back extracted into an aqueous cysteine solution as a Hg-cysteine complex to eliminate interferences from benzene soluble organic constituents in the subsequent gas chromatographic (GC) determination. The aqueous layer was re-acidified with HCl and the liberated CH_3HgCl extracted back into benzene. The final analysis was performed by GC; an electron capture detector was used to measure the eluted CH_3HgCl. Although the Westöö procedure, with some modifications, has been recommended by the U.S. Environmental Protection Agency (77), it is a time consuming procedure. Because the choice of solvents is limited by the use of an electron capture detector, the possibility of using other solvents, e.g., chlorinated hydrocarbons, is not feasible. Partioning in each extraction is also not quantitative. Thus, correction factors are required in the calculations.

A method developed by Watts et al. (78) eliminates the cysteine cleanup by using a simple acetone wash of the fish tissues to remove lipids and other organic molecules that may interfere in the GC analysis. The sample is then acidified with HCl and the liberated CH_3HgCl extracted into benzene for analysis. The Watts procedure, although much simpler, is still susceptible to interferences in the chromatographic analysis from organic species not removed in the acetone wash but co-extracted into benzene with the CH_3HgCl.

In both the Westöö and Watts procedures, the ultimate limits of detection are constrained primarily by the volume of benzene used in the extractions. Attempts to concentrate the CH_3HgCl by evaporation of the benzene solvent results in losses of CH_3HgCl. It has been observed that the total volume of benzene must be kept at 8 mL or greater to avoid loss of CH_3HgCl (78).

A method described by Talmi (71) makes use of a highly selective and sensitive microwave-induced plasma (MIP) as a GC detector for monitoring Hg emissions at 253.7 nm. Samples are homogenized in water, acidified with HCl, and the CH_3HgCl partitioned into a 2 mL volume of benzene for analysis. The selective detection of atomic mercury emissions eliminates interferences from co-extracted organic species provided that the GC is capable of resolving other organomercury compounds which may be present in the sample. Although the method is rapid and very sensitive, microwave plasmas have several operational limitations (61-63). The injection of microliter amounts of species into the plasma; i.e., solvent plug, can decouple the microwave resonant cavity, resulting in total quenching of the discharge. Thus, experimental manipulations are required to remove the solvent from the plasma prior to or after the species to be determined has eluted from the GC. A limitation of MIP sources maintained at low pressure is the buildup of carbonaceous deposits on the walls of the discharge tube from effluents containing carbon, thus periodic cleaning is required.

Methods for the analysis of surface waters for diorganomercury compounds have been very limited. A procedure developed by Dressman (79)

involved extraction of several dialkylmercury species with a mixture of 20% ether in n-pentane, followed by concentration to a 5 mL volume. The extract was then analyzed by GC using a flame ionization detector. The extractions were not quantitative and varied for each compound. The possibility of co-extracting organic interferences severely limits the applicability of the technique.

The previously reported observation that the detection limit of Hg in the APAN afterglow was ∿ 10 pg suggested an evaluation of this excitation source as a specific detector for the GC speciation of Hg. Reported here are the results of applying the GC-APAN system to the determination of methylmercury in fish, water, urine, and sediments; and diorganomercury compounds in water. The results of this study reveal that problems encountered with other GC detectors are eliminated by the APAN approach.

The principal methods used were to isolate methylmercury from samples as methylmercury chloride, followed by extraction into methylene chloride. Diorganomercury compounds were extracted from water with either methylene chloride or carbon disulphide. All extracts were concentrated to 1.0 mL, from which 2 μL aliquots were taken for analysis by GC. Interferences from other co-extracted organic molecules in the GC detection and quantitation of the organomercury species were eliminated by observing the Hg (I) emission at 253.7 nm excited in an APAN afterglow.

Apparatus and procedures

Distilled-in-glass methylene chloride (Burdick and Jackson Laboratories, Inc., Muskegan, Michigan 49442) and "Photrex" reagent grade

carbon disulphide (J. T. Baker Chemical Co., Phillipsburg, New Jersey 08865) were used without further purification. No Hg was detectable when 50 mL of either solvent was evaporated to 1.0 mL. Concentrated HCl (A.C.S. grade) was diluted to 6 N in deionized water for sample acidifications.

A stock solution of methylmercury chloride (Alfa Products, Danvers, Massachusetts 01923) was prepared containing 1.0 mg/mL in methylene chloride. Serial dilutions were prepared containing concentrations of 100 µg/mL to 0.01 µg/mL in 10 mL volumetric flasks.

A stock solution containing a mixture of dimethylmercury, diethylmercury, di-n-propylmercury, diisopropylmercury, dibutylmercury, dihexylmercury, and diphenylmercury (Pfaltz and Bauer, Stamford, Connecticut 06902) in methylene chloride was prepared such that each diorganomercury species was present at 1 mg/mL. Serial dilutions were prepared in the same manner as the CH_3HgCl solutions.

The APAN instrumentation and details of the interfacing to the GC were described in the previous section of this chapter. All filters, vacuum flasks, and separatory funnels used in the extractions were standard with the exception of a specially designed flask, consisting of a 2.0 mL graduated tip on the bottom of a 50 mL round bottom flask, used for concentrating organic extracts (80). The GC column characteristics and operating conditions of the GC-APAN system used in this work are summarized in Table 9. A sample volume of 2 µL was normally used for injection into the GC.

Table 9. Operating characteristics of the GC-APAN system

(I) Chromatographic conditions	
(A) Methylmercury chloride	
Column:	10% SP2401 on 100/120 Supelcoport
Column dimensions:	1/8" O.D. glass, 4 ft. length
Column temperature:	180°C
Column flow rate:	110 mL/min N_2
Interface temperature:	230°C
(B) Diorganomercury compounds	
Column:	4% SE-30/6% SP2401 on 100/120 Supelcoport
Column dimensions:	1/8" O.D. stainless steel, 3 ft. length
Column temperature:	50°C - 210°C at 32°C/min
Column flow rate:	80 mL/min N_2
Interface temperature	210°C
(II) Detector characteristics	
APAN input power:	500 W
N_2 flow rate:	30 L/min
Analytical wavelength:	253.7 nm
Bandpass:	2 nm
PMT voltage:	850 V

For isolation of methylmercury from fish, homogeneous samples of fish tissue were prepared by cutting a ∿ 2.5 cm wide strip from head to tail. The tissue was then finely chopped and pulverized in a tissue grinder. A 1.0 g representative sample was transferred to a 5 cm diameter, medium porosity filter and washed with four 15 mL portions of acetone, followed by two 15 mL portions of methylene chloride to remove water and lipids from the sample, as described by Watts et al. (78). Each washing was removed by vacuum filtration and discarded. The remaining sample was quantitatively transferred to a 50 mL screw-cap bottle, a 20 mL portion of 6 N HCl added, and the mixture vigorously shaken for two minutes. A 20 mL portion of methylene chloride was then added to the extract and the bottle was again shaken for an additional two minutes. The entire contents were then vacuum filtered to remove the tissue and to break up any emulsions that may have formed. The organic layer was separated from the aqueous layer in a 60 mL separatory funnel. The tissue and aqueous layer were recombined in the screw-cap bottle, a second 20 mL portion of methylene chloride added, and the extraction repeated. The organic fractions were combined and concentrated to 1.0 mL on a steam bath for subsequent analysis.

For methylmercury in water, a 100 mL sample was acidified with 20 mL of 6N HCl and extracted twice with 20 mL portions of methylene chloride in a 250 mL separatory funnel. The organic layers were separated from the aqueous layer, combined together, and concentrated to 1.0 mL for analysis. The same procedure was used for methylmercury in urine,

except that only 25 mL samples were used and 10 drops of concentrated HCl were added to acidify the sample. The combined organic and aqueous layers were vacuum filtered to eliminate emulsifications prior to separation.

Contamination of sediments with methylmercury was expected to be a surface phenomenon, thus no breakdown of the sediment particles was attempted. The sediment was dried prior to analysis. A 1.0 g sample was then treated with 10 mL of 6N HCl and extracted with 20 mL of methylene chloride in a 50 mL screw-cap bottle. The sediment was removed by vacuum filtration, and the organic layer separated and concentrated to 1.0 mL for analysis.

For diorganomercury compounds in water, a 1.0 L water sample was extracted three times with 20 mL portions of methylene chloride or carbon disulphide in a 2 L separatory funnel. The organic fractions were then combined and concentrated to 1.0 mL for analysis.

To evaluate the efficiency of the methods described above, samples were spiked by adding 100 µL aliquots from reference CH_3HgCl solutions of appropriate concentration to give methylmercury concentrations of 1.0 ppb and 10 ppb in water samples, 1.0 ppb in urine samples, and 1.0 ppm and 10 ppm in sediment samples. Fish samples known to contain methylmercury were spiked with 2.0 and 20 ppm CH_3HgCl after removal of water from the fish tissue by the acetone washings as described by Watts et al. (78).

For the diorganomercury compounds, a 1 L water sample was spiked with 1.0 mL of a reference mixture containing 1 μg/mL of each compound to give a concentration in water of 1.0 ppb (1 μg/L).

Results and discussion

The APAN afterglow was found to be a very sensitive GC detector for Hg species by monitoring of the atomic mercury line at 253.7 nm, as shown by the detection limits in Table 10. These values represent the absolute amounts of analyte required to give a peak height with signal to background scatter of three. Analytical calibration curves were observed to be linear to approximately 1 μg, well within the range of values expected from analysis of contaminated samples.

The 10% SP2401 column packing gave excellent and reproducible peak shapes for CH_3HgCl as shown in Figure 24 for five sequential 2 ng injections. The negative deflection prior to each peak was caused by the elution of the solvent, which temporarily caused quenching of the spectral background from the afterglow. This quenching effect had no effect on emissions from the sample effluents. An attempt was made to use column packings recommended by others for separating CH_3HgCl, including 15% DEGS (78) FFAP (71), but these packings were found to give considerably broader and tailing peaks.

The 5% SE-30/6% SP2401 column proved to be excellent for separating a number of diorganomercury compounds, as shown by the chromatogram in Figure 20 given in the previous section of this chapter. The resolving power of the column is highlighted by the separation of the di-n-propyl and diisopropyl isomers of Hg.

Table 10. Detection limits for organomercury compounds

Compound	Detection Limit (pg)[a]
Dimethylmercury	2
Diethylmercury	5
Dipropylmercury	10
Dibutylmercury	20
Dihexylmercury	30
Diphenylmercury	50
Methylmercury chloride	50

[a] 2 μL GC aliquot.

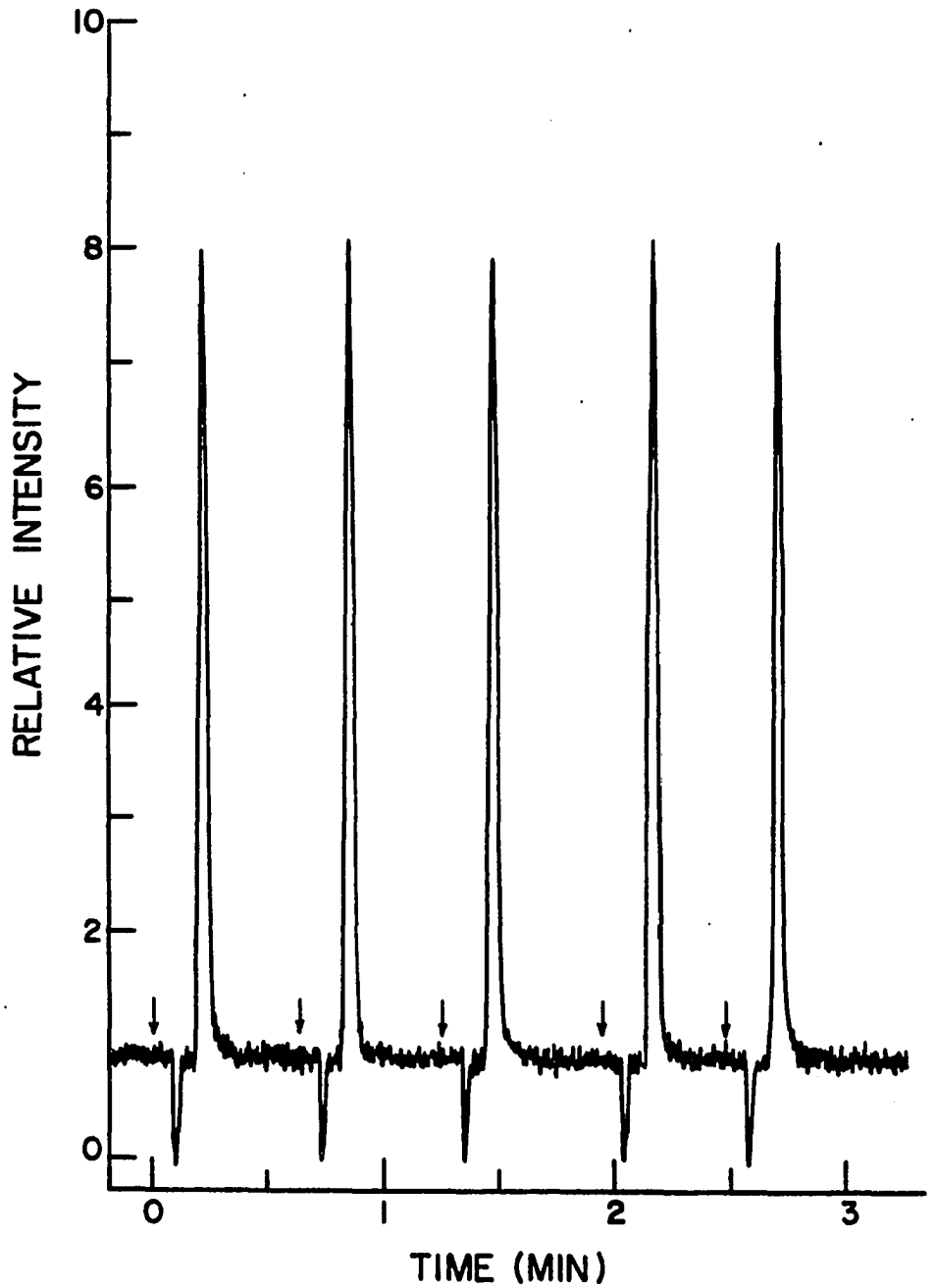

Figure 24. Chromatographic peaks obtained from five sequential 2 μL injections each containing 2 ng of CH_3HgCl. Column temperature: 180°C. Arrows indicate point of sample injection

The results of the analyses and recovery studies for methylmercury in fish, water, sediments, and urine are given in Table 11. The first three fish species were obtained from Canadian lakes suspected of having high levels of Hg contamination.

The precision of the determinations was acceptable, with deviations from the average value of 5% of less obtained from duplicate samples in all cases. An average recovery of 95% was obtained from samples spiked with known amounts of CH_3HgCl.

Removal of emulsions in the extraction process by centrifugation gave no improvement in the recoveries. Apparently negligible amounts of CH_3HgCl were trapped in the emulsified material that was filtered from the urine and fish extractions.

Chromatograms of the samples were remarkably clean, and in all cases exhibited only the CH_3HgCl peak. No other organomercury compounds were detected in the samples used. Organic materials present in the concentrated extracts appeared to have no detrimental effects on the column or detector performance. For example, a comparison of peak heights measured on reference samples injected before and after 60 repeated injections of several fish samples exhibited less than 5% deviation.

Benzene, diethylether, and carbon disulphide were also evaluated as solvents in the development of the methods used for isolation of methylmercury. Benzene was eliminated because of the difficulties encountered in concentrating the extracts to small volumes ($\leq$ 1 mL) without loss of CH_3HgCl. Diethylether proved to be inadequate because

Table 11. Analysis and recovery study results for methylmercury in various sample types[a]

Sample	CH_3Hg Found (ppm)	CH_3Hg Added	CH_3Hg Found	% Recovery
Walleye	10.2 (±0.3)	20.0 ppm	29.3 (±1.2) ppm	95
Lake Trout	1.65 (±0.03)	2.0 ppm	3.55 (±0.13) ppm	95
Small Mouth Bass	4.04 (±0.07)	---	---	--
Carp	0.34 (±0.01)	---	---	--
Surface Water	-b	1.0 ppb	0.96 (±0.02) ppb	96
	-b	10 ppb	9.4 (±0.4) ppb	94
Sediments	-b	1.0 ppm	0.94 (±0.01) ppm	94
	-b	10 ppm	9.4 (±0.2) ppm	94
Urine	-b	1.0 ppb	0.96 (±0.02) ppb	96

[a]All duplicate samples.

[b]Not detected.

of poor partitioning of the CH_3HgCl due to coextraction of HCl. Peak heights obtained from reference CH_3HgCl solutions prepared in carbon disulphide were observed to be only approximately one-fourth the peak heights obtained from identical reference solutions prepared in either benzene, diethylether, or methylene chloride. The reasons for this observed decrease in signal are unknown at this time.

Methylene chloride was found to be the most suitable solvent of those evaluated. The CH_3HgCl was efficiently extracted from acidified aqueous solutions with no apparent decomposition during the chromatographic separations. Concentration of the extracts to as little as 0.1 mL could be achieved without loss of CH_3HgCl.

Recoveries for the diorganomercury compounds at a 1.0 ppb level in water for two different separation methods are given in Table 12. An attempt was first made to elute the water samples through an XAD-2 resin to adsorb the Hg species on the XAD-2 surface. The Hg species were then eluted with 30 mL of methylene chloride and the solvent concentrated to 1.0 mL for chromatographic analysis. The dialkylmercury species, however, appeared to behave in a similar manner observed for hydrocarbons, which give low recoveries due to poor adsorption onto the XAD-2 resin surface (81).

Multiple extractions with methylene chloride or carbon disulphide gave good recoveries, as indicated, for all of the diorganomercury compounds except dimethylmercury. The low recoveries for dimethylmercury suggest that this compound is lost in the solvent concentration

Table 12. Percent recovery of diorganomercury compounds from one liter water samples using column adsorption and solvent extraction techniques

Compound[a]	XAD-2 Column Adsorption[b] Recovery (%)	Solvent Extraction	
		Methylene Chloride Recovery (%)	Carbon Disulphide Recovery (%)
Dimethylmercury	15	23	25
Diethylmercury	25	98	98
Dipropylmercury	28	88	94
Dibutylmercury	35	85	99
Dihexylmercury	30	97	95
Diphenylmercury	80	99	98

[a] 1.0 ppb of each compound (1 µg/L).

[b] Methylene chloride used as eluting solvent.

step because of its high volatility. Carbon disulphide was found to give the best extraction efficiency for the compounds studied. The reasons for the consistently lower recoveries for the dipropyl and dibutyl Hg species when methylene chloride is used as the solvent are not known.

The detection limits obtained for several organomercury species, in reference to the actual water, urine, sediments, and fish samples studied, are summarized in Table 13. The detection limits in Column A are based on the injection of 2 μL aliquots into the GC from a 1.0 mL solvent concentrate for the given sample quantity. The detection limits can be significantly enhanced, as shown in Column B, if sample sizes are increased 5-fold, if extracts are concentrated to 0.1 mL, and if a 5 μL GC aliquot is used.

The rapid, simple, and highly sensitive methods for determining organomercury compounds presented in this communication offer several advantages over previously described methods. The APAN detector exhibits excellent sensitivity, linear analytical calibration curves covering several orders in magnitude, good stability, and high specificity. Extensive sample cleanup is eliminated because species other than mercury present in extracted samples will not interfere in the chromatographic analysis. Most important is the freedom of choice in selecting solvents that are more volatile and less toxic than benzene. This factor has allowed for detection limits in the various environmental samples to be significantly improved over existing methods. These advantages make GC-APAN a viable alternative for the determination of organomercury compounds in food and environmental samples.

Table 13. Detection limits for organomercury compounds in various sample types

Sample	Quantity	Detection Limits (ppb)[a]	(ppt)[b]
Diorganomercurys in:			
Water	1.0 L	0.01 - 0.05	0.4 - 4
Methylmercury in:			
Water	100 mL	0.50	0.4
Urine	25 mL	2	16
Sediments	1.0 g	50	400
Fish	1.0 g	50	400

[a]Extracts concentrated to 1.0 mL; 2 µL GC aliquots.

[b]Sample quantity increased five-fold, extracts concentrated to 0.1 mL, and 5 µL GC aliquots used.

Further Progress with GC-APAN

Capillary column performance in the GC-APAN system

A Hewlett-Packard Model 5710 A gas chromatograph with the capability of using capillary columns was installed to replace the packed column GC used prior to this time. The narrow bore and flexibility of the fused silica capillary columns used, made it possible to insert the column exit directly into the afterglow of the APAN discharge tube, thus eliminating the transfer lines in the interface that were required for packed column operation.

A new discharge tube was also recently designed for use with the GC-APAN system. The discharge region was reduced in length from 40 cm to 15 cm and the tube diameter reduced from 18 mm to 12 mm. The copper electrodes previously used were replaced with platinum electrodes to eliminate problems encountered with oxide formation on the surface of the copper electrodes. The smaller tube was found to operate efficiently at lower flow rates ($\sim$ 15-20 L/min) as opposed to the 30 L/min flow rate used with the larger discharge tubes, thus gas consumption was significantly reduced. The optimum discharge frequency was found to be beyond the range of the power supply used (> 2000 Hz).

Preliminary results obtained from the capillary column, GC separation of a mixture of 10 polynuclear aromatic hydrocarbons yielded peaks that were well resolved with widths characteristic of the performance expected from capillary columns. The major problem encountered was the reproducible elution of the high boiling compounds (i.e., benzo (a) pyrene, . .

M.P. = 176.5°C). This problem was traced to the development of cold spots in the interface region between the GC and the discharge tube. The interface previously used, being a solid-type heating core, only allowed for the temperature to be measured at one point, thus no accurate estimate of the temperature throughout the interface region was possible.

This difficulty was circumvented via an air-heated interface, a diagram of which is shown in Figure 25. The capillary column was guided through a 7 mm O.D. 1 mm I.D. pyrex tube into the discharge tube. The column was heated by two lengths of nichrome wire wound on 3 mm quartz rod and enclosed in a 3.8 cm O.D. brass tube. The inner brass tube was mounted to a 6.4 cm O.D. brass tube and the annular cavity filled with fiberfax insulating material. A thermocouple temperature probe was inserted into the heated cavity so that the tip was adjacent to the pyrex tube. An 8 mm thick brass plate was used to seal the end of the oven where the discharge tube was connected to the interface. Temperatures as high as 325°C have been maintained in this interface with fluctuations of only $\pm$ 5°C.

Comparison of the APAN detector to flame ionization detectors

A chromatogram obtained from a mixture of 10 polynuclear aromatic hydrocarbon compounds with the modified interface in place is shown in Figure 26. A 1 μL injection, containing 4 ng of each compound, was used. It is apparent that the higher boiling compounds were readily eluted and resolved, indicating that the heat distribution in the modified interface was uniform throughout the interface.

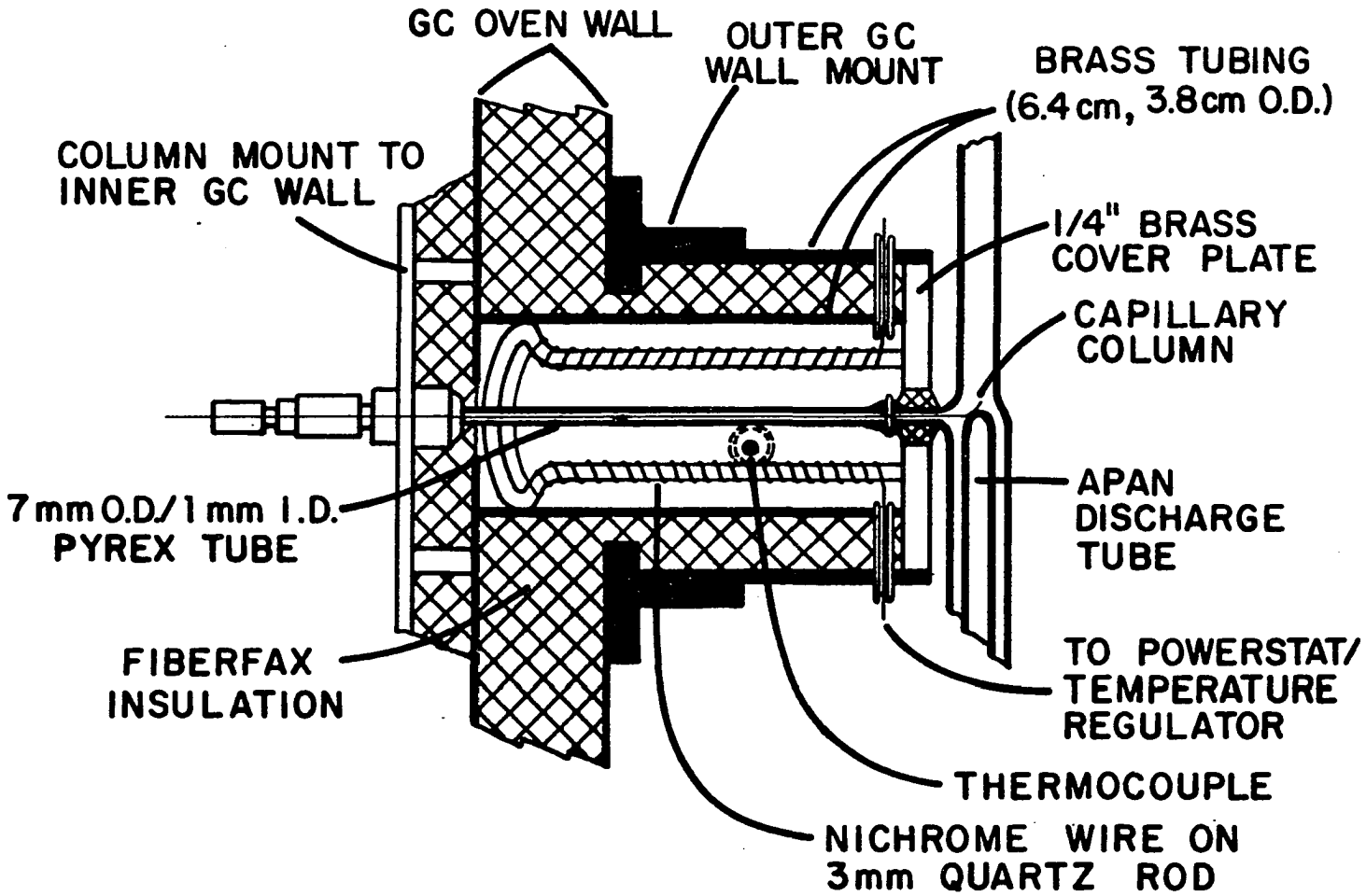

Figure 25. Schematic diagram of the reconstructed interface from the GC oven to the APAN discharge tube for capillary column GC

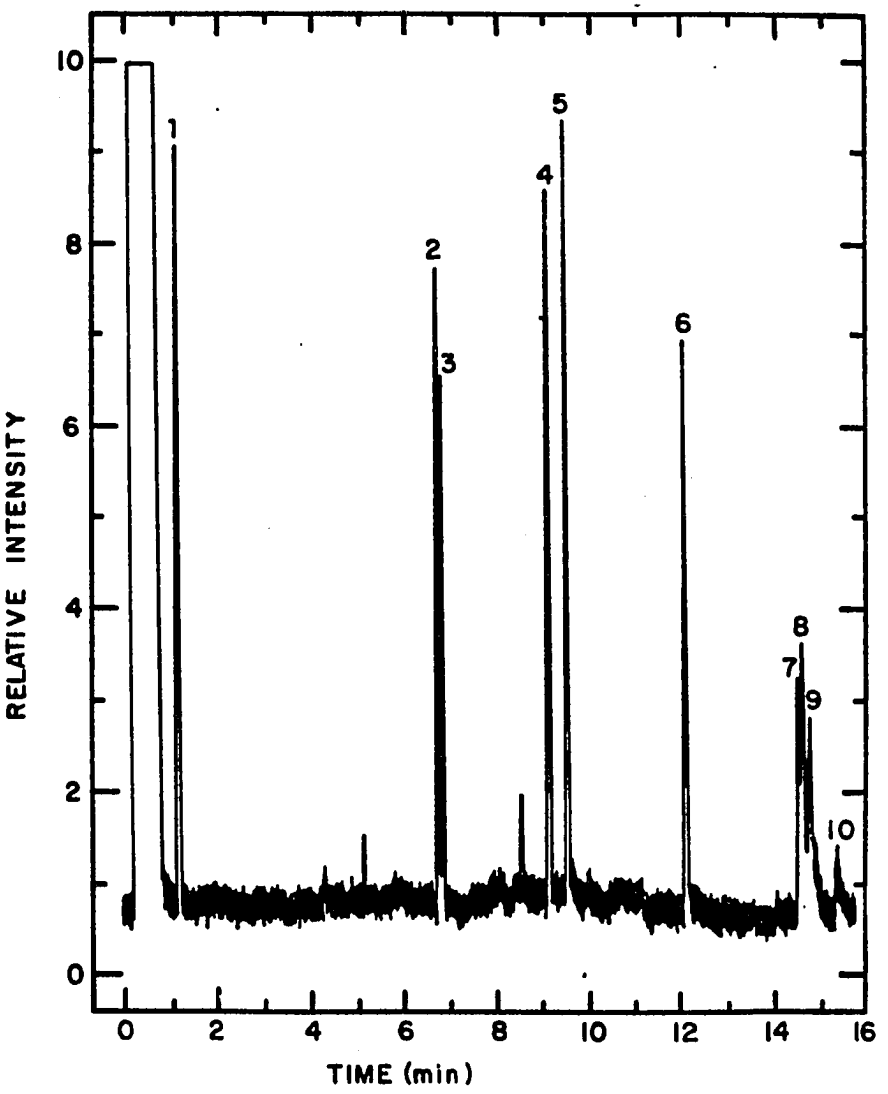

Figure 26. Chromatogram obtained from the separation of a 4 ppm PAH mixture by capillary GC using the APAN detector: (1) napthalene, (2) phenanthrene, (3) anthracene, (4) fluoranthrene, (5) pyrene, (6) chrysene, (7) benzo[e]pyrene, (8) benzo[a]pyrene, (9) perylene, and (10) methylcholanthrene. GC: Hewlett-Packard 5710A; column: SE-54 (14 m length); temperature: 2 min-100°C-8°C/min - 300°C-4 min; amp: 1×10^{7}; wavelength: 388.3 nm

An FID chromatogram obtained from the same mixture containing 1 ng of each compound is shown in Figure 27. Several important comparative observations can be made on the chromatograms shown in Figures 26 and 27. Both chromatograms were observed to yield excellent resolution of the sample mixture. Although the chromatogram from the Carlo-Erba FID appears to give better baseline resolution for the five-ringed isomers, this is primarily due to the longer column length used (30 m as opposed to 14 m). The baseline of the chromatogram obtained with the FID was observed to significantly increase as the column temperature was increased. This change in background has been attributed to column bleed from silicon compounds in the liquid phase of the column. The FID, being a nonselective detector, responds to the silicon compounds being eluted off the column. In comparison, the baseline from the APAN detector remained constant throughout the chromatogram, which can be attributed to selective detection of only the carbon containing species that are eluted from the column. The background noise level of the FID is, however, observed to be much less than that obtained from the APAN afterglow detector. Finally, the Carlo-Erba FID appears to be approximately four times as sensitive as the APAN detector if no attenuation is used, however, the high boiling or late eluting compounds would be obscured due to the increased background from column bleed. Recently, the sensitivity of the APAN detector has been improved by a factor of two, making the sensitivity of the two detectors comparable.

The excellent sensitivity of the GC-APAN system for polynuclear aromatic hydrocarbon compounds, coupled with its proven capabilities as

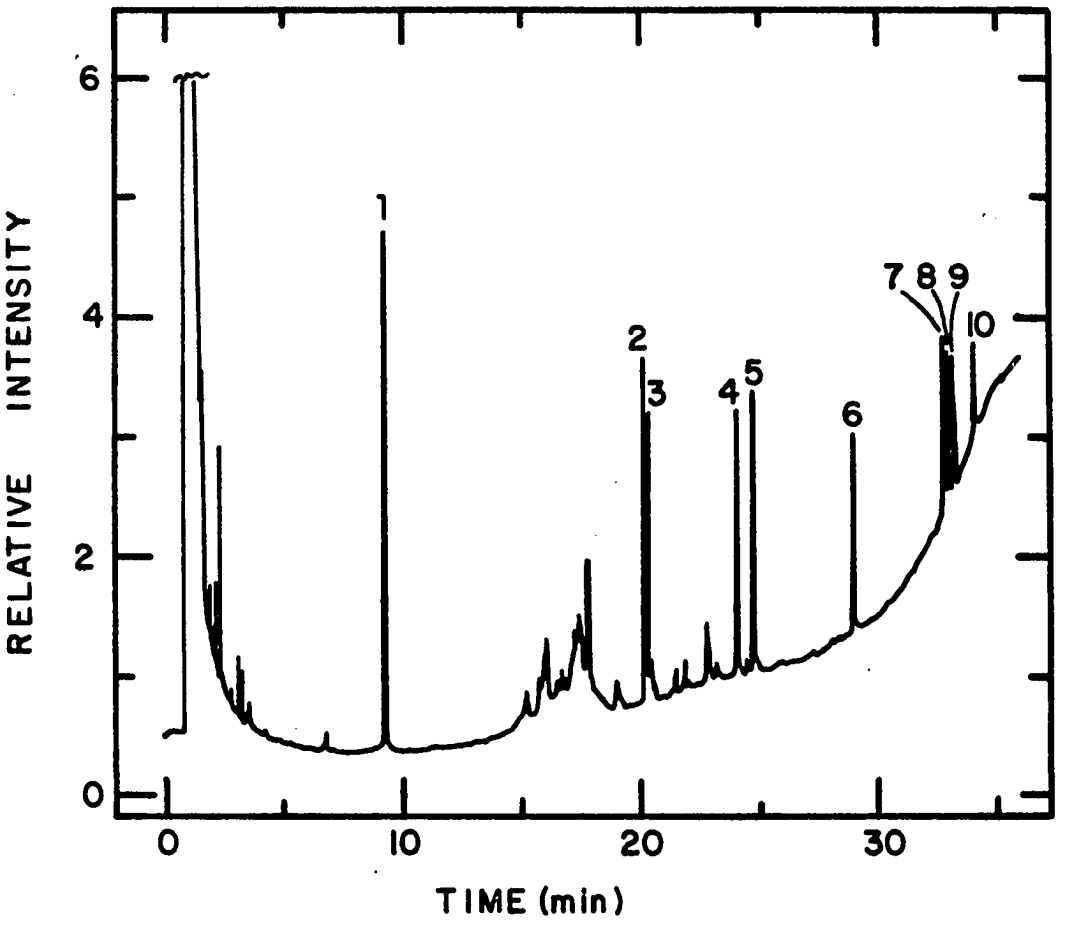

Figure 27. Chromatogram obtained from the separation of a 1 ppm PAH mixture by capillary GC using a Carlo-Erba flame ionization detector: (1) napthalene, (2) phenanthrene, (3) anthracene, (4) fluoranthrene, (5) pyrene, (6) chrysene, (7) benzo[e]-pyrene, (8) benzo[a]pyrene, (9) perylene, and (10) methyl-cholanthrene. GC: Carlo-Erba; column: SE-52 (30 m length); temperature: 5 min-60°C-7.5°C/min - 300°C-4 min; attenuation: x 2

an element selective detector, again makes the APAN afterglow a viable alternative as a GC detector.

CHAPTER III. EXCITATION AND ENERGY TRANSFER CONSIDERATIONS IN THE APAN AFTERGLOW

Spectroscopic Observations in the APAN Discharge and Afterglow

The optical emission observed in both the direct discharge and afterglow regions are compared in Figure 28 (200-400 nm), Figure 29 (400-600 nm), Figure 30 (600-1060 nm), and Figure 31 (1025-1055 nm). All spectra were obtained using a bandpass of 0.3 nm (FWHM). As shown in Figures 28 and 29, emission from the direct discharge was significantly more intense than in the afterglow. Consequently, the spectral recordings from the former had to be substantially attenuated by the factors indicated on the relative intensity axis. No emissions were observed in the afterglow from 600 to 1000 nm. A summary of the species observed spectroscopically in the APAN discharge and afterglow is given in Table 14. Data on the lifetime of the excited states, the transitions and wavelength regions observed, and where they are found in the discharge are included. Potential energy curves for relevant molecular states of N_2 and NO, and atomic states of N and O can be referred to in Figure 32.

Spectroscopic Evidence for Species Observed Only in the Primary Discharge

Only a brief discussion of the species observed exclusively in the primary discharge will be presented, since it is the afterglow which is responsible for the observed analytical results obtained in the previous chapter.

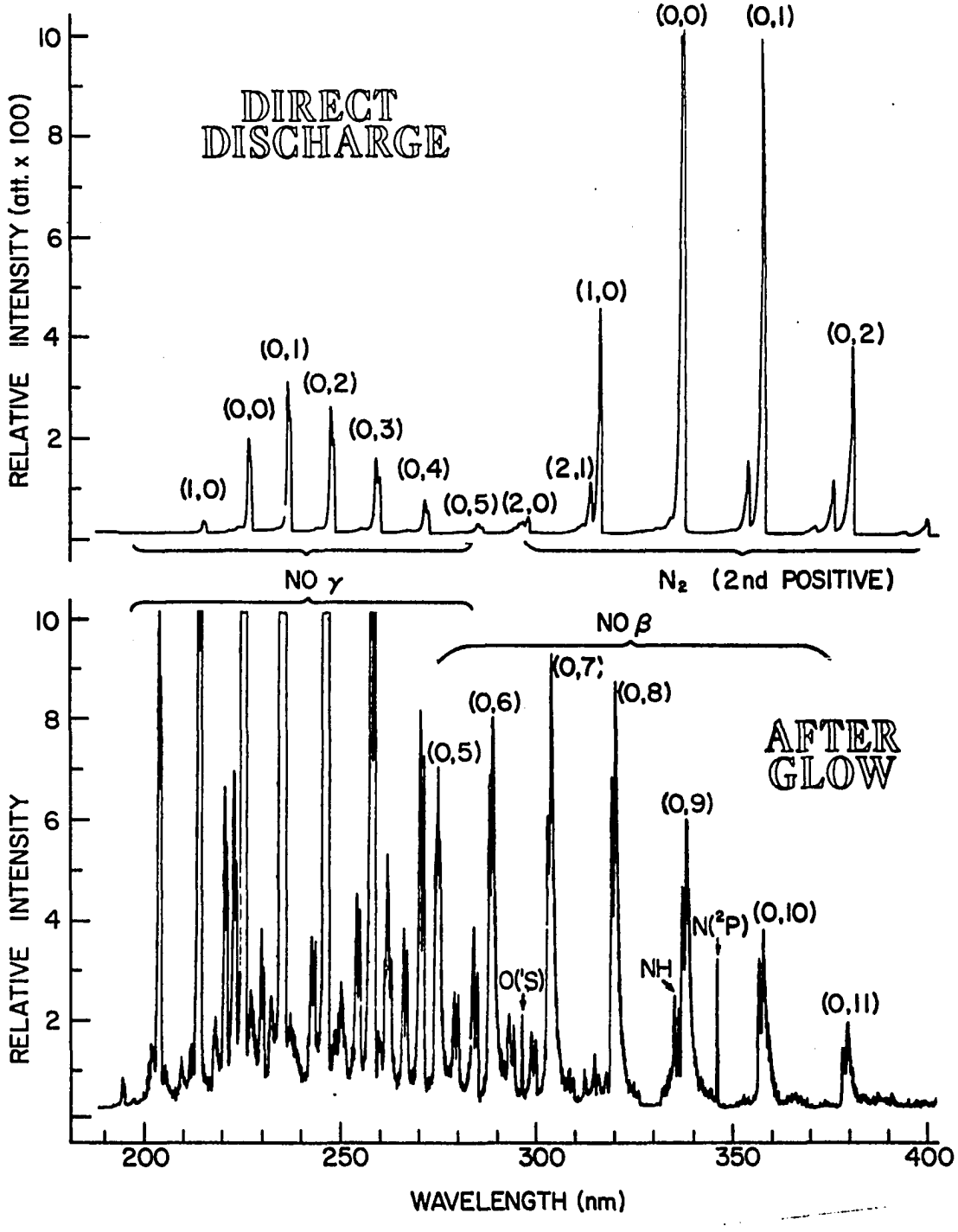

Figure 28. Emission spectra observed in the 200-400 nm region of the APAN discharge and afterglow

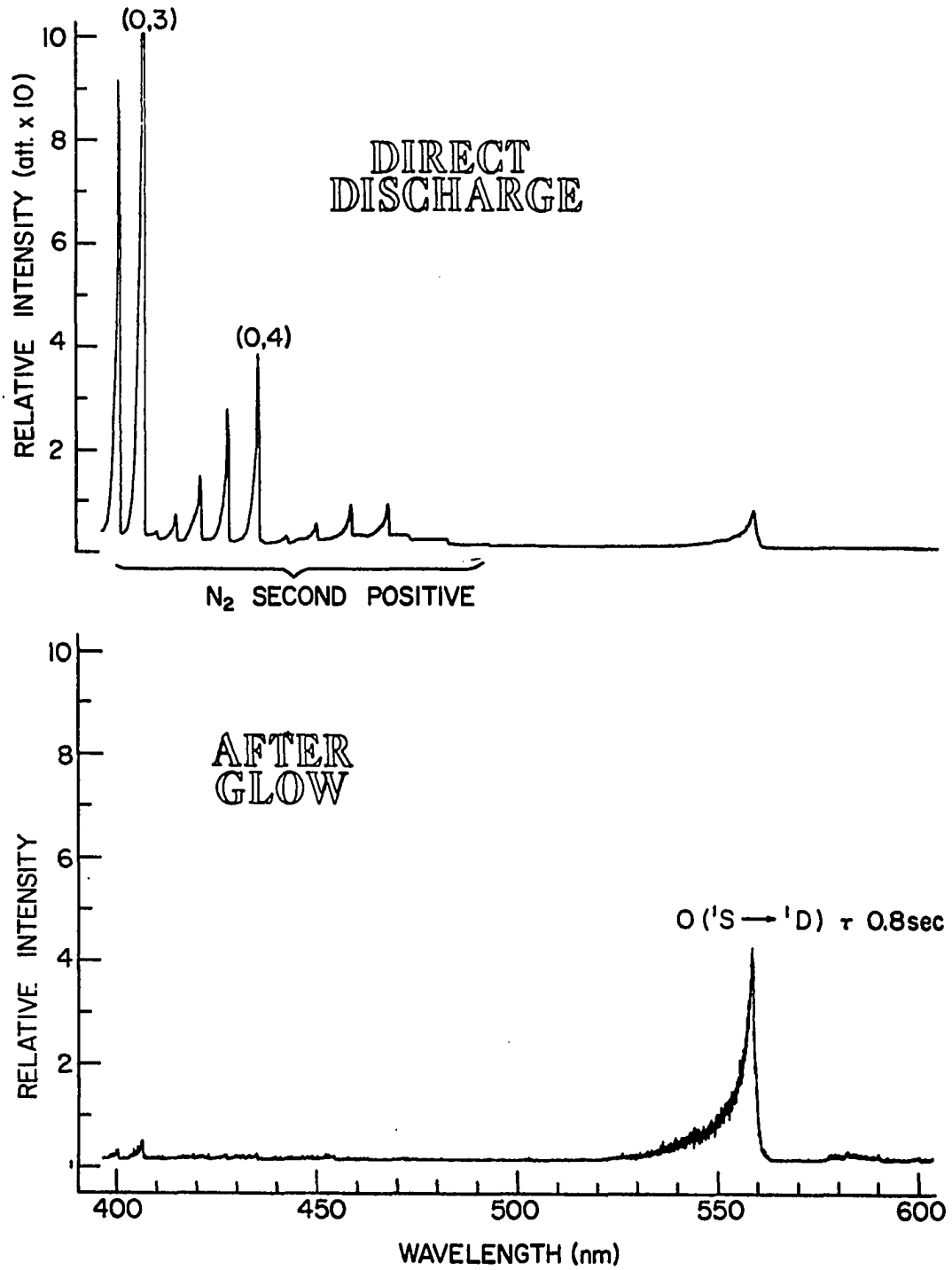

Figure 29. Emission spectra observed in the 400-600 nm region of the APAN discharge and afterglow

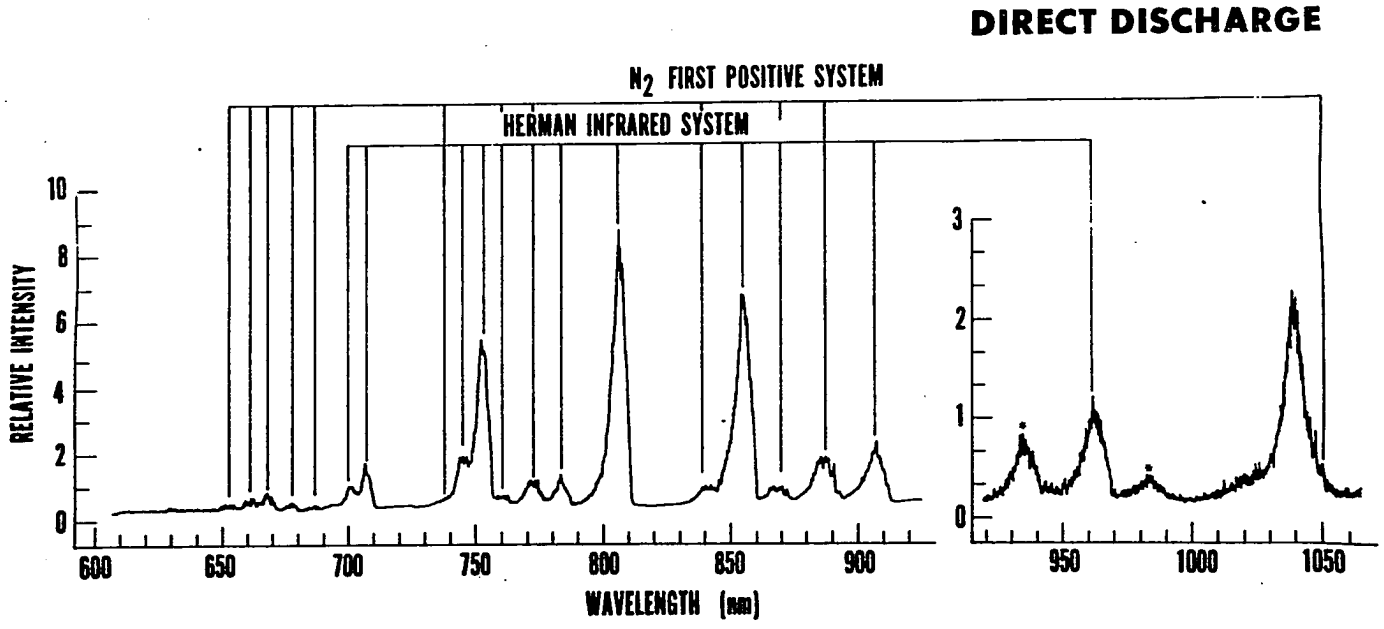

Figure 30. Emission spectrum observed in the 600-1050 nm region of the APAN discharge

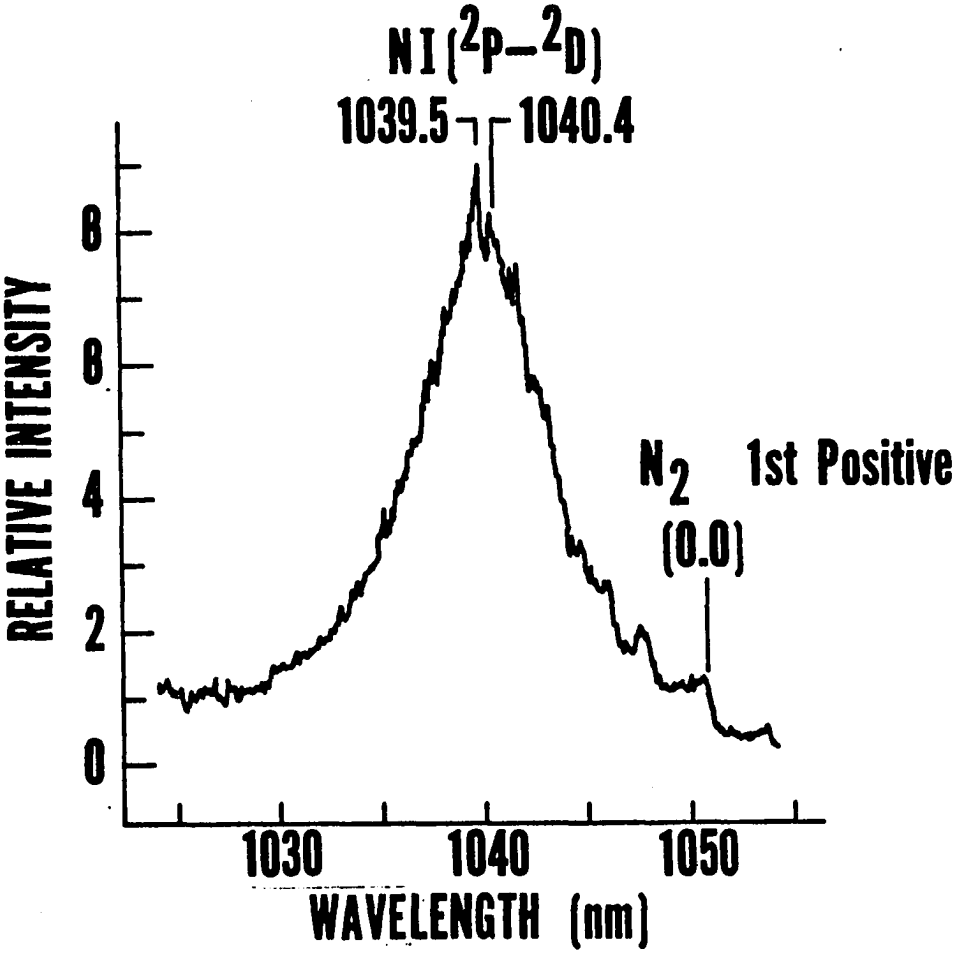

Figure 31. Expanded spectrum of the 1030-1055 nm region showing the resolved N(I) [^{2}P → ^{2}D] doublet and the N_2 (0-0) 1st positive band

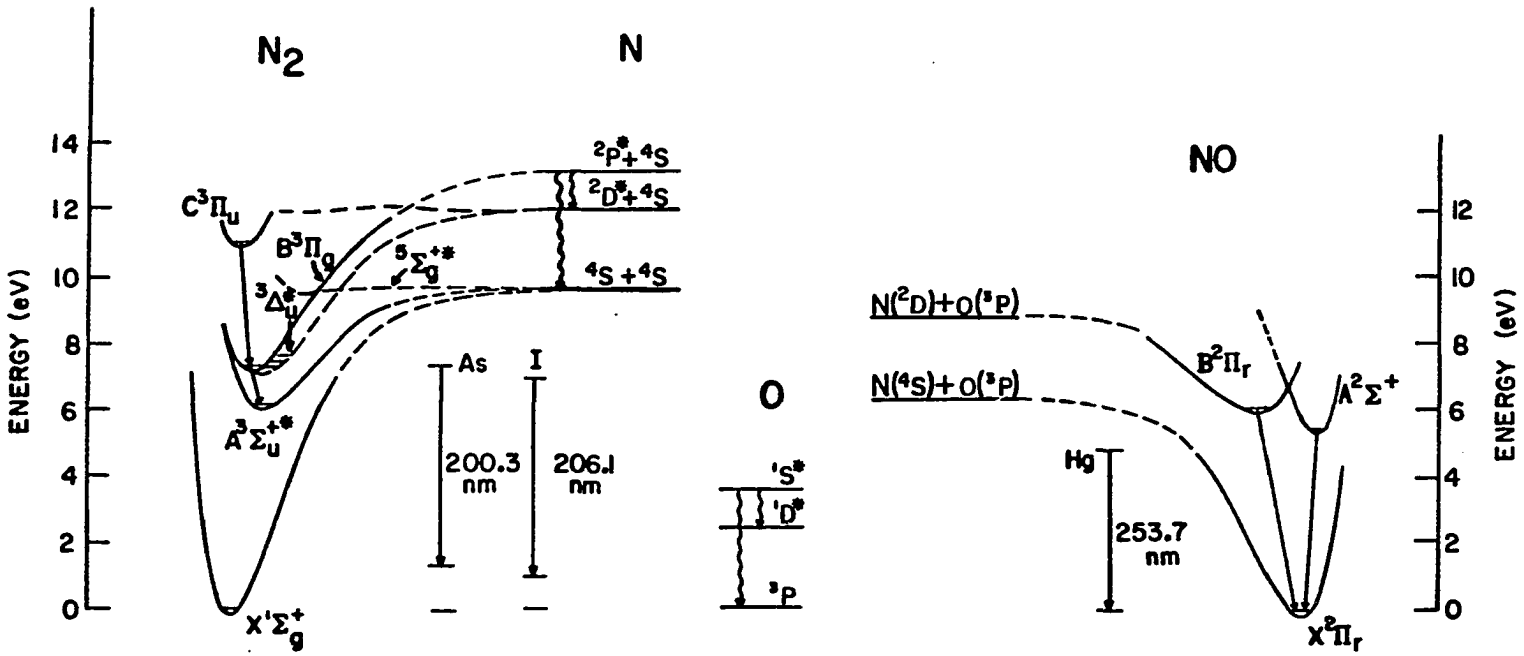

Figure 32. Potential energy diagrams for N_2 and NO, and electronic states of N and O. Only molecular and atomic states observed or presumed to be present in the APAN discharge are shown. Observed emissions designated by ⇃ (forbidden) or ↓ (allowed). Metastable species are designated by asterisks (*). Excited electronic states of As, I, and Hg, from which atomic emission has been observed, are also shown for comparative purposes

Table 14. Molecular and atomic transitions spectroscopically detected in the APAN discharge and afterglow

Species	System	Transition	Wavelength(s) of Observation (nm)	Lifetime (sec)	Detected in: Afterglow	Detected in: Discharge
O	-	$^1S \rightarrow {}^1D$	557.7	0.8	yes	yes
	-	$^1S \rightarrow {}^3P$	297.2	0.8	yes	yes
N	-	$^2P \rightarrow {}^2D$	1039.5, 1040.4	12	yes	yes
	-	$^2P \rightarrow {}^4S$	346.6	12	yes	yes
N_2	1st Positive	$B^3\Pi_g \rightarrow A^3\Sigma_\mu^+$	650 - 1051	a	no	yes
	2nd Positive	$C^3\Pi_\mu \rightarrow B^3\Pi_g$	290 - 500	a	no	yes
	Herman IR	Unknown	700 - 960	-	no	yes
NO	$NO\gamma$	$A^2\Sigma_r^+ \rightarrow X^2\Pi_r$	195 - 290	a	yes	yes
	$NO\beta$	$B^2\Sigma_r \rightarrow X^2\Pi_r$	270 - 380	a	yes	yes
NH	-	$A^3\Pi \rightarrow X^3\Sigma^-$	336.0, 337.0	a	yes	yes

[a]Short lived transitions ($\tau < 1 \times 10^{-6}$ s).

The mechanism of excitation in an ozonizer discharge maintained at atmospheric pressure has been elucidated and will not be presented here (25,82). In general, the nitrogen flowing through the annular cavity of the discharge tube serves as a dielectric for a capacitive-type, AC discharge. The discharge itself consists of a myriad of minute sparks which creates the appearance of a uniform glow. Thus, each spark consists of an extremely weak discharge. Electron excitation in the primary discharge may populate electronic and vibrational excited states of several, if not all, of the molecular N_2 states observed, as well as the formation and excitation of atomic N and O species.

The very intense $N_2(C^3\Pi_\mu \rightarrow B^3\Pi_g)$ second positive emission observed (see Figures 28 and 29) indicates that $N_2(C^3\Pi_\mu)$ and $N_2(B^3\Pi_g)$ species are present in the primary discharge. Both states may be populated by electron excitation or by associative recombination of nitrogen atoms (83) (see Figure 32), although the $B^3\Pi_g$ state is probably primarily populated by the allowed transition from $C^3\Pi_\mu$.

The very weak $N_2(B^3\Pi_g \rightarrow A^3\Sigma_\mu^+)$ first positive emission observed (see Figure 30) indicates that the metastable $A^3\Sigma_\mu^+$ state (τ = 1.9 s) exists in the primary discharge. First positive emissions in low pressure sources are usually rather intense, which indicates that at atmospheric pressure there may be secondary pathways which lead to radiationless deactivation of $N_2(B^3\Pi_g)$. Campbell and Thrush have commented that, at high pressures, the $B^3\Pi_g$ state may be removed by collisional quenching with a second body, presumably ground state N_2 (84). Noxon has observed that at high pressures the emission intensity

of the first positive system decreased significantly, while the Vergard-Kaplan system, $A^3\Sigma_\mu^+ \rightarrow x^1\Sigma_g^+$ (see Figure 32), increased in intensity (26). No attempt was made in the present investigation to detect the Vergard-Kaplan system because of spectral interferences from NOγ emissions.

The transitions responsible for the quite prominent Herman IR system observed in the direct discharge are not known but have been predicted to involve an electronic state of fairly high energy (85). These transitions appear to be unique with respect to being observed in an atmospheric system.

Spectroscopic Evidence for Long Lived Species in the Afterglow

Introduction

Numerous processes occur concurrently in the discharge and afterglow, and it is not easy to isolate the effects of one process from that of another. Many mechanisms have been proposed over the past seventy years to account for the selected features of the afterglow, but they have neither been uniformly applicable to all phenomena present in the afterglow or always self-consistent. To further compound the problem, practically all theory regarding the mechanisms of forming active nitrogen afterglows has been from data obtained in low pressure systems. Thus, the processes through which species are formed, as well as the collisionally induced deactivation and wall deactivation processes which occur, may be vastly different when extrapolating to atmospheric pressure systems.

The properties of the afterglow region are obviously determined by the excited and reactive species possessing liftimes sufficient to survive recombination and/or relaxation processes that substantially depopulate the short-lived energetic states within the primary discharge. Long-lived species may also be formed directly in the afterglow region.

The transitions spectroscopically observed in the afterglow region of the APAN source consisted primarily of emission from atomic N and O, and excited NO molecules.

$\underline{N(^2P)}$

The emission at 346.6 nm arising from the $^2P \rightarrow {}^4S$ transition (see Figures 28 and 32) confirms the presence of the $N(^2P)$ state in the afterglow. In low pressure active nitrogen afterglows, this transition is rarely observed because of the long lifetime (τ = 12 s) of the $N(^2P)$ state (86). It has been postulated that impurities, i.e., O_2, and not nitrogen species, reduces the lifetime of the $N(^2P)$ state at high pressures to give rise to the observed emissions (87).

$\underline{N(^2D)}$

The presence of metastable $N(^2D)$ atoms (τ = 26 h) is confirmed by the $^2P \rightarrow {}^2D$ doublet observed at 1039 and 1040 nm (see Figures 31 and 32). Earlier investigators who utilized electrodeless discharges did not report such observations.

$O(^1S)$

Observation of the forbidden $^1S \rightarrow {}^1D$ transition via the emission of the atomic oxygen line at 557.7 nm (see Figure 29) and the $^1S \rightarrow {}^3P$ transition at 297.3 nm (see Figure 28) confirms the presence of $O(^1S)$ in the afterglow. In addition to direct electron excitation of atomic oxygen in the primary discharge (88), the $O(^1S)$ state may also be populated by metastable $N_2(A^3\Sigma_\mu^+)$ via the following energy transfer process:

$$N_2(A^3\Sigma_\mu^+) + O(^3P) \rightarrow N_2(X^1\Sigma_g^+) + O(^1S) \quad (89) \quad .$$

In low pressure afterglows, the lifetime of the $O(^1S)$ state is 0.8 seconds.

$NO(A^2\Sigma^+)$ and $NO(B^2\Pi_g)$

The presence of $NO(A^2\Sigma^+)$ and $NO(B^2\Pi_r)$ in the afterglow is confirmed by the observed emission from the NOγ system ($A^2\Sigma^+ \rightarrow X^2\Pi_r$) and the NOβ system ($B^2\Pi_r \rightarrow X^2\Pi_r$) (see Figures 28 and 32). Although the $A^2\Sigma^+$ and $B^2\Pi_r$ states are very short lived ($\tau < 10^{-6}$ s), they are apparently generated throughout the primary discharge and afterglow, presumably via the recombination mechanism proposed by Young and Sharpless (90).

$$N + O + (M) \rightarrow NO^* + (M)$$

The third body (M), presumably N_2, may or may not be required for the recombination reaction. The formation of emissive NO species also appears to increase at higher pressures (26).

Evidence for Species Presumed to be Present in the Afterglow but not Observed Spectroscopically

$N(^4S)$

For a number of years there was considerable controversy over whether the chemical activity observed in active nitrogen afterglows was due to atomic or molecular states of nitrogen. Experimental evidence now indicates with considerable certainty that much of the activity is due to $N(^4S)$ atoms. Recombination or collisional processes involving $N(^4S)$ atoms leads to metastable N_2 states (see Figure 32) or observed chemical activity, respectively (84,91). Impurities are known to significantly increase the extent of N_2 dissociation in the primary discharge, oxygen being particularly effective (92). Berkowitz, using mass spectrometric analyses, has estimated that the $N(^4S)$ concentration in low pressure, active nitrogen afterglows to be $\sim$ 0.1% of the total N_2 concentration (93). Measurements by electron spin resonance techniques have also given similar results (94,95). These values, however, cannot be assumed to be of the same magnitude at atmospheric pressure.

$N_2(^5\Sigma_g^+)$

Although there is considerable evidence for the existence of the $N_2(^5\Sigma_g^+)$ state, to date there has been no direct spectroscopic proof of its existence. The $N_2(^5\Sigma_g^+)$ state is generally believed to be populated in the afterglow by three-body recombination of ground state $N(^4S)$ atoms (see Figure 32), N_2 being the third body (91,96). Others have predicted the $N_2(^5\Sigma_g^+)$ state to be in quasi-equilibrium with $N(^4S)$ atoms due to the very shallow potential well (< 0.16 eV), and to be capable of

surviving collisional deactivation processes (93,97). A lifetime of $\sim$ 0.02 seconds has been predicted (97).

$N_2(^3\Delta_\mu)$

The $N_2(^3\Delta_\mu)$ state appears to be the only low-lying, electronically excited molecular state of nitrogen whose exact energy content is not known. There is, however, general agreement that the energy content is on the order of $\sim$ 7.5 eV (9). Transitions to and from the $N_2(^3\Delta_\mu)$ state have been observed only in the Wu-Benesch system (98), which occurs in the 2200-4300 nm region and was not accessible with our instrumentation for investigation. The $N_2(^3\Delta_\mu)$ state has been postulated to be populated through a radiationless, collision-induced transition from the $N_2(^5\Sigma_g^+)$ state (97). Associative recombination of $N(^4S)$ and $N(^2D)$ atoms may also give rise to the $^3\Delta_\mu$ state (see Figure 32). Kenty has estimated that the concentration of $^3\Delta_\mu$ species may be as high as $10^{13}/cm^3$ in afterglows from a N_2-rare gas mixture at pressures of 150 torr (99). His results indicate that the lifetime of the $^3\Delta_\mu$ state is on the order of 1-2 seconds, although the lifetime may be shortened considerably due to susceptibility to deactivation from wall collisions or trace impurities.

$N_2(A^3\Sigma^+)$

The metastable $N_2(A^3\Sigma_\mu^+)$ state (τ = 1.9 s) has been indicated by many investigators to be responsible for observed reactions and emissions from atoms or molecules introduced into active nitrogen afterglows (32,100-102). Formation of the $N_2(A^3\Sigma_\mu^+)$ state may occur through decay

of the $N_2(B^3\Pi_g)$ state, by recombination of two $N(^4S)$ atoms (see Figure 32), or by direct electron excitation in the primary discharge. The lifetime of the $N_2(A^3\Sigma^+)$ state at atmospheric pressure has been predicted to be reduced to 0.1 to 1.0 seconds by collisional quenching or collision-induced emission (26,103).

$N_2(X^1\Sigma_g^+, \nu > 0)$

Vibrationally excited $N_2(X^1\Sigma_g^+)$ ground state N_2 species ($N_2^\dagger$) have also been presumed to be present in active nitrogen afterglows, and may exist in vibrational levels with energy as high as 6.6 eV (104). There is, however, no direct spectroscopic proof of their existence in active nitrogen afterglows. The upper vibrational levels may be produced by recombination of $N(^4S)$ atoms (105), or by direct electron excitation in an electrical discharge (106). Young has suggested that $N_2(A^3\Sigma_\mu^+)$ molecules may be deactivated to highly excited $N_2^\dagger$ states by reactions with $N(^4S)$ atoms (107). A lifetime of 0.05 seconds for $N_2^\dagger$ in lower vibrational states has been determined using microwave excitation at 1.3 torr (108). The reactivity of $N_2^\dagger$ has been demonstrated by strong evidence that Na and K atom lines may be excited by transfer of vibrational energy from highly excited $N_2^\dagger$ (109).

Conclusion

The species which probably are the most important in the reactions with analyte species in the APAN afterglow include electronic states of atomic nitrogen ($N(^4S)$, $N(^2D)$, and $N(^2P)$), and several metastable molecular nitrogen species ($N_2(A^3\Sigma_\mu^+$, $N_2(^5\Sigma_g^+)$, and $N_2(^3\Delta_\mu)$). The possible

interactions of these species with analyte species studied thus far will be presented in the following section.

Interactions of Reactive Species in the Afterglow With Other Molecules and Atoms

The numerous energetic species and processes that occur in the APAN afterglow preclude a conclusive explanation of the energy transfer mechanisms which give rise to atomic or molecular emission from species introduced into the afterglow. Because the gas temperature of the afterglow gases are too low ($\sim$ 150 to 200°C) to provide any significant excitation, it is necessary to resort to collisional transfer of excitation from long lived excited species introduced into or formed in the afterglow. The observed and predicted presence of metastable species in the afterglow invites speculation on their roles in the dissociation-excitation processes to be discussed for the analyte species studied thus far.

The characteristic atomic emission observed from trace levels of the Group IV-VI elements, when introduced as hydrides, will be discussed in detail to demonstrate the complexity involved in postulating a definitive excitation mechanism for such species in the APAN afterglow.

The mechanisms leading to dissociation of the hydrides and excitation of the free atoms can proceed through at least four possible processes; (1) thermal decomposition of the hydride followed by energy transfer from an active species to the free atom; (2) energy transfer from an active species with sufficient energy to cause simultaneous molecular dissociation and atomic excitation; (3) a three body reaction

involving two active species whose total potential energy equals or exceeds that necessary for simultaneous dissociation and excitation; and (4) a sequential process, first involving molecular dissociation of the hydride by one or more active species, followed by atomic excitation.

Little is known on the degree to which thermal dissociation, in relation to other dissociation processes, causes the release of free analyte atoms from the hydrides in the afterglow. All of the hydrides in Groups IV-VI have decomposition temperatures of less than 350°C. Particularly low are H_2Te (0°C), H_2Se (160°C), BiH_3 (150°C), SbH_3 (200°C) (200°C), and SnH_4 (150°C). PbH_4 is thermodynamically unstable and readily decomposes. The operating temperature of the APAN afterglow is typically 150°C, a temperature sufficiently high enough to thermally dissociate the more unstable hydrides. Thus, the only energy requirements from active species in the afterglow would be for atomic excitation (4.02-6.56 eV). This energy could be supplied by a number of active species of nitrogen, including $N_2(A^3\Sigma_\mu^+)$, $N_2(^3\Delta_\mu)$, and $N_2(^5\Sigma_g^+)$, which have energies of 6.16 eV, 7.5 eV, and 9.6 eV respectively. Other species in the afterglow, which include $O(^1S)$ (4.17 eV), NOγ (5.5 eV) and NOβ (5.7 eV) could just as well be possibilities.

A two body energy transfer process, leading to simultaneous dissociation and excitation of the more thermally stable hydrides, appears to be unfavorable due to the relatively high energy requirements involved. It is generally agreed that the maximum energy content in active nitrogen afterglows is on the order of approximately 9.6 eV. Noxon has postulated the same maximum energy content for APAN afterglows

(26). The combined energy for dissociation and atomic excitation for several of the hydride species (i.e., H_2S, AsH_3, GeH_4) in all probability exceeds the maximum energy available in the afterglow. Thus, a purely two body interaction for the more stable hydrides is unlikely.

A three body reaction involving a hydride molecule and two active species in the afterglow could meet some of the necessary energy requirements. Evans and Winkler have suggested that recombination of two ground state $N(^4S)$ atoms could cause the excitation of atoms in the afterglow (28).

$$N(^4S) + N(^4S) + M \rightarrow N_2(X^1\Sigma_g^+) + M^*$$

This type of process is known to produce emission from Hg or Na atoms on recombination of hydrogen atoms (110). The recombination of $N(^4S)$ atoms could provide 9.76 eV of energy, which is probably sufficient for the less stable hydrides. There are no combinations of known active species in the afterglow which could provide sufficient energy for a three body reaction with the more stable hydrides. Furthermore, the relative populations of active species presumed or observed to be present in the afterglow are not known, which precludes any definitive conclusion on how favorable a particular three body process would be.

A sequential reaction mechanism could readily explain how the hydrides are dissociated and the atoms excited. Phillips has proposed consecutive energy transfer steps for species requiring more than 9.6 eV of potential energy (33). He suggested that for $PbCl_2$, successive attacks from metastable nitrogen molecules (N_2^*) could lead to the

observed lead emissions,

$$PbCl_2 + N_2^* \rightarrow PbCl^* + Cl + N_2$$

$$PbCl^* + N_2^* \rightarrow Pb^* + Cl + N_2$$

$$Pb^* \rightarrow Pb + h\nu \quad .$$

Wiles and Winkler have also proposed a similar mechanism involving hydrogen abstraction from phosphine by nitrogen atoms, resulting in the formation of NH and excited PN molecules (29),

$$N + PH_3 \rightarrow NH + PH_2$$

$$N + PH_2 \rightarrow PN^* + H_2$$

$$PN^* \rightarrow PN + h\nu \quad .$$

Sutton has suggested that the observed atomic emissions obtained from hydrides in low pressure afterglows results from the "stripping down" of the hydride molecule by successive attacks of nitrogen atoms, followed by bimolecular energy transfer from $N_2(A^3\Sigma_\mu^+)$ for atomic excitation (36), i.e., for H_2Se,

$$N + H_2Se \rightarrow NH + HSe^*$$

$$N + HSe^* \rightarrow NH + Se$$

$$Se + N_2(A^3\Sigma_\mu^+) \rightarrow Se^* + N_2(X^1\Sigma_g^+)$$

$$Se^* \rightarrow Se + h\nu \quad .$$

Other workers have used atomic emission from Hg to confirm the presence

of $N_2(A^3\Sigma_\mu^+)$ in the afterglow by the reaction (101,111)

$$N_2(A^3\Sigma_\mu^+) + Hg(^1S_0) \rightarrow N_2(X^1\Sigma_g^+) + Hg(^3P_1)$$

$$Hg(^3P_1) \rightarrow Hg(^1S_0) + h\nu \quad (253.7 \text{ nm}) \quad .$$

Sutton has predicted that in their low pressure ($\sim$ 10 torr) active nitrogen afterglow the $N_2(A^3\Sigma_\mu^+)$ concentration is on the order of $10^{13}/cm^3$ (34). Others have suggested that the atomic nitrogen concentration is of the same order in magnitude (112).

Whether the successful dissociation and excitation of the hydrides is the result of energy transfer from atomic or molecular nitrogen species in the APAN afterglow is unresolved at this time. Furthermore, other metastable N_2 molecules of higher energy than $N_2(A^3\Sigma_\mu^+)$ would be necessary in order to excite some of the high energy atomic transitions observed, i.e., As at 200.3 nm (7.54 eV, see Figure 32), Ge at 219.9 nm (6.52 eV). Possible species responsible for excitation of these atomic states could include $N_2(^5\Sigma_g^+)$ and $N_2(^3\Delta_\mu)$. There are also several active species other than nitrogen which could give rise to resonance energy transfer processes. For example, the intense Bi emission at 306.8 nm corresponds to an energy of 4.04 eV, which is very similar to the energy associated with $O(^1S)$ (4.17 eV).

Of the mechanisms proposed for the dissociation and excitation of the hydrides, either thermal dissociation followed by excitation or consecutive energy transfer reactions are the most probable. To pinpoint the exact mechanism and active species responsible is too speculative at this time.

The production of characteristic atomic emission from organometallic compounds, used in the speciation studies via GC, probably occurs through consecutive energy transfer mechanisms. The metal-carbon bonds are relatively stable and would not undergo thermal dissociation at the temperatures maintained in the afterglow. Also, the combined bond and excitation energies are great enough to eliminate the possibility of a single two body or three body energy transfer mechanism.

Phillips has provided an explanation for the molecular emission observed from halogen compounds introduced into active nitrogen afterglows (113). The primary reaction involves $N(^4S)$ atoms,

$$N(^4S) + X_2(^1\Sigma) \rightarrow NX(^3\Sigma) + X(^2P)$$

however, it has been calculated that there is insufficient energy available to electronically excite the NBr or NCl ground state molecules. Excited NCl and NBr species may be produced by a second reaction involving $N(^4S)$ and atomic halogen species, i.e., Br,

$$N(^4S) + Br(^2P) \rightarrow NBr(b^1\Sigma^+)$$

$$NBr(b^1\Sigma^+) \rightarrow NBr(X^3\Sigma^-) + h\nu \quad .$$

The reaction sequence presented is consistent with a slope that approaches approximately two for NCl emission as a function of Cl concentration discussed in the previous chapter. In effect, it would take two Cl atoms to produce one emissive NCl state, thus emission intensity could be expressed in terms of Cl concentration as

$$I_{NCl} = K[Cl]^2$$

where K is an experimental constant. This result is similar to observations from S_2 emissions discussed previously. The nonideal slope actually obtained ($\sim$ 1.8) may be related to further reaction of NBr with active species or by collisional deactivation through nonradiative pathways.

Molecular emission observed from Br_2 and I_2 could arise by energy transfer from a number of active species present in the afterglow. Iodine emission has been believed to be mainly due to energy transfer from $N_2(A^3\Sigma_\mu^+)$ (102).

The intense emission observed from atomic iodine at 183.0 nm in the APAN afterglow requires 8.30 eV of energy for dissociation and excitation. This sequence could occur simultaneously in a two body reaction involving the predicted $N_2(^5\Sigma_g^+)$ state, which contains 9.6 eV of energy. A sequential reaction would necessitate 6.84 eV of energy to promote the atoms to excited states, which could be supplied by $N_2(^3\Delta_\mu)$ at an energy of 7.5 eV (see Figure 32). Once again, no definite answer can be resolved.

Introduction of sulfur containing compounds into active nitrogen afterglows has primarily produced emission from NS (9). Only a few investigators have observed S_2 emission (114,115). Westbury and Winkler have postulated that for H_2S a transition complex with nitrogen atoms occurs which reacts with a second nitrogen atom to form HS radicals (30),

$$N + H_2S \rightarrow [N \cdot H_2S]$$

$$N + [N \cdot H_2S] \rightarrow N_2 + H + HS \quad .$$

The HS radicals recombine to form S_2 molecules,

$$2HS \rightarrow H_2 + S_2 \quad .$$

A mechanism of this type if consistent with the slope of ~ 2 obtained from analytical calibration curves for H_2S presented in the previous chapter. Combination of two sulfur atoms could also occur,

$$2HS \rightarrow H_2S + S$$

$$2S \rightarrow S_2 \quad .$$

However, this mechanism would not be consistent with the slope of ~ 2, since essentially four sulfur atoms would be required to produce one S_2 molecule. Alternatively, the H atoms could be sequentially dissociated from H_2S to leave sulfur atoms, which upon recombination could form S_2 molecules. This type of process could also occur with COS, with the formation of NO and CN occurring. The SO_2 molecule appears to be too stable to be directly attacked by N atoms, although limited decomposition has been observed and attributed to excited nitrogen molecules (116).

The formation of emissive CN species in active nitrogen afterglows has been the subject of extensive investigation, but uncertainty involving the mechanism of formation persists. It has been suggested that CN may be produced in active nitrogen by reactions of N atoms with single carbon containing species (70), i.e., CH_3,

$$CH_3 + N \rightarrow CN + H_2 + H$$

$$CH_2 + N \rightarrow CN + 2H$$

$$CH + N \rightarrow CN + H \quad .$$

The single carbon species are supposedly formed by sequential cracking of the parent compound into smaller alkyl radical chains. Thus, a long and complex chain of reactions is necessary before CN formation can occur. The nonlinearity of calibration curves above 100 ng for hexadecane in the APAN afterglow may be due to depletion of the atomic nitrogen species required, if indeed, nitrogen atoms are responsible for CN formation. If this reasoning is valid, it would be expected that a greater linear dynamic range would be obtained for smaller organic molecules.

The mechanisms presented to explain the observed emission from species studied thus far in the APAN afterglow are admittedly speculations based on evidence accumulated in past investigations. The collection of a more extensive data base is required before the primary and secondary reaction sequences and pathways can be suggested with any semblance of rectitude.

CHAPTER IV. SUMMARY AND OBJECTIVES FOR FUTURE RESEARCH

The analytical utilization of an active nitrogen afterglow produced at atmospheric pressure as a source for the excitation of characteristic emission from a number of elements of environmental interest has been successfully demonstrated. Limits of detection for several elements are comparable to commonly available instrumental techniques. Many of the problems encountered with other element specific detectors for gas chromatography were alleviated by the APAN detector. The GC-APAN system has clearly been demonstrated to be an advantageous and superior analytical combination for the determination of ultra-trace levels of organomercury compounds in environmental samples. Finally, the APAN afterglow may be useful for detecting a number of nonmetallic elements from production of characteristic molecular emission.

A significant potential exists to explore other techniques for production and utilization of APAN afterglows for analytical investigations. Variations in the discharge tube design and modes of sample introduction may further improve the current limits of detection and number of elements detected. A new power supply for production of the discharge, which involves a direct current discharge controlled by a variable low frequency spark gap, is currently being constructed for testing. High frequency electrodeless discharges may also be considered in future investigations.

The analytical potential of using the APAN excitation source for other elements will certainly be of vital importance. All of the elements which have visually been observed to give characteristic atomic

and/or molecular emission in low pressure active nitrogen afterglows are illustrated in Figure 33. Detection of several metallic elements at trace levels by thermal vaporization of the sample into an active nitrogen afterglow has recently been described (117,118). Construction of a thermal vaporization unit for the APAN system would be most advantageous for evaluating the feasibility of detecting elements which have not been investigated up to this time.

Finally, the possibility of using the same experimental design for investigating the analytical potential of afterglows generated from gases other than nitrogen is most exciting. The primary focus would be placed on generating afterglows from helium and argon. Both helium and argon are known to possess several metastable states when generated in low pressure systems (119,120). A list of metastable argon and helium species, including their energies and lifetimes, is given in Table 15. Since the early 1960s, Collins and Robertson (121-123) and Lee et al. (124) have qualitatively described characteristic emission generated from a number of different molecules when introduced into a low pressure helium afterglow. Some interest has also been shown in using argon afterglows for the same purpose (21,125,126). Thus, the potential exists to generate these highly energetic metastable species in the atmospheric pressure discharge system for utilization as a source for analytical emission spectroscopy.

The ability to use a variety of gases for excitation in the same instrumental arrangement would be ideal for analytical purposes. By simply switching to the appropriate gas, the most selective and sensitive

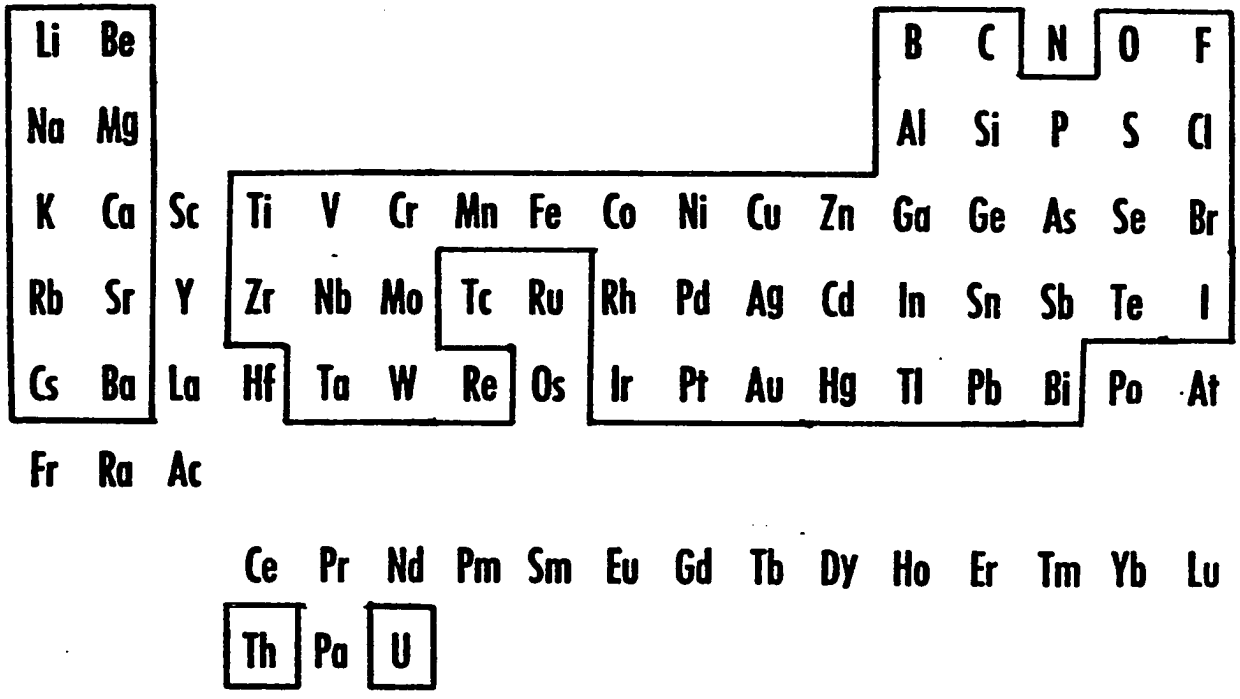

Figure 33. Elements of the periodic table (blocked regions) which have been observed to give characteristic atomic and/or molecular emission in active nitrogen afterglows

Table 15. Metastable species of He and Ar[a]

State	Excitation Energy (eV)	Radiative Lifetime
He (2^1 S)	20.61	19 ms
He (2^3 S)	19.81	>150 min
He_2 ($a^3\Sigma_u^+$)	21.5	> 0.1 s
Ar ($^3P_0$)	11.73	1.3 s
Ar ($^3P_2$)	11.55	1.3 s

[a]Reference 121.

conditions could probably be obtained for each element of interest. Thus, considerable expansion in the capabilities of the instrumentation would be achieved. This feature may be extremely useful when applied as an element selective detector for gas chromatography. A considerable effort will undoubtedly have to be undertaken in order for these capabilities to become a reality.

LITERATURE CITED

1. Morren, M. A. Ann. Chem. Phys. 1865, 4, 293-296.
2. Lewis, E. P. Ann. Physik 1900, 2, 459-465.
3. Lewis, E. P. Astrophys. J. 1900, 12, 8-12.
4. Lewis, E. P. Phys. Rev. 1904, 18, 125-128.
5. Strutt, R. J. Proc. Roy. Soc. 1911, A85, 219-229.
6. Strutt, R. J. Proc. Roy. Soc. 1912, A86, 56-63.
7. Strutt, R. J.; Fowler, A. Proc. Roy. Soc. 1912, A86, 105-117.
8. Strutt, R. J. Proc. Roy. Soc. 1913, A88, 110-117.
9. Wright, A. N.; Winkler, C. A. "Active Nitrogen"; Academic Press: New York, 1968.
10. Phillips, L. F. Can. J. Chem. 1963, 41, 732-738.
11. Lord Rayleigh. Proc. Roy. Soc. 1935, A151, 567-584.
12. Lord Rayleigh. Proc. Roy. Soc. 1940, A176, 1-27.
13. Kenty, C.; Turner, L. A. Phys. Rev. 1928, 32, 799-811.
14. Peyron, M. J. Chim. Phys. 1963, 59, 99-104.
15. McDonald, A. D.; Garskell, D. V.; Getterman, H. N. Phys. Rev. 1963, 130, 1841-1850.
16. Constantinides, P. A. Phys. Rev. 1927, 30, 95-108.
17. Stanley, C. R. Proc. Phys. Soc. (London) 1954, 67, 821-827.
18. Kenty, C. Phys. Rev. 1954, 93, 651-656.
19. Kenty, C. J. Chem. Phys. 1955, 23, 1556-1557.
20. Bennett, W. R. Ann. Phys. (N.Y.) 1962, 18, 367-374.
21. Prince, J. F.; Collins, C. B.; Robertson, W. W. J. Chem. Phys. 1964, 40, 2619-2625.
22. Patel, C. K. N.; Tress, P. K.; McFee, J. H. Appl. Phys. Letters 1965, 7, 290.

23. Groth, W. E.; Oldenburg, O. J. Chem. Phys. 1955, 23, 729-731.

24. Schulze, H. Z. Physik Chem. (Leipzig) 1959, 210, 76-83.

25. Wulf, C. R.; Melvin, E. H. Phys. Rev. 1939, 55, 687-691.

26. Noxon, J. F. J. Chem. Phys. 1962, 36, 926-940.

27. Brocklehurst, B.; Downing, F. A. J. Chem. Phys. 1967, 46, 514-521.

28. Evans, H. G. V.; Winkler, C. A. Can. J. Chem. 1956, 34, 1217-1231.

29. Wiles, D. M.; Winkler, C. A. J. Phys. Chem. 1957, 61, 902-903.

30. Westbury, R. A.; Winkler, C. A. Can. J. Chem. 1960, 38, 334-342.

31. Storr, R.; Wright, A. N.; Winkler, C. A. Can. J. Chem. 1962, 40, 1296-1301.

32. Duthler, C. J.; Brioda, H. R. J. Chem. Phys. 1973, 59, 167-174.

33. Phillips, L. F. Can. J. Chem. 1963, 41, 2060-2066.

34. Capelle, G. A.; Sutton, D. G. Appl. Phys. Letters 1977, 30, 407-409.

35. Capelle, G. A.; Sutton, D. G. Rev. Sci. Instrum. 1978, 49, 1124-1129.

36. Sutton, D. G.; Melzer, J. E.; Capelle, G. A. Anal. Chem. 1978, 50, 1247-1250.

37. Sutton, D. G.; Westburg, K. R.; Melzer, J. E. Anal. Chem. 1979, 51, 1399-1401.

38. Melzer, J. E.; Sutton, D. G. Appl. Spectrosc. 1980, 34, 434-437.

39. For the most current review on hydride methods for atomic spectroscopy, refer to: Robbins, W. B. Anal. Chem. 1979, 51, 889A-899A.

40. Hurd, D. T. "Chemistry of the Hydrides"; John Wiley and Sons, Inc.: New York, 1952.

41. Johnson, D. A. "Some Thermodynamic Aspects of Inorganic Chemistry"; Cambridge University Press: London, 1968; Chapter 7.

42. Vijan, P. N.; Wood, G. R. Analyst 1976, 101, 966-973.

43. Brodie, K. G. Am. Lab. 1979, 11, 58-66.

44. Thompson, M.; Pahlavanpour, B.; Walton, S. J.; Kirkpatrick, G. F. Analyst 1978, 103, 568-579.

45. Thompson, K. C.; Thomerson, D. R. Analyst 1974, 99, 595-601.

46. Smith, A. E. Analyst 1975, 100, 300-306.

47. Thompson, K. C. Analyst 1975, 100, 307-310.

48. Robbins, W. B.; Caruso, J. A.; Fricke, F. L. Analyst 1975, 104, 35-40.

49. Braman, R. S.; Juster, L. J.; Fareback, C. Anal. Chem. 1972, 44, 2195-2199.

50. Braman, R. S.; Thompkins, M. A. Anal. Chem. 1978, 50, 1088-1093.

51. Hwang, J. Y.; Ullicci, P. A.; Malenfant, A. L. Can. Spectrosc. 1971, 16, 100-105.

52. Thompson, K. C.; Reynolds, G. D. Analyst 1971, 96, 771-775.

53. Watling, R. J. Anal. Chim. Acta 1975, 75, 281-288.

54. Braman, R. S. Anal. Chem. 1971, 43, 1462-1467.

55. Drinkwater, J. E. Analyst 1976, 101, 672-677.

56. Fiorino, J. A.; Jones, J. W.; Capar, S. G. Anal. Chem. 1978, 48, 120-125.

57. Belcher, R.; Bogdanski, S. L.; Henden, E.; Townshend, A. Analyst 1975, 1000, 522-523.

58. Farwell, S. O.; Rasmussen, R. A. J. Chromatogr. Sci. 1978, 14, 224-234.

59. Chau, Y. K.; Wang, P. T. S. Water Qual. Bull. 1978, 3, 8-11.

60. Grant, N. Environment 1971, 13, 3-14.

61. McCormack, A. J.; Tong, S. S. C.; Cooke, W. D. Anal. Chem. 1965, 37, 1470-1476.

62. McLean, W. R.; Stanton, D. L.; Penketh, G. E. Analyst (London) 1973, 98, 432-442.

63. Van Dalen, J. P. J.; Coulander, P. A.; de Galen, L. Anal. Chim. Acta 1977, 94, 1-19.

64. Quimby, B. D.; Uden, P. C.; Barnes, R. M. Anal. Chem. 1978, 50, 2112-2118.

65. Beenakker, C. I. M. Spectrochim. Acta 1977, 32B, 173-187.

66. Lloyd, R. J.; Barnes, R. M.; Uden, P. C.; Elliot, W. G. Anal. Chem. 1978, 50, 2025-2029.

67. Treybig, D. S.; Ellebracht, S. R. Anal. Chem. 1980, 52, 1633-1636.

68. Windsor, D. L.; Denton, M. B. Appl. Spectrosc. 1978, 32, 366-371.

69. Windsor, D. L., Denton, M. B. J. Chromatogr. Sci. 1979, 17, 492-496.

70. Safrany, D. R. "Progress in Reaction Kinetics", Vol. 6; Permagon Press: New York, 1972; Chapter 1.

71. Talmi, Y. Anal. Chim. Acta 1975, 74, 107-117.

72. Miettinen, J. K.; Rahola, T.; Hattula, T.; Rissane, K.; Tillander, M. Ann. Clin. Res. 1971, 3, 116-122.

73. Jensen, S.; Jernelov, A. Nature (London) 1969, 223, 753-754.

74. Fishbein, L. "Chromatography of Environmental Hazards - Metals, Gaseous, and Industrial Pollutants", Vol. 2; Elsevier Scientific Pulbishing Company: New York, 1973; Chapter 7.

75. Westöö, G. Acta Chem. Scand. 1966, 20, 2131-2137.

76. Westöö, G. Acta Chem. Scand. 1967, 21, 1790-1800.

77. "Manual of Analytical Methods for the Analysts of Pesticide Residues in Human and Environmental Samples"; Thompson, J. F., Ed.; Environmental Protection Agency: Research Triangle Park, NC; Section 1-13A.

78. Watts, J. O.; Bayer, K. W.; Cortez, A.; Elkins, Jr., E. R. J. Assoc. Off. Anal. Chem. 1976, 59, 1226-1233.

79. Dressman, R. C. J. Chromatogr. Sci. 1973, 107, 472-475.

80. Junk, G. A.; Richard, J. J.; Grieser, M. D.; Witiak, D.; Witiak, J. L.; Arguello, M. D.; Vick, R.; Svec, H. J.; Fritz, J. S.; Calder, G. V. J. Chromatogr. 1974, 99, 745-762.

81. Junk, G. A.; Ames Laboratory, Iowa State University: Ames, Iowa; private communication.

82. Hague, R.; Von Engel, A. J. Electronics 1974, 36, 239-246.

83. Bauer, E.; Bartky, C. D. J. Chem. Phys. 1965, 43, 2466-2476.

84. Campbell, I. M.; Thrush, B. A. Proc. Roy. Soc. (London) 1967, 296A, 201-221.

85. Carroll, P. K.; Sayers, N. D. Proc. Roy. Soc. (London) 1953, 64, 1138-1144.

86. Kaplan, J. Phys. Rev. 1934, 45, 675-677.

87. Oldenburg, O. Phys. Rev. 1953, 90, 727-730.

88. Donahue, T. M.; Zipf, E. C.; Parkinson, J. D. Planet. Space Sci. 1970, 18, 171-178.

89. Henriksen, K. Planet. Space Sci. 1973, 21, 863-871.

90. Young, R. A.; Sharpless, R. L. J. Chem. Phys. 1963, 39, 1071-1102.

91. Anketell, J.; Nicholls, R. W. Rep. Prog. Phys. 1970, 33, 269-306.

92. Young, R. A.; Sharpless, R. L.; Stringham, R. J. Chem. Phys. 1964, 40, 117-119.

93. Berkowitz, J.; Chupka, W. A.; Kistiakowsky, G. B. J. Chem. Phys. 1956, 25, 457-466.

94. Marshall, T. Bull. Am. Phys. Soc. 1962, 7, 133-136.

95. Marshall, T. J. Chem. Phys. 1966, 44, 1715-1720.

96. Bayes, K. D.; Kistiakowsky, G. B. J. Chem. Phys. 1960, 32, 992-1000.

97. Wright, A. N.; Winkler, C. A. J. Chem. Phys. 1963, 67, 172-177.

98. Wu, H. L.; Benesch, W. Phys. Rev. 1968, 172, 31-35.

99. Kenty, C. Bull. Am. Phys. Soc. 1962, 7, 640-644.

100. Wright, A. N.; Nelson, R. L.; Winkler, C. A. Can. J. Chem. 1962, 40, 1082-1097.

101. Brennen, W. R.; Kistiakowsky, G. B. J. Chem. Phys. 1966, 44, 2695-2702.

102. Mandl, A.; Ewing, J. J. J. Chem. Phys. 1977, 67, 3490-3494.

103. Zipf, E. C. J. Chem. Phys. 1963, 38, 2034-2035.

104. Herman, R. Ann. Phys. (Paris) 1945, 20, 241-246.

105. Benson, S. W.; Fueno, T. J. Chem. Phys. 1959, 31, 1338-1343.

106. Chen, J. C. Y. J. Chem. Phys. 1964, 30, 3513-3518.

107. Young, C. R. A. Can. J. Chem. 1966, 44, 1171-1178.

108. Kaufman, F.; Kelso, J. R. J. Chem. Phys. 1958, 28, 510-517.

109. Starr, W. L.; Sharo, T. M. J. Chem. Phys. 1966, 44, 4181-4186.

110. Bonhoeffer, K. F. Ergel. Exakt. Naturw. 1927, 6, 201-208.

111. Young, R. A.; St. John, G. A. J. Chem. Phys. 1968, 48, 2572-2574.

112. Dondes, S.; Harteck, P.; Kung, C. Z. für Naturw. 1964, 19, 6-12.

113. Raxworthy, K. S.; Phillips, L. F. Can. J. Chem. 1964, 42, 2928-2930.

114. Smith, J. J.; Meyer, B. J. Mol. Spectrosc. 1964, 14, 160-172.

115. Pannetier, G.; Ressaun, O.; Ardet, I.; Goudmand, P. Bull. Soc. Chim. France 1966, 25, 313-318.

116. Brown, R.; Winkler, C. A. Angew. Chem. 1970, 9, 181-196.

117. Na, H. C.; Hornung, S. D.; Niemczyk, T. M. 31st Pittsburgh Conference on Analytical Chemistry and Applied Spectroscopy, 1981; Atlantic City, NJ; Paper No. 173.

118. Dodge, W. B.; Allen, R. O. Anal. Chem. 1981, 53, 1279-1286.

119. Kolts, J. H.; Setser, D. W. In "Reactive Intermediates in the Gas Phase", Setser, D. W., Ed.; Academic Press: New York, 1979, Chapter 3.

120. Golde, M. F.; Thrush, B. A. Rep. Prog. Phys. 1973, 36, 1285-1364.

121. Collins, C. B.; Robertson, W. W.; Ferguson, E. E.; Matsen, F. A. J. Am. Chem. Soc. 1962, 84, 676.

122. Collins, C. B.; Robertson, W. W. Spectrochim. Acta 1963, 19, 747-751.

123. Collins, C. B.; Robertson, W. W. J. Chem. Phys. 1964, 40, 701-712.

124. Lee, F. W.; Collins, C. B.; Waller, R. A. J. Chem. Phys. 1976, 65, 1605-1615.

125. Ave, W. A.; Paramasigamani, V.; Kapila, S. Mikrochim. Acta 1978, 1, 193-200.

126. Ave, W. A.; Paramasigamani, V.; Kim, J. H. Can. J. Chem. 1981, 59, 1439-1448.

ACKNOWLEDGEMENTS

The guidance and patience of Arthur P. D'Silva during the course of this work is greatly appreciated. His trust in my capabilities ultimately provided me with the materials and knowledge to successfully complete this work. I wish also to especially thank Dr. Velmer A. Fassel for his many helpful suggestions and support throughout my graduate studies, and for his critical review and helpful suggestions during the writing of this dissertation.

Special recognition must be given to John Richard, with whom many long hours of discussion and experimentation were spent in developing the APAN system as a GC detector. His analytical expertise is a valuable asset for those who work with him. The work of two summer assistants, Tami Jensen and Jane Moeller, who were significant contributors to the organomercury speciation studies, is also appreciated.

I would like to express my thanks for the splendid work done by all of the people in the support facilities of the Ames Laboratory. Special thanks to Harold Hall for his patience and glassblowing expertise during construction and repair of the many discharge tubes used in this work.

I also wish to thank my parents, Bobby and Phyllis Rice, for their continued support. Although their understanding of my work was very limited, they have always displayed extreme gratification for what I have tried to accomplish in my life.

Finally, the greatest recognition must go to my wife, Tonya. She encouraged me during many times of self-doubt and futility, displayed patience during times of impatience, and endured many sacrifices in her

own educational pursuits while providing love for the treasure which we both share in our son, Micah. Although the many long hours spent away from my family will never be regained, the experiences we have shared in the past will undoubtedly create a better world for all of us in the future.